FE Modeling of interacting indentation, flexural and delamination damage in lap joints of composites

SALMAN KHALID
NUST201362426MCEME35113F

Supervisor
DR. RIZWAN SAEED CHOUDHRY

DEPARTMENT OF MECHANICAL ENGINEERING
COLLEGE OF ELECTRICAL & MECHANICAL ENGINEERING
NATIONAL UNIVERSITY OF SCIENCES AND TECHNOLOGY
ISLAMABAD

AUGUST, 2016

FE Modeling of interacting indentation, flexural and delamination damage in lap joints of composites

SALMAN KHALID

NUST201362426MCEME35113F

A thesis submitted in partial fulfillment of the requirements for the degree of

MS Mechanical Engineering

Thesis Supervisor:

DR. RIZWAN SAEED CHOUDHRY

Thesis Supervisor's Signature: _____

DEPARTMENT OF MECHANICAL ENGINEERING

COLLEGE OF ELECTRICAL & MECHANICAL ENGINEERING

NATIONAL UNIVERSITY OF SCIENCES AND TECHNOLOGY,

ISLAMABAD

AUGUST, 2016

Declaration

I certify that this research work titled *"FE Modeling of interacting indentation, flexural and delamination damage in lap joints of composites"* is my own work. The work has not been presented elsewhere for assessment. The material that has been used from other sources it has been properly acknowledged / referred.

Signature of Student

SALMAN KHALID

NUST201362426MCEME35113F

Language Correctness Certificate

This thesis has been read by an English expert and is free of typing, syntax, semantic, grammatical and spelling mistakes. Thesis is also according to the format given by the university.

Signature of Student

SALMAN KHALID

NUST201362426MCEME35113F

Signature of Supervisor

Copyright Statement

Acknowledgements

First of all, I would like to express my gratitude to Allah SWT for all the blessings and benevolence which helped me to complete this task in terms of integrity and completeness. I would also like to thank people who have helped and guided me in this research and provided all possible assistance throughout the time of working on the thesis. It is a pleasure for me to thank those who made this thesis possible.

I gratefully thank my thesis supervisor, Assistant Professor Dr. RIZWAN SAEED CHOUDHRY for his support, encouragement and guidance in different problems concerning the topic to reach my targets. His continuous support, co-operation and encouragement were the keys for successful completion of this research work. I am also thankful for his tireless efforts during the review of the manuscript. In short, without his guidance, support and precious time, this work was impossible for me.

I am grateful to my Guidance and Evaluation Committee (GEC) and for taking time from his tough schedule to attend my thesis presentations. I am really obliged for letting my defence be an enjoyable moment and for his brilliant comments and suggestions.

I would like to thank the entire honourable faculty and staff of Mechanical Department of College of E & ME whose professional approach and vision groomed me as a sound person both technically and morally.

The last and most important thanks goes to my family, who always supported me in all my pursuits. I would like to thank them for all their love and encouragement

Abstract

Composite lap joints are essential for various applications such as aircraft wings, piping networks, sporting equipment and civil engineering works. The low velocity impact on such joints is a common occurrence in real life situations. The response of these joints under such impacts is quite complex. This involves multiple interacting damage modes that may occur within plies (fiber and matrix damage), at interfaces between plies (delamination) and at the bond interface (joint failure), indentation, flexural and shearing loads caused by impact. These may lead to significant degradation of joint strength without apparent complete failure. Thus it is very important to predict the response and behavior of such joints under impact.

Many researchers have dealt with problem of impact damage modeling, however these approaches are either too complex or require material parameter that may not have clear physical meaning. Thus, the objective of the study was to demonstrate a consistent set of methodology for evaluation of damage parameters for built in damage progressive models in ABAQUS and validating the methodology by applying on a lap joint impact problem. The damage model used in a previous study (Choudhry et al. IJIE, 80 (2015)) is improved to include laminate damage in addition to delamination and bond failure. The study follows a continuum damage modeling approach. Different progressive damage models for composite materials that are available in the literature were studied/reviewed by the author. Hashin damage model is one of the built in progressive damage model in ABAQUS. In this study, Hashin damage model is used for modeling laminate failure in this study. The model is implemented using plane stress elements (continuum shell). Mesh convergence and reduction in overall computational cost is an important consideration for such models. This point is discussed extensively in current work. The results of simulations are validated against experimental data of previous study. The study will be helpful for practicing engineers, as it provides them with the consistent and easy to use methodology for evaluating damage parameters for practical impact simulation problem.

Table of Contents

List of Figures

List of Tables

Chapter 1

Introduction

1.1 Motivation

The use of adhesively bonded composite lap joints for joining method is increasing day by day in industries, due to its advantages, over mechanical fasteners such as bolts, screws and rivets. In comparison of these mechanical fasteners, these joints are not only barren of localized stress concentration but these joints also provide less weight and cost saving features. Products made from woven fiber reinforced polymer matrix composites can benefit from adhesive as these can be made using a single manufacturing process, therefore saving the manufacturing and assembly cost.

Single lap joint is the simplest form of adhesive joint and these are used in many industrial applications such as aircraft wings, piping networks and civil engineering works. These joints are subjected to impact in real life situations and evaluating the failure response due to these impacts are very important for their safe operations. Different types of failures occur in lap joints. Both, delamination and inplane damage are the most common failure due to transverse impact on a lap joint. In this study a detailed overview of delamination and inplane damage, and there effect on lap joints due to the low velocity impacts is shown.

The main emphasis of this study is to provide a design criteria for both delamination and laminate damage, to ensure the lap joint remains safe due to impact (in a low velocity regime) for different overlap widths.

1.2 Problem description

Composite lap joints are essential for various applications such as aircraft wings, piping networks, sporting equipment and civil engineering works. The low velocity impact on such joints is a common occurrence in real life situations. It involves multiple damage modes that may occur within plies (fiber and matrix damage), at interfaces between plies (delamination) and at the bond interface (joint failure). The severity of damage, the damage modes, and the interaction between them depends on multiple factors such as joint geometry, material properties of the laminate and

the adhesive, impact velocity and point of impact relative to joint geometry. Therefore it is very important to find the response and behavior of joints under such impacts.

To model such complex impacts different analytical approaches are used in literature [1].But these techniques are limited to simpler impact cases where complicated factor such as transverse shear deformations does not play any significant role. Also the plate and impactor geometries are limited for simple cases. The stiffness values depend on the particular plate geometry and boundary conditions due to which these analytical approaches remains very limited in scope. In order to overcome these limitations, numerical models are used. Although there has been a lot of work regarding the impact (low and high velocity) on various types of composite materials, the study of the transverse impact on lap joints and the characterization of damage modes resulting from such an impact has only recently started to attract attention of researchers (for example see ref [2], [3]) and still has great scope for further research.

Delamination is a major mode of failure in laminated and woven fibre composites subject to a low velocity impact. There are other failure modes like matrix cracking and fibre failure, but delamination, which is basically debonding between adjacent laminas, significantly reduces the strength of the laminate [4], [5]. Polymer composites are highly susceptible to internal damage even under low velocity transverse loading [6]. This is due to their ability to absorb energy which in turn depends on the properties of the fibres, matrix and the interface between the two. It is known that woven fibre polymeric composites exhibit less internal damage than their unidirectional counterparts because the damage growth between the layers is constrained by the collapsing weave [7].

Despite recent development of sophisticated analysis techniques a design engineer in industry tasked to design composites products, most often has access to only Commercial finite element codes such as ABAQUS™, which do offer generalized built-in capability of progressive damage analysis for implementing any of the models cited above in literature. Implementing these however, often require the use of user subroutines and is generally way beyond the capability of an average user and would require extensive validation even for simplest of problems.

Most of the industry users thus tend to stick to the built-in damage models provided by these software. Using such models it is possible to predict in-plane and delamination damage modelling through meso-level homogenized models with discrete interface (cohesive) regions between the

plies. While the delamination prediction using the cohesive zone approach has been reasonably successful and is straight forward to implement in terms of both model generation and input parameters, the same is not true for lamina failure (in-plane failure within a ply) using the built in (Hashin) progressive damage model. The primary difficulty is that it requires input of softening parameters in terms of either damage mode dependent fracture toughness or corresponding final displacement at failure and unlike the measurement of fracture toughness for delamination growth in mode I, II or mixed mode, here the definition of these input parameters is not straight forward due to heterogeneous nature of failure that results in multiplicity of possible damage mechanisms for a given intended crack propagation modes.

In this study, a consistent set of methodology is developed for evaluation of damage parameters for built in damage progressive models in ABAQUS and validating the methodology by applying on a lap joint impact problem. The previous work [8] was done on delamination and debonding damage due to transverse impact for a lap joint. The impact at varying velocities is modelled using a hemispherical indenter and the responses have been gauged at four different velocities over the four different overlap width of the joint that is co-cured and has fully enclosed boundary conditions along all edges. In this work the damage model is improved to include laminate damage in addition to delamination and bond failure. The delamination and bond failure was modeled using cohesive zone approach. The model was implemented using plane stress elements. The result of this study were compared with the previous published experimental and numerical work.

1.3 Aims and Objectives

The main aim of the study is to demonstrate a consistent set of methodology for evaluation of damage parameters for the built in Hashin progressive damage models in ABAQUS and validating the methodology by applying on a lap joint impact problem. The previous work [8] was done on delamination and debonding damage due to transverse impact for a lap joint. In this work the damage model is improved to include laminate damage in addition to delamination and bond failure.

There are basically three damage types in the composites, delamination, matrix cracking and fibre damage. In this study, the damage modes in focus are both delamination and laminate damage which includes matrix cracking and fiber failure. Different progressive damage models developed for composite materials and available in the literature are applied to this problem. The results from

these approaches are compared in term of prediction accuracy, computational cost and requirement of input parameters (material data).

The substantial objectives to help achieve this aim are:

- A detailed review to develop a comprehensive understanding of the work which has already been done for the transverse impact on a lap joint. This included a thorough grasp on Finite Element modeling and Simulation Software (ABAQUS) for modeling our impact problem.
- Literature review to develop an up-to-date understanding of the various numerical, experimental and analytical techniques being used to define damage modes in composite lap joints.
- Verification of the model by running some of the cases which were already covered in the previous work.
- Detail study of Hashin Failure criteria (built in damage progressive model in ABAQUS) which includes the strong understanding of both damage initiation and damage evolution parameters.
- Implementation of Hashin failure criteria on uni-directional composite material for the determination of material parameters. In this study, Hashin is implemented for IM7-8552.
- Validation of results with the available experimental results in the literature.
- Determination of material parameters (fracture toughness) for a single lap joint of woven fiber glass reinforced polymeric composite.
- Validation of results with the available experimental results in literature.
- Implementation of determined parameters on lap joint impact problem for modeling both delamination and laminate damage for different velocities(in low velocity regime) and for different overlap widths
- Validation of model by comparing FE simulation results with the experimental published results
- Proposing an improved damage model for a single lap joint of woven fabric reinforced polymeric composites.

1.4 Methodology

Overall Methodology adopted is shown in the following chart:

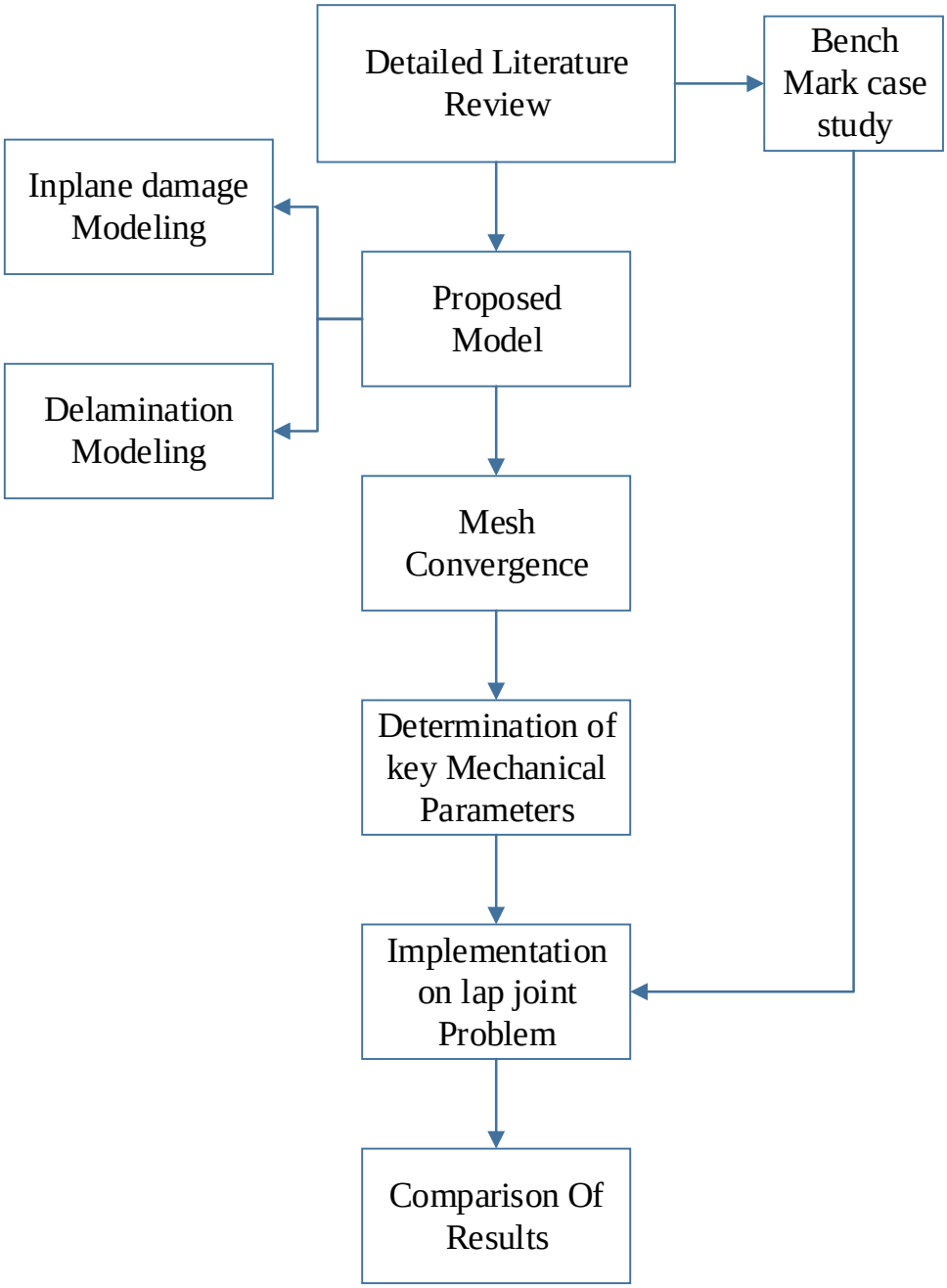

1.4.1 Summary of Methodology

First an extensive literature review was carried out to determine the appropriate approach. Different approaches were used for inplane progressive damage modeling in literature review. Two main approaches focused in our literature review are Hashin damage and VUMAT for woven fabric. Abaqus has built in material model for Hashin and VUMAT. Other approaches can be used but writing their own subroutine for the material model. For industrial environment, other approaches donot remain feasible to apply and VUMAT require extensive data. However, Hashin is widely acceptable but require material parameters which would be important to find first before implementation. Therefore, for implementing Hashin Damage model, benchmark case study is selected. In the proposed model, the delamination and bond failure is modeled using cohesive zone approach (as done in bench mark case study). Progressive damage modeling approach based on Hashin criteria is implemented for modeling laminate failure (new addition in this model). And the determination of key mechanical properties for Hashin damage propagation model using a new simulation approach (new addition). The model will be implemented using plane stress elements (continuum shell). Mesh convergence and reduction in overall computational cost will be important consideration for such models. The results of simulations will be validated against experimental data of previous study.

1.5 Contribution

- Although Hashin and cohesive zone modeling approach is available in literature but accuracy of models employing both of these aspects for impact problem were not demonstrated before in published literature.
- New proposed technique to determine fracture toughness in longitudinal tension mode as applicable for Hashin damage model in ABAQUS.
- Further validation of characteristic overlap width concept proposed in earlier studies.

Chapter 2

Literature Review

2.1 State of Art in Impact Damage Modeling in composite joints

In this section, some of the relevant work regarding the characterization, propagation and simulation of delamination and laminate damage has been reviewed.

E.J Barbero et al. [9]

In this paper, a novel methodology is presented for the determination of material properties for progressive damage analysis model implemented in Abaqus. This methodology is based on fitting Progressive damage analysis results to available published experimental data. This model is compared with the available E-glass epoxy laminates experimental results. Abaqus Progressive damage analysis model's sensitivity to h- and p- refinement is also covered in this study.

R.C Batra et al. [10]

A low velocity impact on a fiber reinforced polymeric laminated composite resulting in damage initiation and damage progression is studied in this manuscript. The results are compared with the experimental results. Damage is initiated when one of the Hashin failure criteria is satisfied and further damage evolution is modeled by an empirical relation proposed by another authors. In this study 3-D elements are chosen as compared to plane stress elements. A user defined subroutine is implemented for this model in Abaqus. User defined subroutine based on a micromechanics approach calculates average stress and check whether the Hashin Failure criteria meets or not. If the damage initiation criteria is initiated in material, it develops the further damage developed and provide it to FE. Delamination is modeled by cohesive zone approach. Various damage modes agrees with the experimental results available in literature.

Vaidya et al. [11]

The author conducted numerical dynamic simulation of composite lap joints under low velocity transverse impacts. A lap joint of 25 mm width was subjected to a low velocity impact test. Three different lap joint samples in terms of adhesives used were tested. In the paper, the author

compared the stresses generated during in plane loading and the transverse loading. The static elastic analysis of the lap joint in both the in-plane and transverse loading cases was done by using ANSYS while the dynamic response was simulated by using the 3D Finite element software LS-DYNA. The results showed that the magnitude of the peel stress in transverse impact loading was higher than that in in-plane loading, due to deflection. The failure initiation in the transversely impacted lap joint starts from the edge of the lower adherend and is always under mixed mode, but as the crack propagates the stress state primarily changes to mode II. This was in clear contrast to inplane loading where the stress state during fracture initiation is primarily shear (mode II) dominated. To check the dependence of failure energy and load on the increase in the overlap width of the joint, tests were carried out in a 75-mm-wide specimen as well and showed an increase.

Reeder et al. [12]

This paper introduces a new framework for visualizing 3D fracture criteria to cater for the mode III loading component. As a first step, the power law fracture criterion was used and it was justified that this criterion has trouble matching the mixed-mode toughness values in the critical high mode I region, and the situation would have only got worse by the introduction of mode III. A 3-D fracture criterion based on the B-K criterion was therefore proposed, which shows good results in the mode I and mode II loading region for a wide range of materials. In this criterion, unlike the power low criterion, the values of mixed-mode toughness were lower than any of the pure mode toughnesses. Although these values cannot be fully confirmed, until experimental techniques to gauge mixed-fracture toughness with known percentages of mode II and mode III are developed, this technique is a way forward and has already been introduced in ABAQUS. The basic assumption for this technique were that relationship between mode I and mode III toughness is similar to the relation between mode I and mode II toughnesses and that a linear interpolation can be established between mode II and mode III.

Hashin et al. [13]

Four different failure modes- compressive and tensile fiber and matrix modes are modelled which results in a piecewise smooth failure surface. The main theme of the study is to present a failure criteria for unidirectional fiber composites. The failure criteria is not smooth but piecewise smooth

which models a distinctive fiber failure modes. This criteria is more realist physically as compared to smooth failure criterions.

M.V. Donadon et al. [14]

In this paper, a 3 dimensional failure model is used for calculating the material response of composite laminated structures under the impact is presented. The study is based on continuum damage mechanics approach and permits the handling of energy dissipation linked with each failure mode irrespective of mesh refinement and orientation of fracture plane. LS-DYNA is used for implementation of material model with in 3d elements and its proven to be proficient of reproducing experimental results with good accuracy response in terms of absorbed energy, static and dynamic responses and degree of damage.

Panding Wang et al. [15]

Analytical and experimental study is carried out for determining mechanical behaviour of composite bolted joints under dynamic loading. A novel technique is introduced for dynamic stiffness and quasi static stiffness of composite bolted joint by presenting mass spring model having strain rate dependent elastic modulus. By using composite laminate theory in combination of Tsai- Hill theory the model is capable of calculating the strain rate dependent elastic modulus and strength of bolted joint. Stiffness and strength calculated from this model shows a good agreement with the experimental results. The results shows that under impact loading stiffness and strength is significantly higher than quasi static state.

Reyes et al. [16]

In this study the low velocity impact response on three layered laminates consisting of woven glass fiber and polypropylene has been investigated on 100 X 100 mm panels of two different fiber volume fractions – 50/50 and 20/80 configurations. The fiber content in the panels formed by stacking pre-pegged layers is approximately 60% by weight and the velocity range of the impactor is between 4 to 16 J. The impact response was modeled using an energy balance model and it can be used to evaluate the maximum impact force and the resultant deflection within this energy range. In order to understand the failure modes in a better way, some of the samples were prepared and observed through Scanning Electron Microscope. It was observed that at low energy impacts

i.e. at 4 and 8 J, there are not traces of matrix cracking except for the small indentation at the site of impact. When the energy increases to 12 J and subsequently 16 J, there is some fiber–matrix delamination. That however is extremely localized and the major failure mode is fiber breakage. It was also revealed that the woven thermoplastic composites have excellent energy absorption capabilities, and at high impact energies, they dissipate a significant portion of the kinetic energy into permanent failure mechanisms. The thermoplastic woven composites can therefore be used in energy absorbing structures. The paper also details the repair process of the composite after the impact. The flexural strength and modulus of the composites decrease as the impact energy increases, and it can be restored by using a simple compression molding process.

Cesim et al. [17]

The paper discusses the impact response on woven composites, having various weave angles between the interlacing yarns. It details a method of creating a woven composite with small weaving angle out of an orthogonal glass woven fabric, and without the help of a weaving machine. It is basically a shearing process in which the base material is modified a bit to ensure that the volume fraction of the fabric remains the same. The impactor had a velocity of 4.3 ms-1 for impact testing. A velocity sensor and a data acquisition system were also used, which allowed for the determination of impact characteristics like peak force, contact duration, maximum deflection and absorbed energy.

The impact response has been discussed on the basis of load-deflection curves and an energy profile, and the study has further been verified with the help of detailed images of the specimens which were impacted. The study concludes that the energy absorption capacity and impact perforation threshold energy of the woven fiber composites can be significantly improved by using small weaving angles between interlacing yarns, also sheds light on the reasons behind the argument. Woven composites with small weaving angles have lower bending stiffness. They ate hence more flexible and allow for larger contact duration, meaning a larger effective displacement and energy absorption capability. These composites also have a smaller fiber crimp, which means that there are lesser resin rich interstices, a higher fiber volume fraction and fiber pullout.

Duana et al. [18]

In this study, a high velocity transverse impact of circular cylinder has been simulated on a panel of plain-woven Kevlar fabric. LS-DYNA has been used to perform the three dimensional finite element analysis in which the impactor is assumed to be rigid. The study examines the velocity profile of the impactor at various stages of impact and also signifies the effect of different boundary conditions on the nature of perforation damage at different test velocities. Three different boundary conditions have been used and the velocity range is 200 – 400 ms^{-1}.

Results from the study show that upon impact, the velocity of the projectile reduces significantly, before the drop becomes gradual. The sudden velocity drop is due to the momentum transfer between the projectile and the local fabric that it directly impacts. Results from the modeling effort show that during initial stage of the impact, the projectile velocity drops very quickly. Then as the damage starts to move in the form of mechanical waves, the decrease in velocity becomes gradual. When the velocity was low, 200 ms^{-1}, boundary condition greatly influenced the fabric deformation, stress distribution, energy absorption and failure modes. However at higher velocities, the damage is so instantaneous that the boundary conditions donot really come into play.

S.T. Pinho et al. [19]

An extensive review of methods for the experimental description of fracture toughness with fiber braking failure modes of composite laminates. Tensile failure collection of work reveals a diverse approach in terms of size, data reduction and specimen configuration, in spite of the being an ASTM standards. Best techniques are acknowledged and scope of work is given for future prospects. Compressive failure work is less wide-ranging. Overview of composite failure modes including translaminar fiber tensile failure, translaminar fiber compressive failure and interlaminar damage modes is described comprehensively. This reviews finds that substantial amount of research steps are needed to be taken before a resistance curve is fully described.

E. Martin et al. [20]

In this study, thin 3D-woven SiCf/SiC samples were impacted with low velocity projectiles of varying diameters and energies at room temperature. The thickness of all test specimens was 1.4 mm and they were clamped on all four sides with the help of a steel fixture. It was revealed that

the extent of damage and the energy absorbed by the composites was dependent on the diameter of the hemispherical indenter and the energy with which it is released. The evaluation of the damage caused by the impactor was done using a combination of optical microscopy, a non-destructive technique in thermography and post-impact tensile tests. The analysis revealed that the formation of micro matrix crack and fibre breakage was localized under the impactor tip – no delamination is observed outside this zone due to the weave structure of the specimen. As the energy of the impact increased the diameter of the indented zone also increased. Indentation at the back is only observed after a low energy barrier is crossed, and ranges have also been defined when complete perforation takes place.

Rajesh et al. [21]

This study gives an insight into the experimental observations due to the result of a low-velocity impact on woven glass fibre epoxy matrix composite laminates. For the experimentation three different plates of thickness 2, 4 and 6 mm are used and the drop/fall weight test is used for low velocity impact. A number of tests with energies ranging from 7.85 – 35.23 J were carried out and the specimens were then viewed through optical microscopy. This study does not deal with lap joints and mainly focuses on the energy-displacement and energy-strain relationships caused by the impactor at varying energy levels.

Qin et al. [22]

The study investigates the strain energy release rate with the change in the delamination size was studied, both experimentally and numerically. A simple beam model was used to construct the scenario and graphite-epoxy composites were used as adherend for numerical simulation. The results were depicted in the form of graphs relating the variation of the stress energy release rate with the change in the length of the crack tip. These results were then verified experimentally, by using Hexcel T2G_190-12"-F263 graphite/epoxy prepreg and Cytec 300-2M adhesive film, manufactured both for unidirectional and cross ply tests. Delamination was introduced by inserting thin Teflon films during manufacture. All the joints were loaded at 220 MPa and the resultant damage behavior was captured using on-line video microscopy.

J. Neumayer et al. [23]

In this manuscript, the author investigated the effect of delamination on bonded joint in impact simulations. A cohesive element approach is used to simulate the delamination failure in bonded joints on a full scale structural level. The main aim of the study was to compute the through thickness of adherend analytically in which the cohesive elements represents the complete behavior of adherend. Delamination results was validated numerically by single lap joint case study. The results were in a good correlation with each other. The model not only computed delamination initiation, it measured the joint strength too. The convergence behaviour of the model was improved.

W. Wagnera et al. [24]

Failure analysis in an adhesive joint of laminated composites cannot be accurately performed without the evaluation of critical energy release rates or fracture toughnesses, which depend upon the mode mix ratios**.** The paper makes an attempt to relate these critical energy release rates as a function of the mode mix and both experimental and numerical approaches have been adopted in this regard. The material under investigation in this paper is unidirectional Hexcel IM7/8552 carbon/epoxy composite, joined by film adhesive Cytec FM 300 M. In the experimental part, three tests namely Double Cantilever Beam (DCB) test, Mixed Mode Bending (MMB) test, End Notch Flexure (ENF) test have been carried out for the determination of pure mode I, pure mode II and mixed mode I/II loading conditions, in which the mode mix ratios are controlled. Load deformation curves were produced to quantify the experimental investigations. To check which initiation fracture toughness, $G_{c,\text{ non-linear}}$ or $G_{c,\text{ maximum}}$, can be used for failure analysis, numerical simulation is carried out using shell elements for representation of the composite laminates and cohesive zone elements, using traction-separation law, for the interface. The simulation results revealed no interlink with the experiment values of critical energy release rates. Through trial and error method though, the critical energy release at specific mode mixed were fitted in the load deformation curves, and these values were then compared to the ones available in literature. The best fit was observed for the B-K criterion.

Xiaohu Yao et al. [25]

Damage analysis of composite laminated structures subjected to low velocity impact is modeled. Two kinds of stacking sequence were used and drop weight tests were carried out. Experimental teste were conducted by using ultrasonic C-Scan and delamination area of each interface was

measured. Numerical modeling was done by using cohesive zone approach. Delamination model's efficiency was discussed and the damage model was validated by experimental results. The results of numerical model was found to be agree with the experimental results. Delamination shape was made for composite laminates and it was found that around the impact point, delamination areas was distributed symmetrically and the delamination shape depends on the ply angles near the interface.

Hyonny Kimb et al. [26]

This paper deals with effects of transverse impact of hailstones on single lap joint of composite materials. The material used for the fabrication of the single lap joint is a carbon/epoxy pre-preg and an epoxy film is used as an adhesive. This single lap joint is clamped, and then centrally impacted with 50.8 mm diameter ice spheres. The impacted specimens were inspected by ultrasonic C-Scan. The damage areas in the samples were observed through optical microscopy. Based on this visual analysis, ranges were defined at which there was no, little, and high damage at the lap joint. It was observed that there was no damage below 210 J; between 210 and 250 J, localized damage occurs in the overlap region. However above 250 J, delamination starts to take effect from the back side joint free edge. It was noted that the delamination occurred in laminas adjacent to the adhesive layer before propagating into other layers. The observations were then verified by running a simulation in ABAQUS. The ice impact was modeled by using LS-DYNA 3D software and it was then imported to ABAQUS. The plies and the adhesive layer were modeled with separate layers of three dimensional elements having elastic material properties. The results showed that the delamination occurred in plies which had the highest peel and shear stresses. The study dealt with 'high' velocity impact in lap joints of unidirectional composite. The contact situation analyzed is between two deformable bodies rather than a rigid and deformable body.

2.1.1 Concluding Remarks

In all the papers discussed above, for predicting both inplane and out of plane damage initiations several approaches were used in literature. Donadon et al. [14] developed a continuum damage models that predicts both in-plane and out of plane failure initiation using strength based criterion for each mode and then uses respective fracture toughness values to effect failure propagation. On the contrary Pinho [27] used a similar approach for the in-plane damage propagation, however he used cohesive zone elements for modelling delamination failure.

In general the wide variety of progressive damage modelling methodologies cited in literature can thus be broadly classed in one of these categories as follows:

1. The ply discount analysis (deterministic)
2. Models involving probabilistic estimates of strength
3. Models involving continuum damage models that utilize strength or strain based failure prediction for failure initiation and fracture energy (or energy release rate ERR) limited propagation models
4. Models using cohesive zone (interface elements) for prediction of delamination and in-plane failure.
5. A combination of type 2 and 4
6. A combination of type 3 and 4.

Within each of these categories the choice of failure theory used and the shape of the softening curve vary widely. In the review paper [19] Pinho and Laffan et al. discuss six different notched tests to determine the longitudinal failure mode fracture toughness (translaminar fracture toughness). It will be discussed in detail later that these values of initiation and propagation fracture toughness cannot be directly used as an input to the built Hashin-damage progression model in Abaqus™ as it uses a strength based initiation criteria and linear elastic response up till failure initiation. Thus although the nomenclature is similar, the experimental initiation values do not necessarily correspond with the strength based values used as an input in Abaqus™. Similarly the experimentally determined propagation values may not correspond with the propagation values used in Abaqus™. The presence of discrete cohesive zones in the model to simultaneously model delamination can even further complicate the data input parameters as the meanings of traditionally measured terms are further obscured as the experimental data normally pertains to a laminate rather than an individual lamina or interface zone. In literature it was not clear that how to measure the fracture toughness values associated with various damage models used in ABAQUS.

2.2 Details of Benchmark case study

Low velocity impact on single lap joint of woven fibre-reinforced polymeric composites has been discussed in detail in the PhD work of R.S.Choudhry [28], and it is that very work which has formed the basis of this thesis. In this work, the main focus was to ascertain the damage

mechanisms – both in the laminates and at the interfaces - within the lap joint when the transverse low velocity impact occurred at the center. Co-cured joints having matching adherends were used in the experimental phase, meaning that the main focus was on the physical characteristics of the bonded joint, rather than the choice of adhesive which was used [28].This was a significantly important choice considering the amount of effect that the choice of adhesives can make to the evolution of damage in a lap joint or a bonded surface. Although less commonly used in high end applications due to tendency of lateral deflection, a single lap joint was used as it is the simplest joint configuration which can be used as a building block for complex joints. The study had two comprehensive phases, experimental and numerical.

2.2.1 Model Geometry

The schematic representation of single lap joint is shown in Fig (2.1)

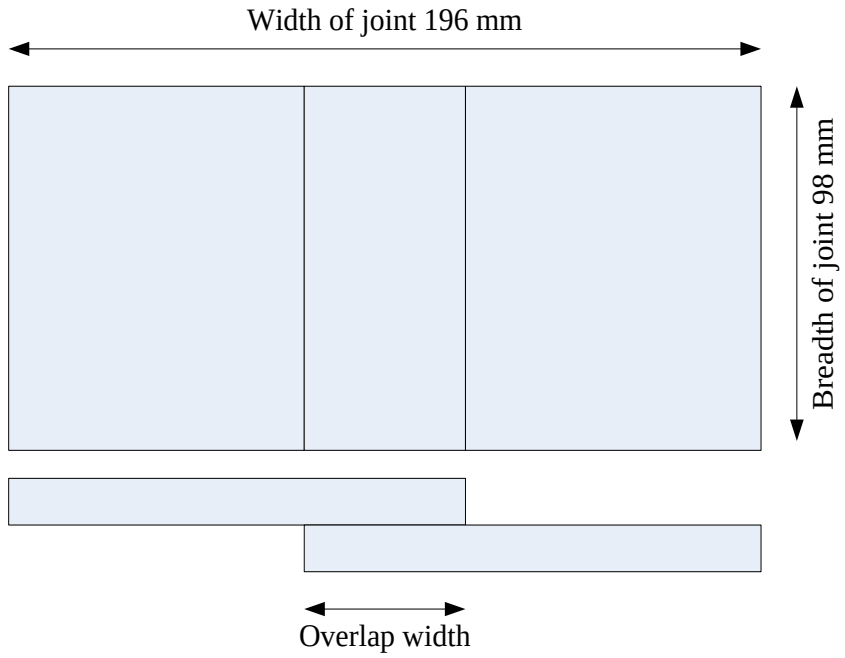

Fig 2. 1-Schematic Representation of Single Lap joint

2.2.2 Specimen Details

The specimen were made using Primco-SL246/40, a glass fibre/phenolic pre-preg, which is based on an 8 harness satin weave fabric. The resin content in each pre-preg is 40 percent, and four such pre-pregs formed one adherend. The layup was done with the help of a single sided tool, which

was vacuum-bagged later. A flipping stacking sequence $[0/0f]_2$ in the warp direction was followed, and the co-curing was done at a Quickstep ^{TM} plant at the University of Manchester, England [28].

2.2.3 Experimental Phase

Specimens having four different overlap widths – 21, 25, 36 and 46 mm - were prepared and were installed in an impact rig. To ensure a fully clamped boundary condition, baffles having the same material type and width same as the joints were placed around the boundaries of the specimen. A pressure measuring film was used to gauge the intensity of the impact on the lap joint. A total of 52 impact tests for centric loading were carried on different overlap widths, within a velocity range of 4.02 ms^{-1} to 9.6 ms^{-1} – energy range of 1.64 J to 8.01 J [28]. Some of the samples were tested for residual bond strength and to evaluate the properties required for the Finite Element (FE) model. These tests included mixed mode bending tests for determining the fracture energies at various mode mixes, three rail shear test for shear modulus and tensile tests for tensile modulus.

2.2.3.1 Visualization techniques

The main focus of the experimental work was to assess the various damage modes, and for that three different damage characterization techniques used, including Through Transmission Photography, Ultrasonic C-Scan and X-ray micro tomography [28].

(i) Transmission Photography

The first technique used for damage characterization was Through Transmission photography. This method is used for thin composite surface, made up of glass fibre only, due to their semi-transparent nature. The basic idea is to illuminate the surface significantly from the back side and then capture the image using a camera. In this case, the composite sample was illuminated by placing it over the glass top of a slide projector, whose light diffuser had been removed. The images were taken by a Nokia D200 camera. The snaps were taken before and after the impact, and the comparative results showed that the damaged zones grew darker. The method does illustrate the places where the damage occurs; differentiating between the indented and delaminated zones as well, but does not give complete understanding of the damage mechanism.

(ii) Ultrasonic C-Scan

The Ultrasonic C-Scan is a very popular and effective technique in the non-destructive analysis of metals, but in composites, it cannot be completely relied on due to the number of interfaces and irregular fibre patterns. These variables therefore make the scan less reliable and more

complicated. The method however does provide some insight to damage, and on some accounts, more than through transmission photography.

(iii) X-Ray Micro Tomography

The damage details gathered from both Ultrasonic C-scan and through transmission photography were not thorough enough to establish a good understanding of the damage characterization – they only indicate the overall damaged area at the overlap region and are two dimensional - therefore the study focussed mainly on a computed tomography technique, which constructs a volume from its cross sectional projections, called the X-Ray Micro Tomography (XMT). In this method, x-rays were used to create the cross sectional projections. Given that different constituents of a structure absorb x-rays to a different extent, the internal microstructure can be revealed by this technique - different absorption rates result in a contrast and this difference can be used to comprehend the microstructure. The significance of the contrast in the XMT analysis was one of the major reasons behind selecting glass fibre/phenolic composites rather than carbon epoxy composites. By using this technique, damage at any location within a structure can be observed by generating three dimensional surface models, along any desired cross section, at any depth and angle, and we can exactly locate the position, connectivity and extent of the delamination.

2.2.4 Finite Element and Simulation Phase

(i) Material Model

In that study [28], FE modelling of the bonded joints, a homogenised meso-scale model was used, which used shell elements with an elastic lamina material model in ABAQUS. The 3D continuum shell elements were preferred to the 3D solid elements due to the computational cost and aspect ratio.

In between any two adjacent laminas, a layer of cohesive zone elements has been inserted to model the interface. In this work, the author used seven different FE models, but the most compact material model for the lamina [28] was used in the final three cases and was based on the following equations;

$6_{11} = Q_{11}.\varepsilon_1 + Q_{12}.\varepsilon_2$ $\quad \tau_{12}=G_{12}\,\gamma_{12}$ for $\tau_{12} \leq \tau_{nl}$

$6_{22} = Q_{21}.\varepsilon_1 + Q_{22}.\varepsilon_2$ $\quad \tau_{12}=\tau_{nl}+G_{12}^{nl}.\,\Delta\,\gamma_{12}$ for $\tau_{12} > \tau_{nl}$

In the above equations 6_1 and ε_1 are normal stresses and strains in the x-direction, 6_2 and ε_2 are the stresses and strains in the y direction.

$$Q_{11} = \frac{E_1}{1 - v_{12}.v_{21}}$$

$$Q_{22} = \frac{E_2}{1 - v_{12}.v_{21}}$$

$$Q_{21} = Q_{12}$$

$$v_{21} = \frac{E_2}{E_1}.v_{12}$$

In the case of shear stresses, it was observed at higher velocities, that the in-plane shear stresses were high enough to cause a non-linear behaviour. The shear non-linearity of the composite thus had to be taken into account and it was done so by using the piece wise bilinear approximation. This bilinear curve is defined by three variables - G_{12}, τ_{nl} *and* G_{12}^{nl}

τ_{nl}= Stress level after which the non-linear shear behaviour starts. It is calculated through the three rail shear test.

G_{12}^{nl} = Shear modulus for non-linear region

τ_{12} and γ_{12} are the shear stress and strain in the x-y plane

This material model, excluding the interface and the joint, was built with continuum shell elements, and the material definitions were implemented by defining a user subroutine interface VUMAT [28][23] in ABAQUS/Explicit. The subroutine was programmed in [29] FORTRAN and the resultant model was in-plane, orthotropic and elastic with shear nonlinearity.

(ii) Cohesive Elements

The next step involved the embedding of layers of cohesive zone elements between each lamina. The bond interface was also modelled using these cohesive zones, each with a thickness of 3 μm. These cohesive elements are a special group of elements which have been incorporated in ABAQUS to simulate the response of the interfaces in bonded joints of composites and other materials, when the integrity of the bond is of interest. In this specific case, the cohesive elements have been added at the interfaces to determine the location, extent and the connectivity of various delamination fronts [28].

(iii) Traction-Separation Law

There are three approaches through which cohesive elements can be defined – continuum, constitutive and traction-separation description. For a very thin interface, such as the one used in this scenario, the traction-separation based approach is ideal.

In this method [29], the thickness of the interface is so small that the macroscopic stiffness based response can be ignored, meaning that there is a direct relationship between the traction τ_i at the interface and the relative displacement δ_i. To do so, the constitutive thickness of the element must be kept equal to one, irrespective of the actual geometric thickness. Stiffness used to relate traction with the displacement is thus defined as a penalty value and is defined by;

$K_I^0 = K_I \,.\, \tau_i^c$

Where

K_I^0 =Penalty stiffness Value

$K_I > IE5$ and $K_I < IE7$

$\tau_i^c = (i = 1, 2, 3)$ are inter laminar tensile and shear strengths, in the first and the second direction respectively.

(iv) Damage Initiation

There are two steps to damage characterization inside the cohesive zone interfaces – damage initiation and evolution. The damage initiation will start when a certain criteria or a failure index is surpassed. There are several damage initiation criterions available in ABAQUS, but based on the proximity of the experimental and numerical delamination results, the author chose Quadratic Nominal Stress Criteria (QUADS) [30].

Failure Index=FI=$\left\{\frac{\tau_1}{\tau_i^c}\right\}^2 + \left\{\frac{\tau_2}{\tau_2^c}\right\}^2 + \left\{\frac{\tau_3}{\tau_3^c}\right\}^2$

As soon as the failure index exceeds one, failure of the element initiates.

(v) Damage Progression

The next step is the evolution of the damage. Every damage initiation index should have a damage evolution law associated with it; otherwise the damage modelling process cannot be undertaken.

The aim of this evolution law is to describe the progressive reduction of material stiffness once the failure has initiated.

In the traction separation definition [30], a scalar damage parameter (D) will be used, which combines the effect of all active damage mechanisms. The value of this parameter ranges from 0 to1 and the tractions are reduced as its function.

$$\tau_1 = (1 - D).\bar{\tau_1} \qquad \text{for} \qquad \bar{\tau_1} \geq 0$$

$$\tau_2 = (1 - D).\bar{\tau_2}$$

$$\tau_3 = (1 - D).\bar{\tau_3}$$

In the above formulation, it has been assumed that pure compressive deformation or stress state does not initiate damage. In other words, the compressive stiffness of the cohesive zone elements will not be degraded.

(vi) Benzeggagh-Kenane (BK) criteria

The damage propagation in the cohesive zone elements depend on the mode mix definition, which can be specified in terms of either displacement or fracture energy. In this work, the mode mix which quantifies the relative proportions of normal and shear deformation has been specified in terms of fracture energy using the Benzeggagh-Kenane (BK) criteria [28] [29].Three modes of loading have been shown in the figure 2.2 below;

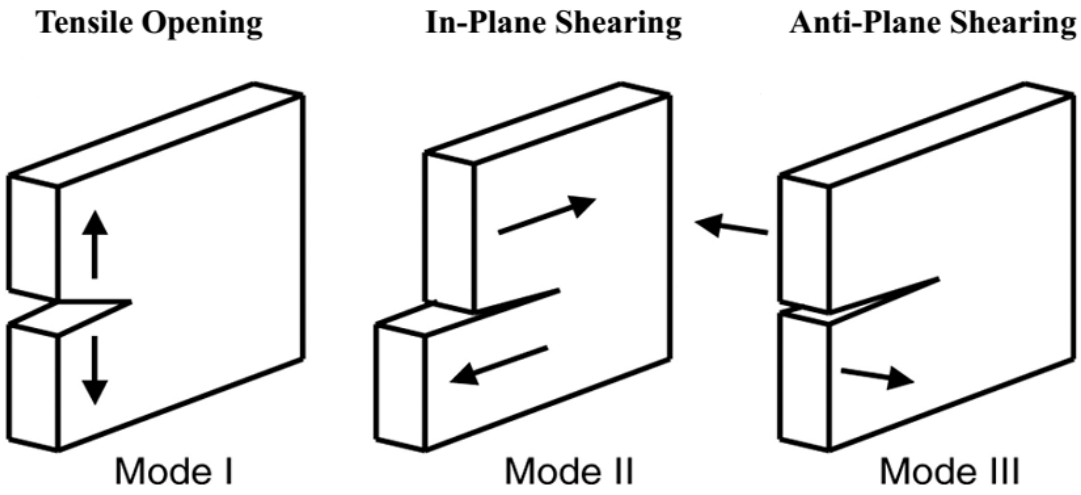

Fig 2. 2- Three modes of loading

This criterion, which is used when the critical mode III fracture energy is not known, and can be assumed equal to the critical mode II fracture energy. It is mathematically expressed as;

$$G^C = G_n^C + \left\{ (G_S^C - G_n^C) . \left(\frac{G_S}{G_T} \right)^n \right\}$$

Where;

$G^C =$ Mode mix fracture energy

G_n^C and G_S^C are critical fracture energies required to cause failure in the normal and the first shear direction.

$$G_S = G_S + G_T$$

n= material parameter

As far as the material models for the laminas and the interface are concerned, they will remain the same for the analysis carried out in the current master's thesis.

Finite Element Simulation

In order to carry out dynamic simulation for impact analysis, explicit time Integration was used on ABAQUS.

Model Geometry and Boundary Conditions

Model Geometry and boundary conditions used in that model is shown in Fig. 2.3 [8]. The boundary conditions are closely approximated to the boundary conditions as described in actual experimental setup conducted [8]. Finite Element simulation were carried out for all impact velocities on all overlap widths used in the experiments [8]. The impactor was modelled as an analytical rigid and the impactor was bound to move along a z-axis. Frictionless 'hard contact' was defined for modeling the dynamic interaction between the lap joint and the projectile.

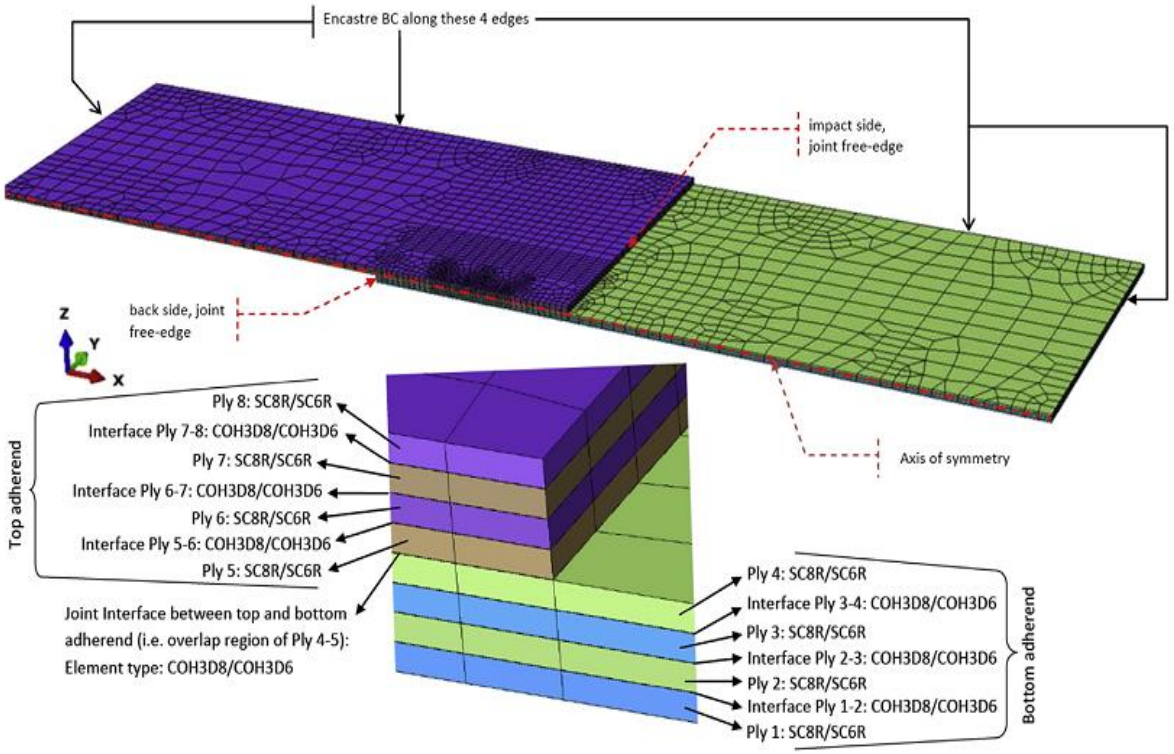

Fig 2.3 [8] **Converged Mesh and boundary conditions (Half Lap joint shown for visualization purpose)**

2.2.5 Failure Modes

The experimental results clearly distinguished three major damage modes, each having further classifications. They were the micro damage modes, delamination/disbond, and the macro damage modes [28].

(i) Micro Damage modes

This is the failure damage which occurs directly under the tip of the hemispherical indenter. This damage depends upon the elastic nature of the lap joint and only takes place once the energy of the hemisphere is large enough to overcome the elastic threshold. There are four ways in which macro damage can take place - micro indentation, fibre tow splitting or loosening, local fibre tow rupture and micro matrix cracks.

(ii) Delamination/Disbonding

Any interface failure which runs continuously for an area of 1x1 mm, causing a minimum separation 0.1 mm, has been categorized as delamination in this study [7]. Delamination which takes place at the bond interface is called disbonding. For the centric loading case, maximum delamination damage occurs at the bond interface, with varying amount of adherend delamination depending upon the overlap width and impact velocity also observed. Delamination at the bond interface has two modes of propagation, one under type 1 loading, is smaller width joints, and other under mixed mode with type 2 being more significant.

(iii) Macro Damage modes

This is more common in higher overlap width joints, when type 2 loading becomes more significant under mixed mode. Delamination is at a minimum in these cases, which results in more energy being absorbed. This absorbed energy results in more amplified damage to the lap joint. The damage can be categorized as macro indentation or bulge, matrix cracks and fibre push/pull out.

It is pertinent to mention that in order to cater for adherend failure modes other than delamination failure theories including the Maximum Stress Criterion, Tsai-Wu Criteria and LARC03 were also implemented in the material model. They have not been discussed in detail as the focus of current study is only on delamination and it’s mapping [28].

Chapter 3

Methodology

3.1 Proposed Model

The previous work [8] was done on delamination and debonding damage due to transverse impact on a lap joint. In this study, damage model is improved to include laminate damage (inplane damage) in addition to delamination and bond failure. Different progressive damage models were available in literature. One of the built in progressive damage model in Abaqus™ is named as Hashin damage model and it is a generalization of the models originally formulated for modelling delamination using cohesive zone elements in Abaqus [9]. The study follows continuum damage modeling approach. Progressive damage modeling based on Hashin criteria is implemented for modeling laminate failure. Thus determination of key mechanical properties (fracture energies) for those four damage modes defined in Hashin damage criterion was an important part of the study. ABAQUS provides a built in capability in specifying the damage in terms of Hashin theory using an energy approach.

3.1.1 Model Details (Hashin Damage Model)

Hashin damage model combines the elements of continuum damage models and linear elastic fracture mechanics and thus the damage initiation is predicted by using effective stresses within a strength based criterion and damage propagation is controlled using a damage variable that evolves (i.e. reduces the effective stresses) in relation to the fracture toughness of the material in a particular crack propagation mode.

This model requires a plane stress, linear, orthotropic elastic material definition before damage initiation. Equation 1a, and 1b describe the pre-failure and post failure response of each effectively homogenised lamina within the composite laminate.

$$\boldsymbol{\tau} = C \cdot \boldsymbol{\varepsilon} \tag{1a}$$

$$\boldsymbol{\tau} = C_d \cdot \boldsymbol{\varepsilon} \tag{1b}$$

Where $\boldsymbol{\tau}$ is the in-plane stress tensor (expressed in contracted notation used in Abaqus™), $\boldsymbol{\varepsilon}$ is corresponding the in-plane strain tensor, C is the in-plane stiffness matrix and C_d is the reduced or damage in-plane stiffness matrix.

In component form the pre-failure response can be expressed as

$$\begin{Bmatrix}\tau_1\\ \tau_2\\ \tau_4\end{Bmatrix} = \begin{bmatrix} E_1/\Delta & \nu_{21}E_1/\Delta & 0 \\ \nu_{12}E_2/\Delta & E_2/\Delta & 0 \\ 0 & 0 & G_{12}\end{bmatrix} \cdot \begin{Bmatrix}\varepsilon_1\\ \varepsilon_2\\ \gamma_4\end{Bmatrix} \quad (2a)$$

$$\begin{Bmatrix}\tau_5\\ \tau_6\end{Bmatrix} = \begin{bmatrix} G_{23} & 0 \\ 0 & G_{13}\end{bmatrix} \cdot \begin{Bmatrix}\gamma_5\\ \gamma_6\end{Bmatrix} \quad (2b)$$

In these equations for the material property definition 'E_1' is the elastic modulus of composite in the longitudinal direction (i.e. along the direction of long axis of fibre in a unidirectional lamina), E_2 is the elastic modulus of composite in transverse direction, i.e. transverse to the direction of fibre reinforcement within the plane of lamina), G_{12} is the in-plane shear modulus and G_{23} and G_{13} are the out of plane (transverse) shear modulus. Due to the plane stress assumption the through thickness stress i.e. in the '3' direction is assumed to be zero. The material parameter Δ is defined as,

$$\Delta = 1 - \nu_{12}\nu_{21} = 1 - \nu_{21}{}^2 . E_1/E_2 \quad (2c)$$

A basic limitation of this model is that the compressive and tensile modulus is assumed to be equal, which may not be strictly true for composites. This is however not generally considered a big limitation as the difference between tensile and compressive elastic modulus is usually small.

Note that the component ordering in the stress and strain tensor in the contracted notation used in Abaqus™ Explicit is different from the standard contracted notation. Thus in equations 2a and 2b, $\tau_1 = \tau_{11}, \tau_2 = \tau_{22}, \tau_4 = \tau_{12}, \tau_5 = \tau_{23}\ and\ \tau_6 = \tau_{13}$ are the components of the Cauchy stress tensor (true stress). The model uses a homogenized description of the lamina (i.e. fibre and matrix are represented by a single element with an effectively homogenized stress field). Hashin Damage initiation and damage evolution is discussed below.

(i) Hashin Damage Initiation

These criteria consider four different damage initiation mechanisms: longitudinal tension, longitudinal compression, combined transverse tension and shear, and combined transverse compression and shear.

1. **Longitudinal tension** – referred to in Abaqus™ manual [31] as fibre tension mode – is predicted by the equation;

$$F_f^t = \left(\frac{\hat{\tau}_1}{X_T}\right)^2 + \alpha\left(\frac{\hat{\tau}_4}{S_L}\right)^2 \quad (3a)$$

2. **Longitudinal compression** – referred to in Abaqus™ manual [31] as fibre compression mode – is predicted by the equation;

$$F_f^c = \left(\frac{\hat{\tau}_1}{X_c}\right)^2 \quad (3b)$$

3. **Combined transverse tension and shear** – referred to in Abaqus™ manual [31] as matrix tension mode – is predicted by the equation;

$$F_m^t = \left(\frac{\hat{\tau}_2}{Y_T}\right)^2 + \left(\frac{\hat{\tau}_4}{S_L}\right)^2 \quad (3c)$$

4. **Combined transverse compression and shear** – referred to in Abaqus™ manual [31] as matrix compression mode – is predicted by the equation;

$$F_m^c = \left(\frac{\hat{\tau}_2}{2S_T}\right)^2 + \left[\left(\frac{Y_c}{2S_T}\right)^2 - 1\right]\frac{\hat{\tau}_2}{Y_c} + \left(\frac{\hat{\tau}_4}{S_L}\right)^2 \quad (3d)$$

Terms 1-4 are used in order to emphasize that the FE Mesh is at homogenised lamina level, thus the failure modes do not represent constituent (micromechanical) failure. In these equations the strength terms have the usual meanings i.e. X_T and X_C are the tensile and compressive strengths respectively of the UD lamina in the longitudinal (fiber) direction. Y_T and Y_C are the tensile and compressive strengths respectively of the UD lamina in the transverse direction. S_L and S_T are the longitudinal and transverse shear strengths respectively of the UD lamina and α is a coefficient that determines the contribution of the shear stress to the longitudinal tension criterion (equation 1). F_f^t, F_f^c, F_m^t and F_m^c are indexes which shows whether the criterion for damage initiation in a damage mode has been satisfied or not. Damage initiation starts when any of the indexes exceeds the value of 1.0.

(ii) Damage Evolution

The further loading after the damage initiation criteria is satisfied will cause the degradation of material stiffness coefficients. The damage evolution uses the critical energy release rates Gci, which are material property with i = F_f^t, F_f^c, F_m^t and F_m^c corresponding to the four damage modes.In

general the constitutive relations are expressed in stress-strain relations. Each damage mode has an associated fracture toughness associated to it.The equivalent stress and equivalent displacement for all the damage modes [32] are as follows:

1. **For longitudinal tension ($\sigma_{11} \geq 0$)**

$$\delta_{ft}^{eq} = Lc.\sqrt{< \varepsilon_{11} >^2 + \alpha {\varepsilon_{12}}^2} \quad (4a)$$

$$6_{ft}^{eq} = (< 6_{11} >< \varepsilon_{11} > + \alpha\, 6_{12})/(\, \delta_{ft}^{eq}/Lc) \quad (4b)$$

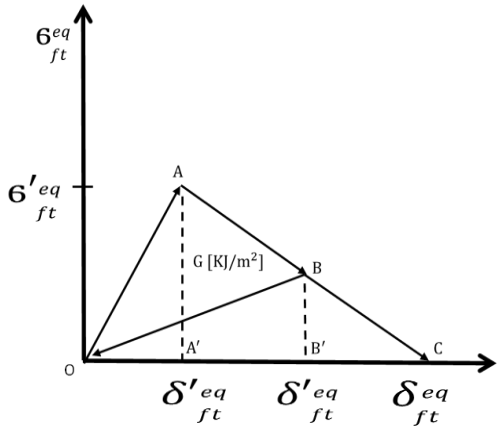

Fig 3. 1(a) Equivalent Stress versus Equivalent Displacement plot [33]

2. **For longitudinal compression ($\sigma_{11} < 0$)**

$$\delta_{fc}^{eq} = Lc < -\varepsilon_{11} > \quad (4c)$$

$$6_{ft}^{eq} == (< -6_{11} >< -\varepsilon_{11} >/(\frac{\delta_{fc}^{eq}}{Lc}) \quad (4d)$$

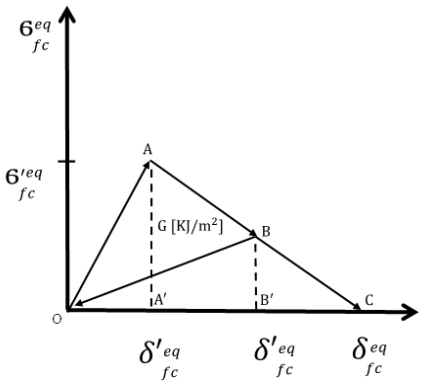

Fig 3.1 (b) Equivalent Stress versus Equivalent Displacement plot [33]

3. **Transverse Tension and Shear ($\sigma_{22} \geq 0$)**

$$\delta_{mt}^{eq} = Lc.\sqrt{< \varepsilon_{11} >^2 + {\varepsilon_{12}}^2} \quad (4e)$$

$$6_{mt}^{eq} = \frac{< 6_{22} >< \varepsilon_{22} >+ 6_{12}\varepsilon_{12}}{\frac{\delta_{mt}^{eq}}{Lc}} \quad (4f)$$

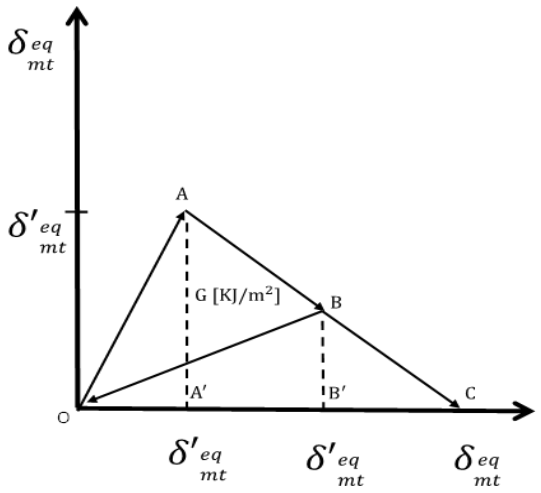

Fig 3.1 (c) Equivalent Stress versus Equivalent Displacement plot [33]

4. **Transverse Compression and shear ($\sigma_{22} < 0$)**

$$\delta_{mc}^{eq} = Lc.\sqrt{< -\varepsilon_{22} >^2 + {\varepsilon_{12}}^2} \quad (4g)$$

$$6_{ft}^{eq} == (< -6_{22} >< -\varepsilon_{22} > +6_{12} + \varepsilon_{12})/(\frac{\delta_{mc}^{eq}}{Lc}) \quad (4h)$$

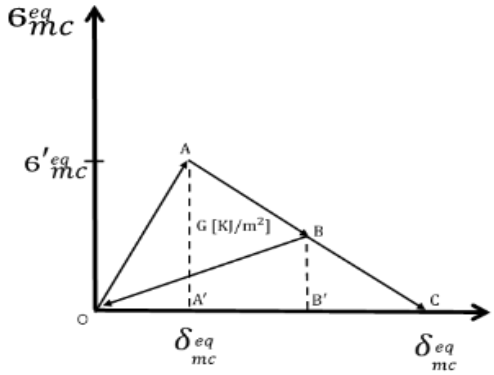

Fig 3.1 (d) Equivalent Stress versus Equivalent Displacement plot [33]

For each failure mode you must specify the energy dissipated due to failure, G^c which corresponds to the area of the triangle OAC in Fig 3.1. The values of δ_{eq}^{f} for the various modes depend on the respective G^c values. Unloading from a partially damaged state, such as point B in Fig 3.1, occurs along a linear path toward the origin in the plot of equivalent stress vs. equivalent displacement; this same path is followed back to point B upon reloading as shown in the Fig 3.1 [33].

In ABAQUS, in order to remove the mesh dependency problem, characteristic length is introduced. Where L_c is defined as the characteristic length of the element. Abaqus manual claims that by using equivalent displacement instead of strain in the formulation of damage model the mesh dependence has been eliminated. In plane stress elements, the characteristic length is calculated as the square root of the area of the reference surface of the smallest element. In this approach direct reduction of stiffness is not carried out to run PD simulations rather an energy approach analogous to that used for modelling delamination is used. The values of δ_{eq}^{0} for the various modes depend on the elastic stiffness and the strength parameters specified as part of the damage initiation definition [31].

3.2 Determination of key mechanical property (Fracture toughness)

3.2.1 Details of FE tensile test setup

Determination of material parameters is the most important part of this study. In order to model laminate failure, fracture toughness (G_{ci}) of the material is required. Fracture toughness can be find experimentally as well as predicted accurately by using Finite Element based approach. Hashin is generally used for unidirectional composites [13] but we extend this damage model to woven GFRP. In this respect, unidirectional composite IM7-8552 carbon epoxy [34] and woven GFRP [8] is taken in to account for the prediction of fracture toughness (G_{ci}). Model Geometry and boundary conditions are closely approximated to experimental setup [28]. Ply was meshed using a single layer through the thickness of reduced integration continuum shell elements i.e. 8 node, reduced integration, hexahedron (SC8R). Force displacement curves are computed for different elements sizes. We can see the results are mesh dependent. The energy dissipated is specified in per unit volume. In ABAQUS, in order to remove the mesh dependency problem, characteristic length is introduced. There are four different damage modes, as described above, required to model the progressive damage. Each mode has an associated fracture toughness value. In this study, longitudinal fiber tensile mode is calculated for both unidirectional composite IM7-8552 carbon epoxy [34] and woven GFRP [8] and for the rest of three modes, brittle fracture assumption is

taken. However, this assumption is true for unidirectional composite, but for woven fabric material, other modes should be taken in account too for correctly prediction of the progressive damage model. Then Equivalent stress- displacements curves are plotted for longitudinal fiber tensile mode. From area under the curve (G_{ci}) is calculated for all the cases. Tensile tests are performed on different number of elements until the convergence in strain energy per unit area is achieved. Strain energy per unit area for both cases (woven fabric and IM7-8552) are shown below. First the mesh sensitivity tests are carried out for IM7-8552 and the results are validated with literature experimental results and then the same mesh sensitivity tests are carried out for woven fabric [8] and the results are compared with the experimental results found in literature. The material properties of IM7-8552 is shown in Table 3.1 and the material properties used for woven GFRP is already shown in Table 2.4. The initial value input for woven fabric, for fracture energy (longitudinal fiber tensile mode) is calculated from the area under the load displacement curve, Fig 5.2 [28]. For the rest of the modes, brittle fracture assumption is taken. And for IM7-8552 case, the initial value input, for fracture energy (longitudinal fiber tensile mode) is taken a random value.

Table 3. 1 Material Properties of Woven Fabric [8]

Property	**Units**	**Value**
E_1	MPa	24200
E_2	MPa	23100
G_{12}	MPa	3850
G_{23}	MPa	1930
v_{12}	-	0.2
F_{1t}	MPa	336
F_{2t}	MPa	295.8
F_{1c}	MPa	-298

F_{2c}	MPa	-309
F_6	MPa	57.2
$G_C\ F_f^t$	KJm^{-2}	5.2 (initial guess)
$G_C F_f^c$	KJm^{-2}	0
$G_C F_m^t$	KJm^{-2}	0
$G_C F_m^c$	KJm^{-2}	0

Table 3. 2 Material Properties of IM7-8552 [34]

Property	**Units**	**Value**
E_1	MPa	162100
E_2	MPa	8960
G_{12}	MPa	4690
G_{23}	MPa	4690
v_{12}	-	0.36
F_{1t}	MPa	2560
F_{2t}	MPa	64.1
F_{1c}	MPa	-1690
F_{2c}	MPa	-286
F_6	MPa	53.5
$G_C\ F_f^t$	KJm^{-2}	5.2 (initial guess)
$G_C F_f^c$	KJm^{-2}	0

$G_C F_m^t$	KJm^{-2}	0
$G_C F_m^c$	KJm^{-2}	0

3.2.2 Finite Element tensile tests for IM7-8552

Fracture toughness KJ/m^2 is calculated at every iteration ranging from one element up to 625 elements until the convergence is achieved. Convergence criteria is set to be achieved, until the percentage difference between two mesh sensitivity tests is less than 5 percent. In this case, we started achieving convergence at around 320 elements and we got the converged value of around 31.8 KJ/m^2 when number of elements reached at 625 as shown in Fig. 3.2. Fig. 3.3 is showing the percentage difference plot. We can see the percentage difference is less than 5 percent between two successive iterations when the convergence is achieved.

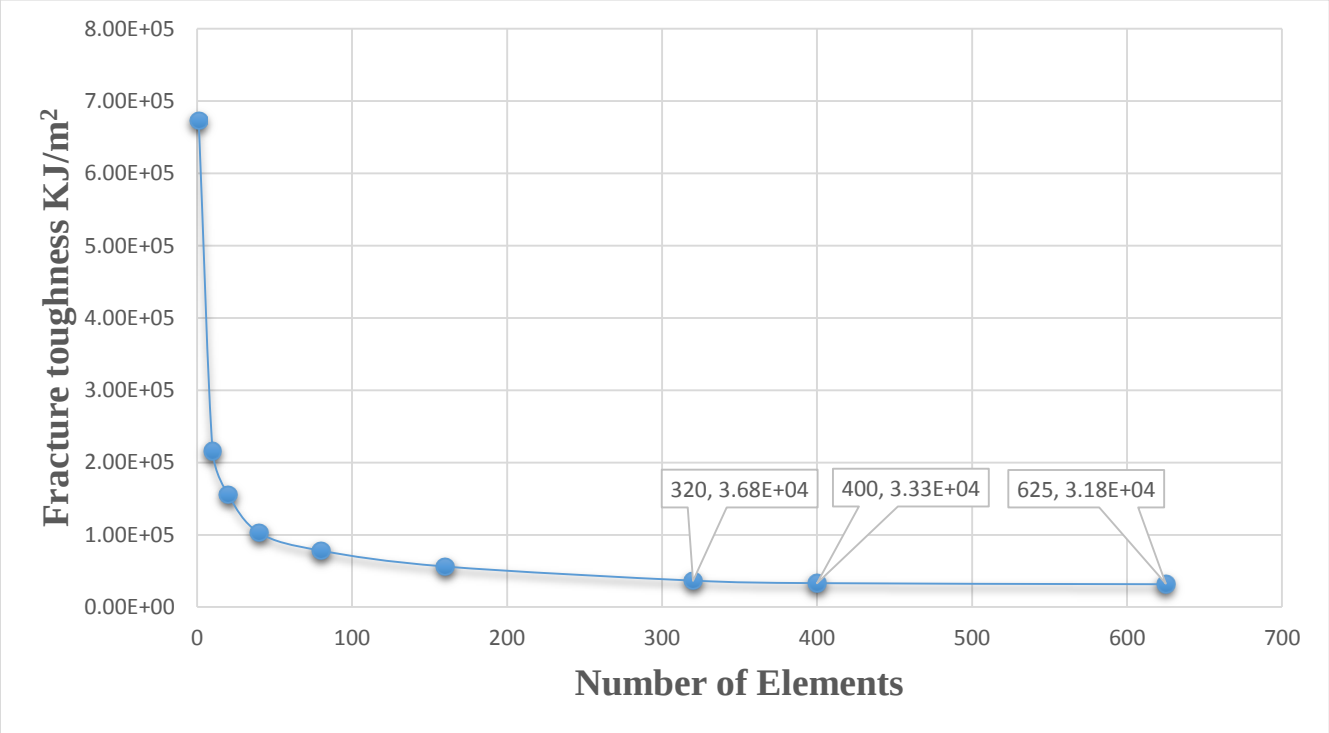

Fig 3. 2Convergence of Fracture toughness KJ/m^2 with respect to Number of elements

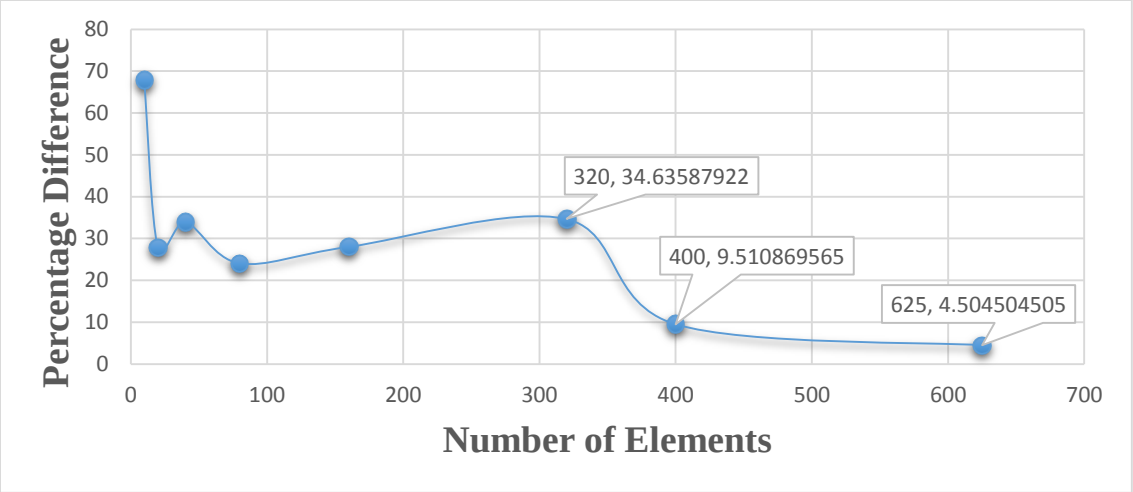

Fig 3. 3 Percentage difference plot as compared to Number of elements

3.2.3 Experimental Results and Comparison

In literature, published experimental translaminar fracture toughness is given [19] . Summary of data obtained from characterization of tensile and compressive translaminar failure modes is shown in Fig 3.4 [19].

Study	Specimen configuration	Material system	G_{ic}^{0} (kJ/m^2)	
			Initiation	Propagation
Tension				
Vaiyda and Sun [53]	CNT	AS4/3501-6	220.6	–
Pinho et al. [26]	CT	T300/913	91.6	133.0
Laffan et al. [27]	CT	T300/920	56.1	65.2
Catalanotti et al. [30]	CT	IM7/8552	97.8	133.3
Laffan et al. [29]	CT	IM7/8552	112.7	147.2
Teixeira et al. [59]	CT	T800s/M21	152.0	237.0
Compression				
Pinho et al. [20]	CC	T300/913	79.9	–
Catalanotti et al. [30]	CC	IM7/8552	47.5	–
Laffan et al. [57]	4PB	IM7/8552	25.9	–

Fig 3. 4[19] Summary of data obtained characterization of tensile and compressive translaminar failure modes

From Fig. 3.4, it can be seen that different authors have calculated the translaminar fracture toughnesses of different material system at initiation and propagation with respect to different specimen configuration. Catalanotti et al [35] and Laffan et al. [36]has calculated the fracture toughness value of 97.8 KJ/m^2 and 112 KJ/m^2 respectively at initiation by compact tension test. By compliance calibration method, Catalanotti et al [35] has calculated the fracture toughness value of 47.5 KJ/m^2. And by 4 point bend test [37], the estimated calculated value of fracture toughness at initiation is 25.9 KJ/m^2. By changing the specimen configuration a large variation in fracture toughness values are seen. Fracture toughness value calculated by Finite Element tensile tests in our study is 31.8 KJ/m^2 which lies in between compliance calibration [35] and 4 point bend test [37].

3.2.4 Finite Element tensile tests for Woven Fabric

Fracture toughness KJ/m^2 is calculated at every iteration ranging from one element up to 625 elements until the convergence is achieved. Convergence criteria is set to be achieved until the percentage difference between two mesh sensitivity tests is less than 5 percent. We can see in Fig 3.5 as we increase the number of elements we started achieving convergence at around 400 elements and we got the converged value of 4.75KJ/m^2. Figure 3.6 represents the percentage difference plot which shows the convergence is achieved until the percentage difference between two successive iteration is less than 5 percent.

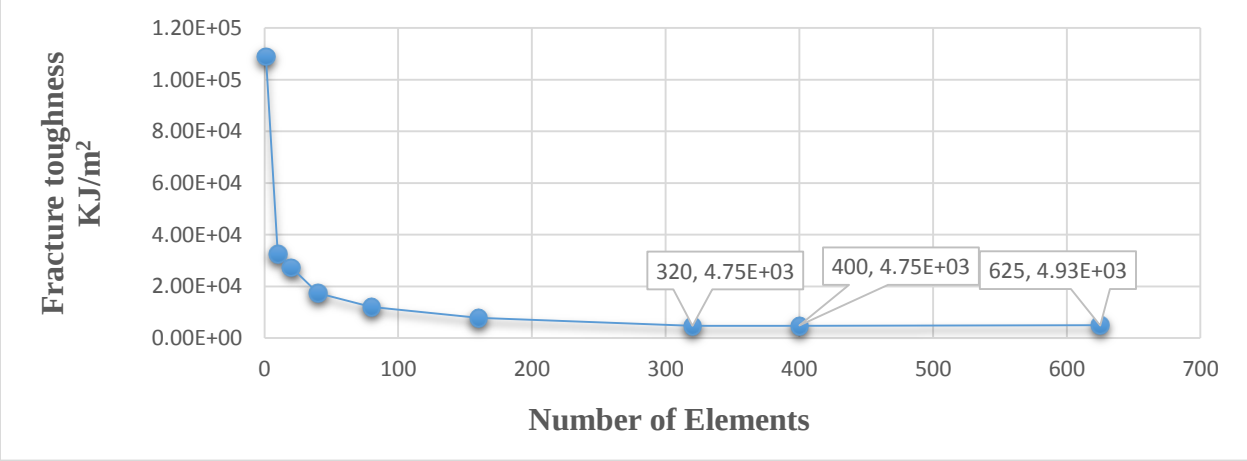

Fig 3. 5Convergence of Fracture toughness KJ/m^2 with respect to Number of elements

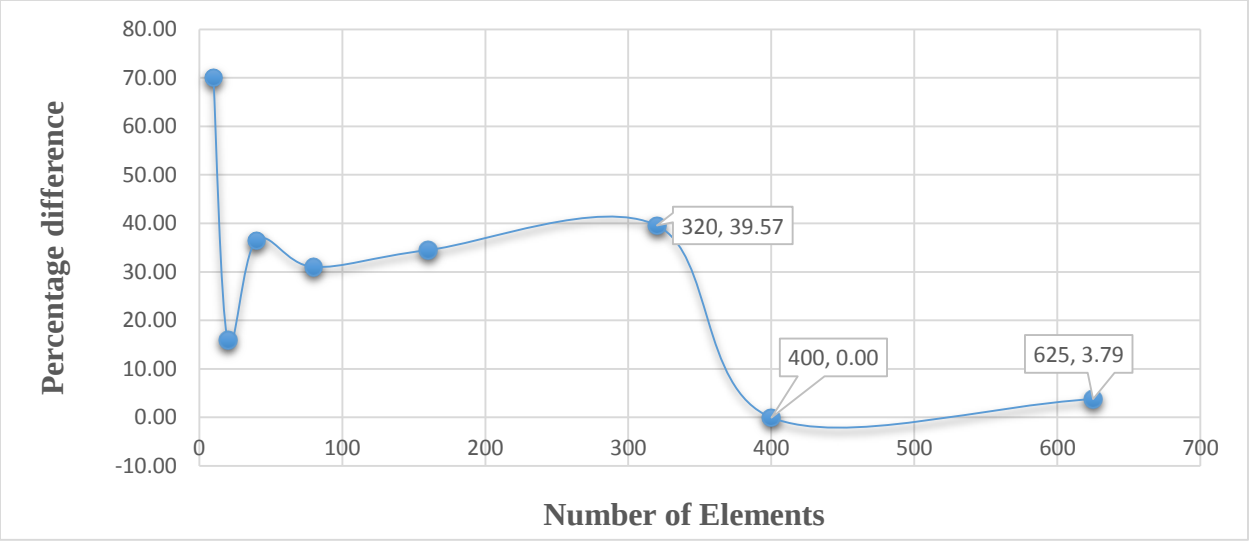

Fig 3. 6 Percentage difference plot as compared to Number of elements

3.2.5 Experimental Results and Validation

In literature [38], tensile stress strain curve for this material is given as shown in Fig 3.7. At the converged mesh when the number of elements reached 400, stress strain curve is computed from our FE tensile test and plotted as shown in Fig 3.8. Area under the curve was computed for both experimental and as well as Finite Element tensile test. Strain energy density in KJ/m^3 computed from the Fig 3.7 is 2700 kJ/m^3. And the Strain energy density in KJ/m^3 calculated from Finite Element Tensile test data is 2390 kJ/m^3. Which shows our Finite Element tensile test results are in a good agreement with the Experimental results.

After determination of fracture toughness value for a woven fabric case, we considered a single lap joint problem [8] as our case study for modelling delamination as well as laminate damage, thus validating the methodology by comparing with the previous experimental results.

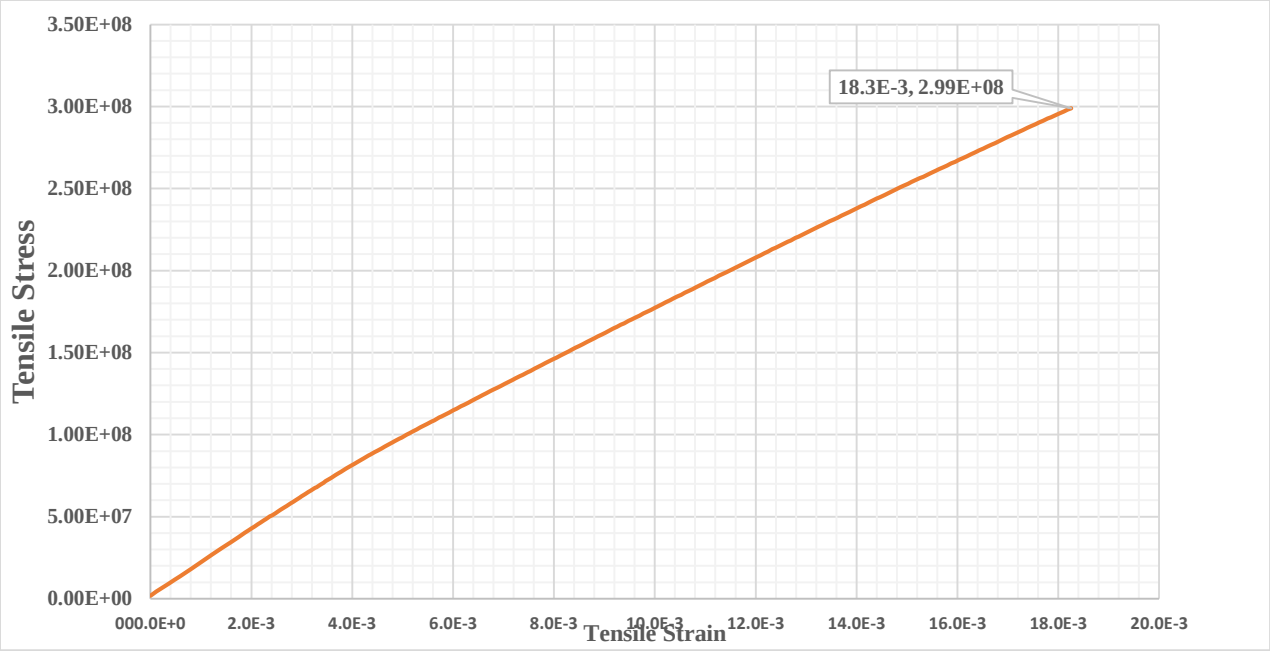

Fig 3. 7 Experimental Tensile Stress Strain curve [38]

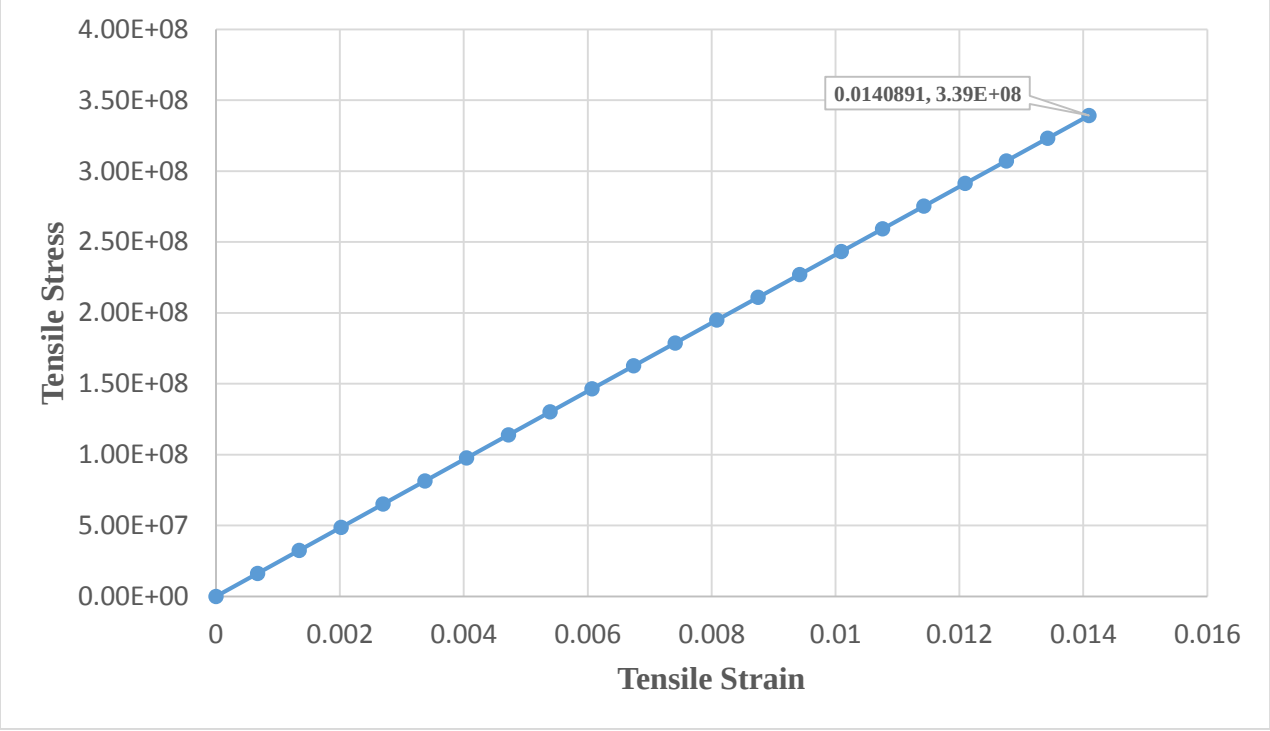

Fig 3. 8 FE Tensile Stress Strain curve

3.3 FE Modeling of Single Lap Joint

Explicit time Integration was used on FE software package ABAQUS/Explicit for impact analysis.

3.3.1 Model Geometry and Boundary Conditions

Model Geometry and the boundary conditions are closely approximated to the boundary conditions as described in actual experimental setup conducted [8]. FE simulation were carried out for all impact velocities on all overlap widths used in the experiments [8]. The impactor was modelled as an analytical rigid and the impactor was bound to move along a z-axis. Frictionless 'hard contact' was defined for modeling the dynamic interaction between the lap joint and the projectile.

3.3.2 Mesh Details

Each ply in the model was meshed using a two layers through the thickness of reduced integration continuum shell elements (i.e. 8 node, reduced integration hexahedron (SC8R) and 6 node, reduced integration wedge (SC6R). The bond interface was modeled using a separate layer of elements (i.e. 8 and 6 node, three dimensional cohesive zone elements (COH3D8 and COH3D6). This is shown in the zoomed view of mesh in Fig 3.10. Delamination between the plies and the disbonding at the bond interface was modeled using cohesive zone approach. The joint interface in the overlap region was also modeled as using similar cohesive elements. These cohesive elements were generated using offset mesh .And the plies were modeled as a 3 dimensional continuum shell elements. When the shear loading is large, the elements may distort and allow interpenetration of plies. This was prevented using refined mesh at the impacted zone and increasing the number of elements through the thickness. Another source of mesh dependency for modeling progressive damage in laminate by using Hashin was greatly reduced by using characteristic length.

3.3.3 Mesh Convergence

The mesh in XY plane in the overlap region and in particularly the (indentation zone) was denser than the other regions. In a 36 mm lap joint, for a converged mesh as shown in Fig. 3.9, total number of elements are over (0.1 million) 128366 including 89664 linear hexahedral elements of type SC8R, 37697 linear hexahedral elements of type COH3D8, 720 linear wedge elements of type SC6R and 285 linear wedge elements of type COH3D6.

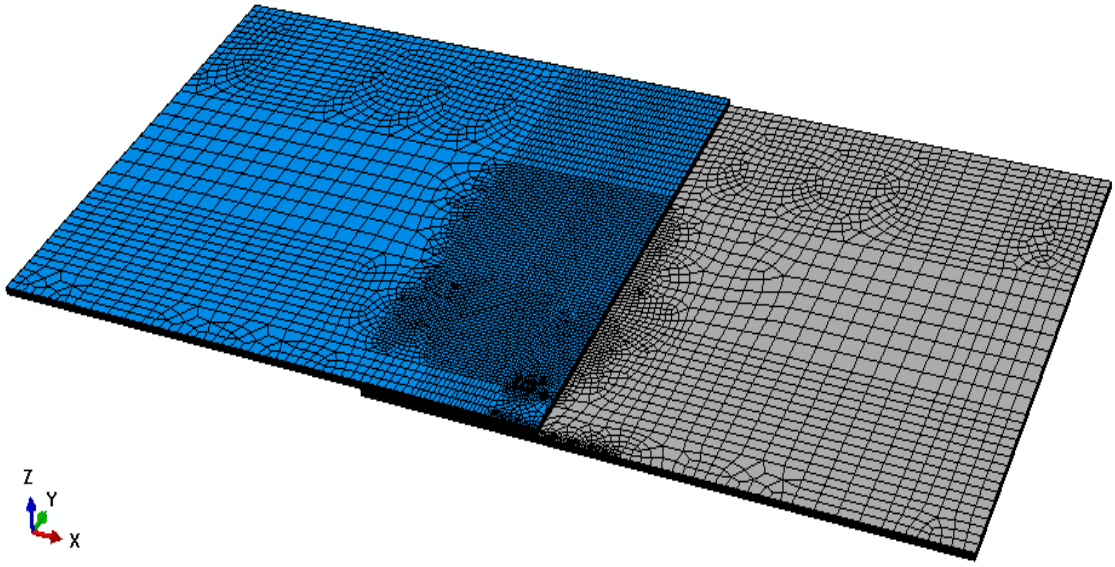

Fig 3. 9 Converged Mesh for a 36 mm single lap joint

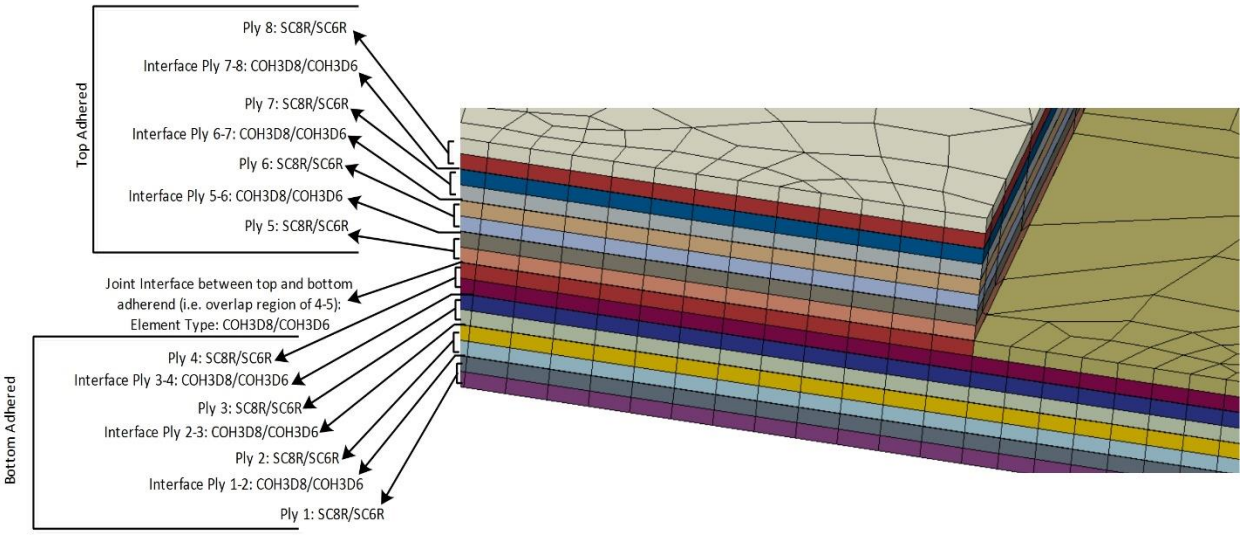

Fig 3. 10 Zoomed View of Mesh

Each ply has two elements through the thickness. In a zoomed view, top adherend and bottom adherend is fully labeled. Top ply is named ply 8 and the bottom most ply in bottom adherend is

Ply 1. Between two plies, there is an interface ply, it was modelled using cohesive zone layer. There is a joint interface between top adherend and bottom adherend (i.e. overlap region between ply 4 and 5).

3.3.5 Material Model and failure criteria

The material properties used for modeling cohesive zone elements are shown in Table 3.3.

Table 3. 3 Material properties for plies used in FE models for continuum shell elements [8]

Property	**Units**	**Value**
Density of composite	Kg/m^3	1566.3
E_1	MPa	24.2
E_2	MPa	23100
G_{12}	MPa	3850
G_{23}	MPa	1930
v_{12}	-	0.2
F_{1t}	MPa	336.6
F_{2t}	MPa	-298.4
F_{1c}	MPa	295.8
F_{2c}	MPa	-309.4
F_6	MPa	57.2
G_C F_f^t	KJ/m^2	4.75

Table 3. 4 Material Properties of Cohesive Elements [8]

Property	**Units**	**Value**
Density of resin	Kg/m^3	1085
Knn=K_I^0: Penality stiffness in mode-1	MPa	$4.44x10^7$
K_{ss}=K_{II}^0: Penality stiffness in mode-II	MPa	$2.22x10^7$
Ktt=K_{iii}^0: Penality stiffness in mode-III	MPa	$2.22x10^7$

$\boldsymbol{\tau_I^C}$: Interlaminar tensile strength	MPa	44.4
$\boldsymbol{\tau_{II}^C}$=$\boldsymbol{\tau_{III}^C}$: Interlaminar shear strenght		
G_{1C}	KJ/m^2	0.425
G_{IIC}	KJ/m^2	0.905
η		4.8
Softening		Exponential

3.3.4 Time Steps

In ABAQUS, you can either let a simulation run at default time steps, or can actually define intervals at which you require more detailed analysis. This is done by using the time points which basically allow you to generate irregular sampling. The purpose is to carry out a finer analysis at the critical points of your simulation, thus attaining finer details. In the present case, bigger time steps were defined at the start of the impact when the impactor starts to move towards the lap joint, and as the surface of the impactor and the joint start to interact, the number of the steps were increased gradually. This not only helped in attaining more reliable results at the business end of the impact, but also saved a bit of simulation time, something which was of essence. One more important factor, which can affect the results of our analysis, is that of vibration, which are experienced when the projectile starts to bounce off the lap joint due to inertia and boundary constraints. These vibrations can significantly increase the delamination damage in the overlap width and in case of smaller widths, can result in a complete disbond due to peel separation. An intentional effort was therefore made to rule out this factor from our analysis, and to do so, the maximum time for the impact step was reduced from 3.5 ms to 1.92 ms. this also helped in significantly reducing the running time of the simulation.

Chapter 4
Results and Validations

4.1 Cases Investigated

After the Finite element modeling of lap joint, simulations run were carried out at 4 different velocities -4.0, 5.5, 6.7 and 7.9 for all the four overlap widths as described earlier in chapter 2. A total of 16 simulations were performed to collect the data for further parametric analysis, the details of which will follow. The results of these simulation were validated by the experimental results found in literature [8].

The delamination and in plane(laminate) damage patterns obtained from these simulations in the form of images, which were then cropped and processed to determine the percentage damage at each interface. This analysis was done using the **ImageJ** [39] freeware. These damage areas were measured after 1.81ms of the first impact and the value of the scalar damage variable 'D' has been limited between 0.9 to 1 to focus only on the completely failed elements. The main principle behind using ImageJ was to determine the percentage of delamination and laminate damage that was done by evaluating the colour differential. As can be seen from Fig 4.1 given below, the delaminated surface at an interface is represented by the red and the rest of the interface retains a blue background. After the image is processed, the entire delaminated area turns red while the background maintains its colour.

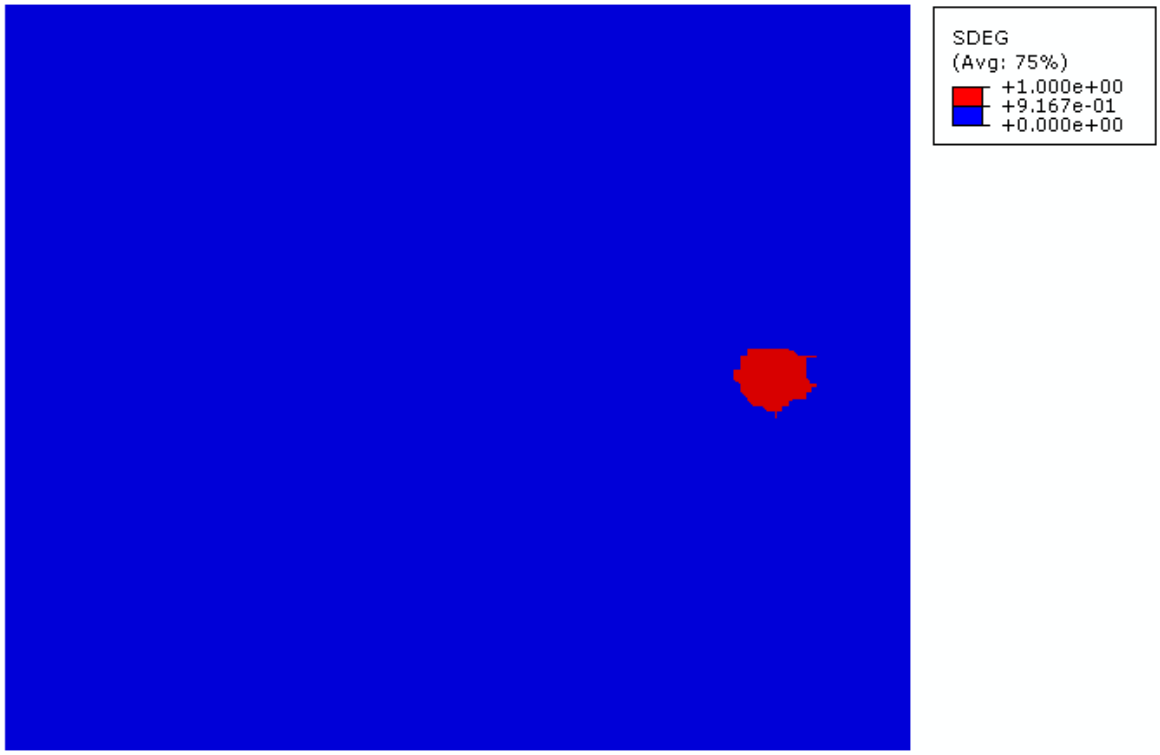

Fig 4. 1 Delaminated interface

1. To start the process of determining the percentage delaminated area within the interface, the first step is to launch Image J.
2. Copy the macro [40] in Clipboard.txt.
3. From the Image J toolbar, click File --- New ----- System Clipboard. The text will automatically be pasted and macro toolbar will also open.
4. Now from the Image J toolbar select the image, which has to be processed.
5. After the image is opened, using the macro toolbar, go to Macros and click on Run Macro.
6. You will get the percentage of delaminated surface in a separate window.

4.2 Delamination Results

Impact simulations ware carried out for four impact velocities on each overlap region of lap joint model. There will be four cases with respect to overlap regions (21, 25, 36 and 46) mm. In each case results of four impact velocities will be shown and discussed which will be later validated by experimental results [8].

4.2.1 Case Number 1- 21 mm overlap width

In this case, results of 4 impact velocities (4, 5.5, 6.7 and 7.9) ms^{-1} will be shown and discussed. Percentage delamination damage areas were calculated, by plotting the damage variable (SDEG) for cohesive zone elements. These damage areas were measured after 1.81ms of the first impact.

(i) Impact Velocity 4 ms^{-1}

Damage area plots were calculated for each interface, which are shown below in Fig 4.2. The maximum damage was seen to be observed at first and second layer from the top. Due to very low velocity, damage didn't reached to the bottom layers. As we will be moved towards the higher velocities, the damage started to grow, it will be discussed later on in next coming up cases. Finite element based plots of all interfaces of 21mm lap joint at $4ms^{-1}$ at1.81 ms after the first impact is shown in Fig 4.2.

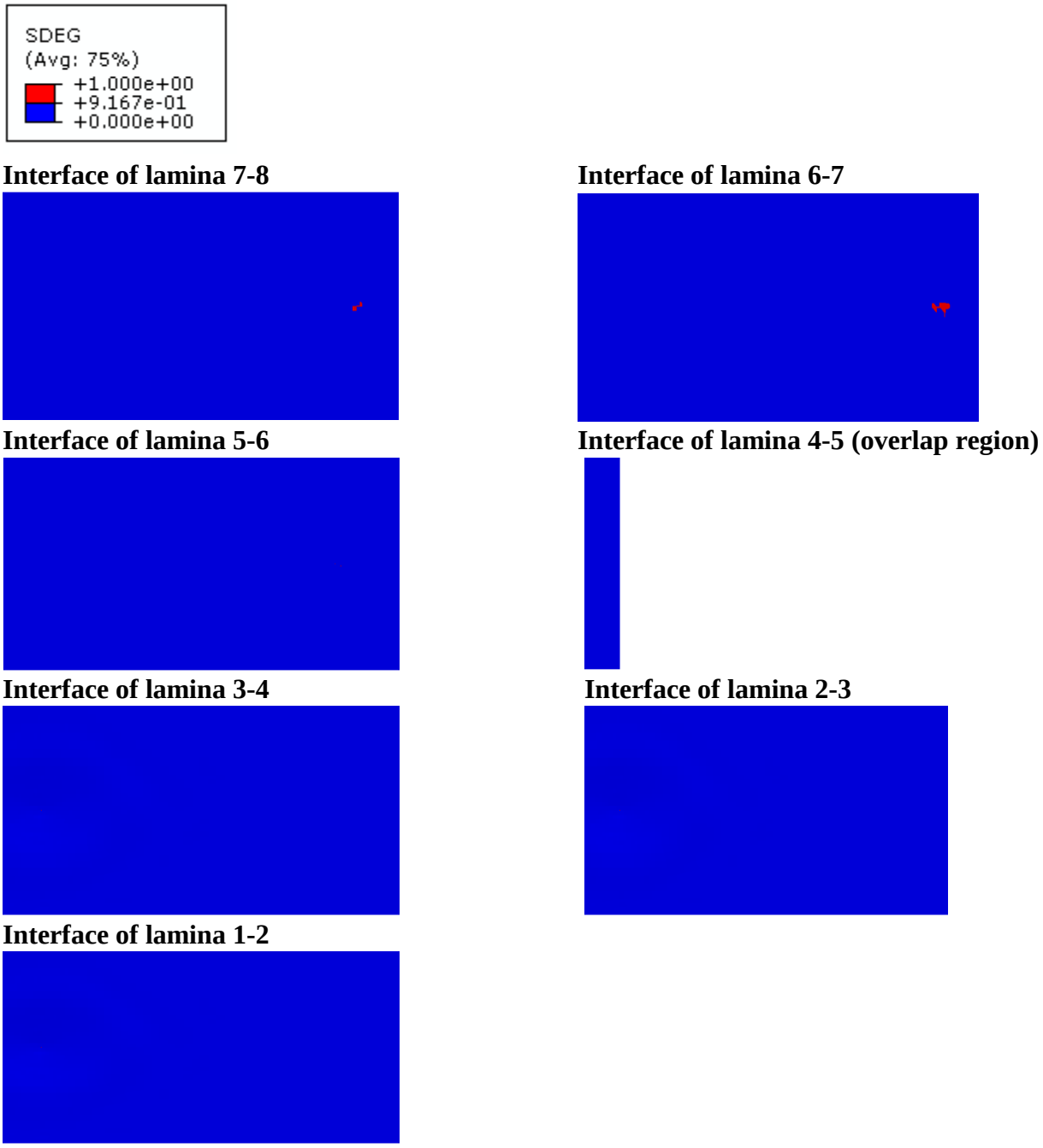

Fig 4. 2 FE based damage area plots for all interfaces of lap joints of 21 mm at 4ms^{-1}

(ii) Impact Velocity 5.5 ms^{-1}

Similarly, damage area plots were calculated for each interface, which are shown below in Fig 4.3. The maximum damage was seen to be observed at the two top interfaces. But in this case, damage reached to lower interfaces too as shown in Fig 4.3. These damage areas were measured after 1.81ms of the first impact.

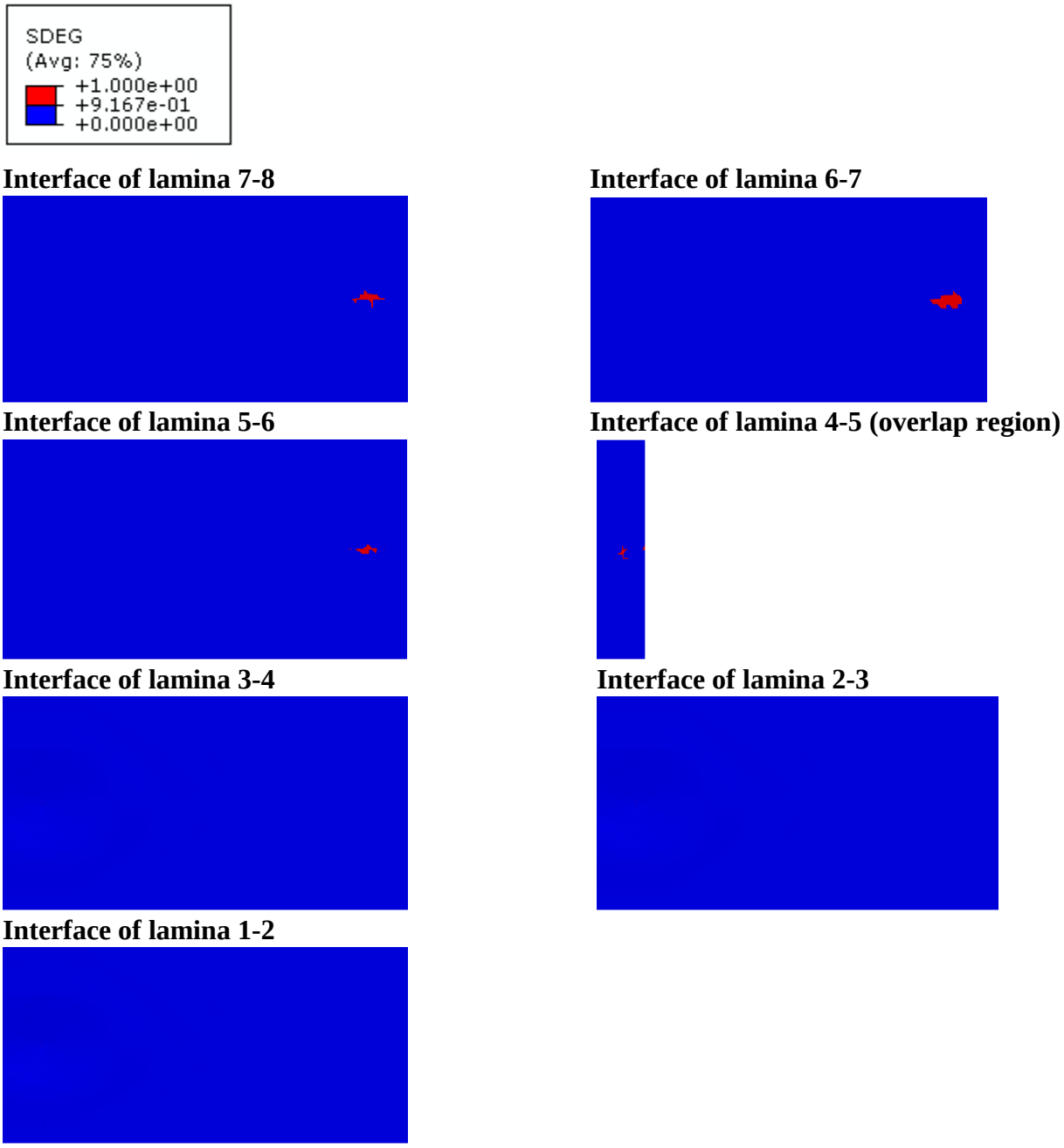

Fig 4. 3 FE based damage area plots for all interfaces of lap joints of 21 mm at 5.5 ms^{-1}

(iii) Impact Velocity 6.7 ms^{-1}

Damage area plots were calculated for each interface, which are shown below in Fig 4.4. In this case, we see unusual behavior, the maximum damage was seen to be observed at the two top interfaces. Damage areas are increased as compared to last two cases. These damage areas were measured after 1.81ms of the first impact.

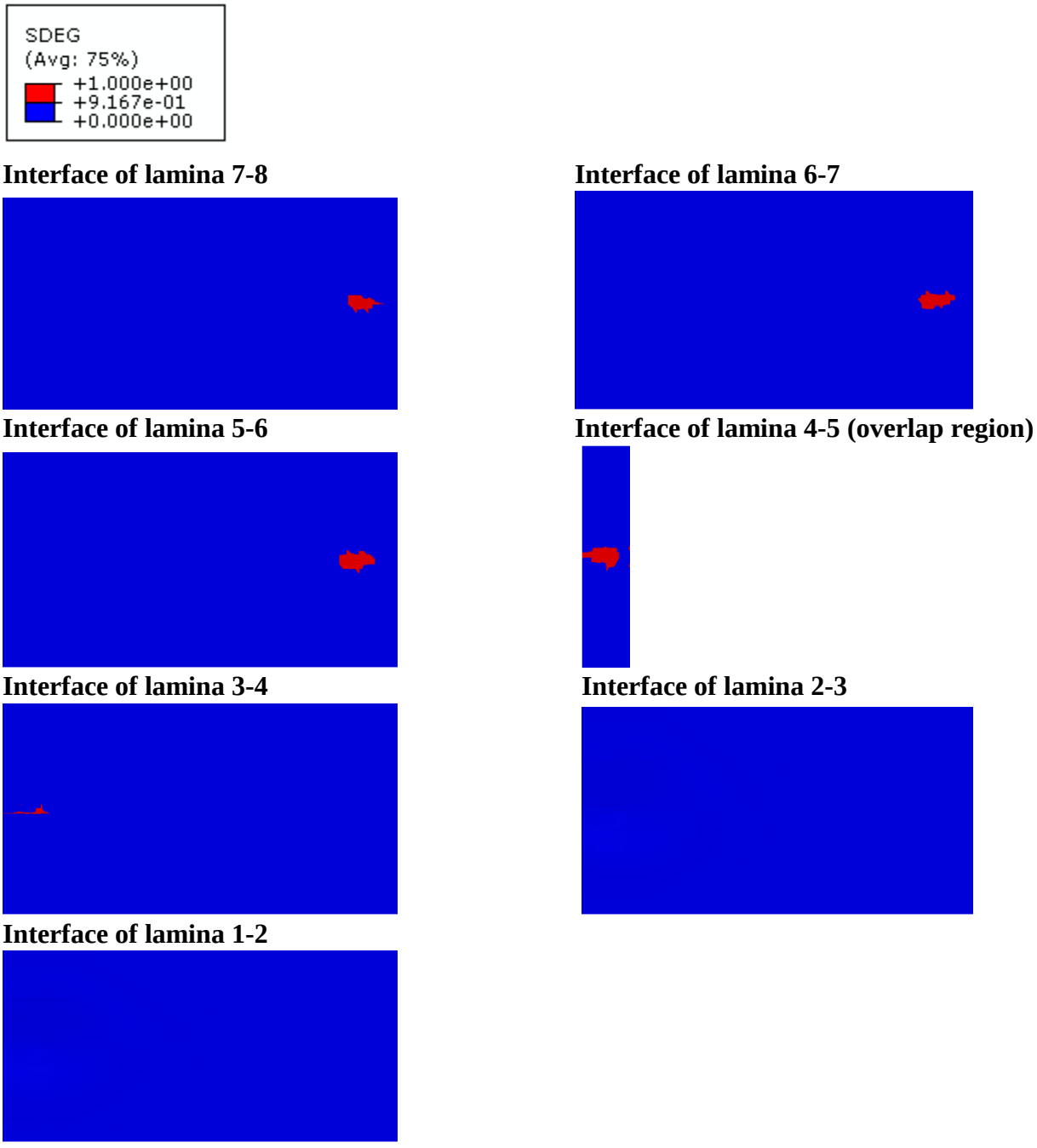

Fig 4. 4 FE based damage area plots for all interfaces of lap joints of 21 mm at 6.7 ms^{-1}

(iv) Impact Velocity 7.9 ms^{-1}

Damage area plots were calculated for each interface, which are shown below in Fig 4.5. In this case, the maximum damage was seen to be observed at the interface of lamina 6-7. Damage areas are increased as compared to last two cases. These damage areas were measured after 1.81ms of the first impact.

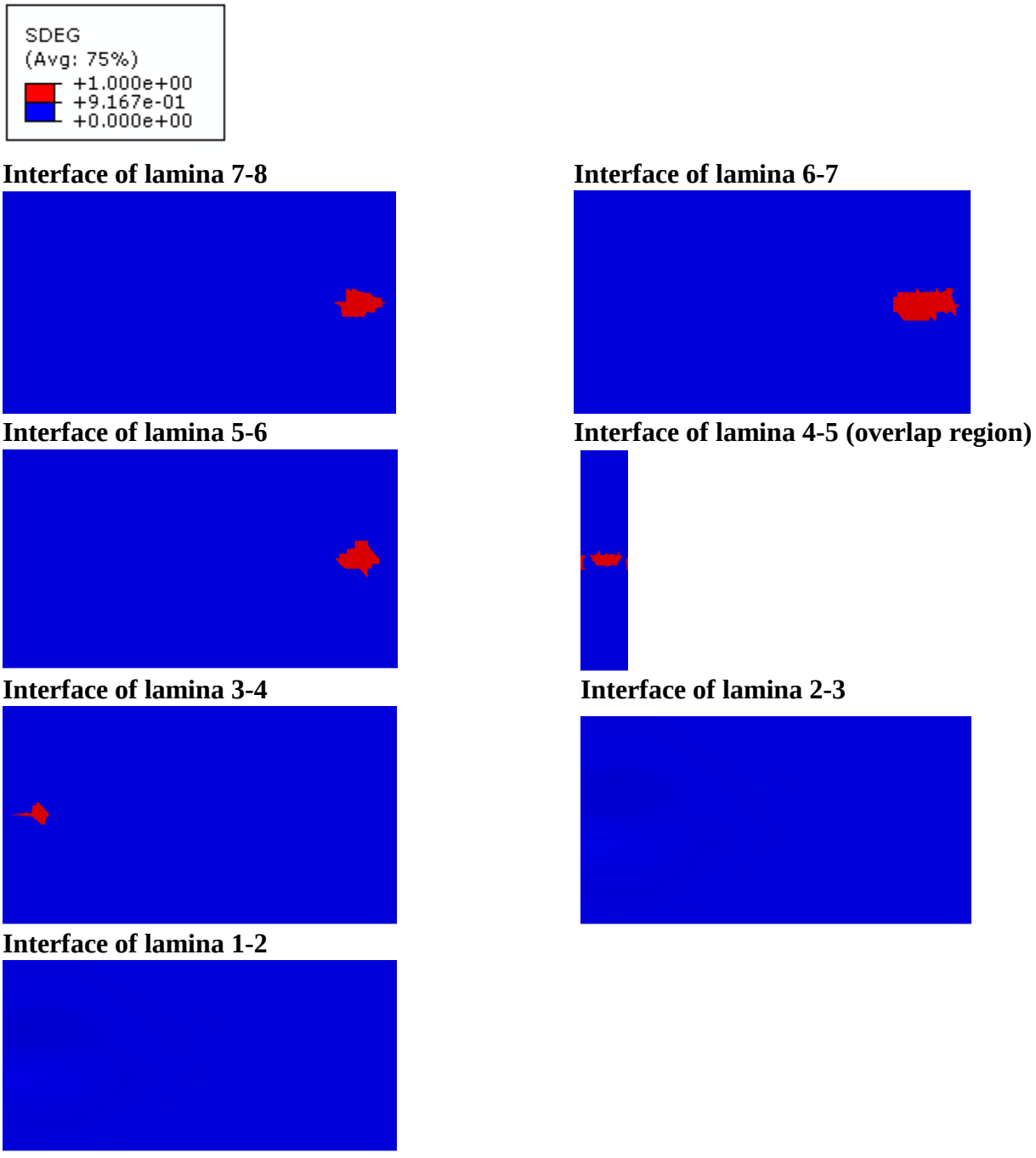

Fig 4. 5 FE based damage area plots for all interfaces of lap joints of 21 mm at 7.9 ms^{-1}

(v) Comparison of Case 1- 21 mm overlap joint results with respect to impact velocities

It has been observed that, the maximum delamination area arises at the interface of lamina 6-7 at all impact velocities in 21 mm overlap joint. And the damage areas started to grow, as the impact velocities increases from 4 ms^{-1} to 7.9 ms^{-1}. The comparison of delamination areas expressed as percentage are of overlap is shown in Fig 4.6. These percentage delamination areas are calculated

at the maximum delaminate interface, which in our case is interface of lamina 6-7. Fig 4.6 shows that, the percentage delamination area increases as impact velocities increases and the maximum percentage delamination area is 8.93 % percent at 7.9 ms^{-1}.

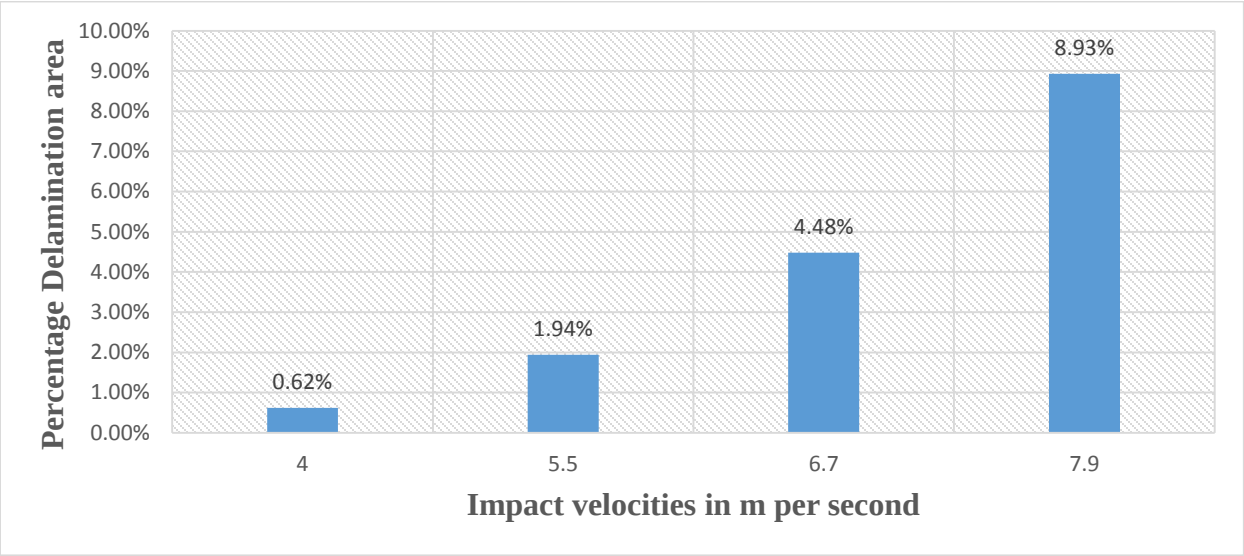

Fig 4. 6 Comparison of Percentage delamination area expressed as percentage of total area of overlap

4.2.2 Case Number 2- 25 mm overlap width

Damage area plots were calculated for each interface, which are shown below in Fig 4.7. The maximum damage was seen to be observed at first and second layer from the top as observed in last case for a 21 mm overlap width. Finite element based plots of all interfaces of 25mm lap joint at 4ms^{-1} at 1.81ms after the first impact is shown in Fig 4.7.

(i) Impact Velocity 4 ms^{-1}

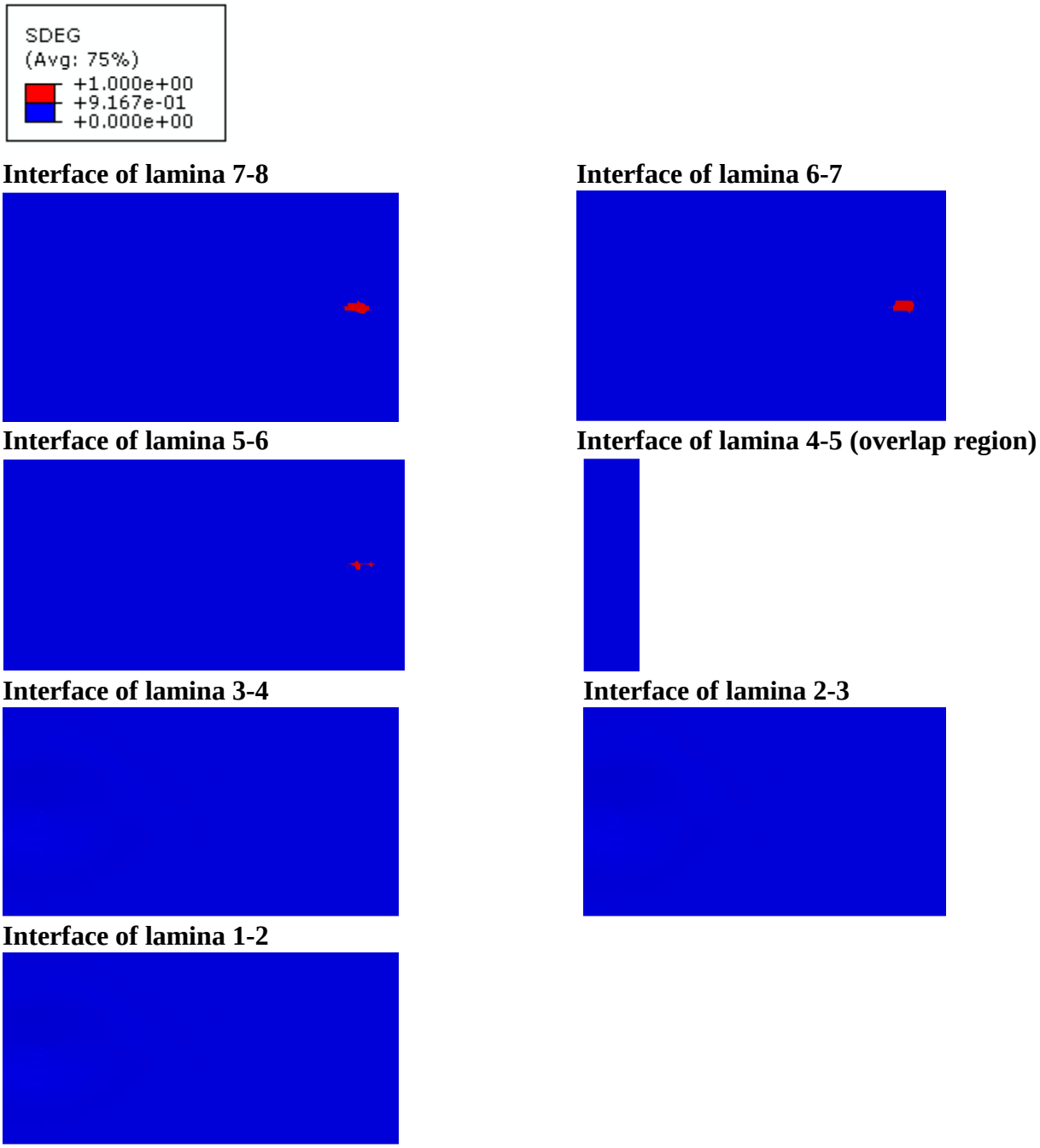

Fig 4. 7 FE based damage area plots for all interfaces of lap joints of 25 mm at 4ms^{-1}

(ii) Impact Velocity 5.5 ms^{-1}

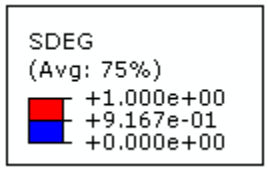

Interface of lamina 7-8

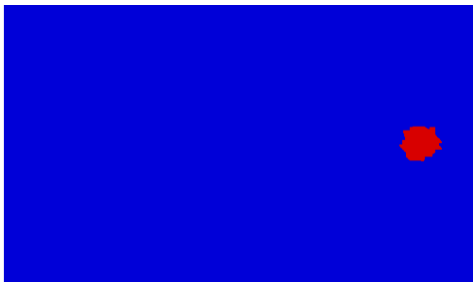

Interface of lamina 6-7

Interface of lamina 5-6

Interface of lamina 4-5 (overlap region)

Interface of lamina 3-4

Interface of lamina 2-3

Interface of lamina 1-2

Fig 4. 8 FE based damage area plots for all interfaces of lap joints of 25 mm at 5.5ms^{-1}

(iii) Impact Velocity 6.7 ms^{-1}

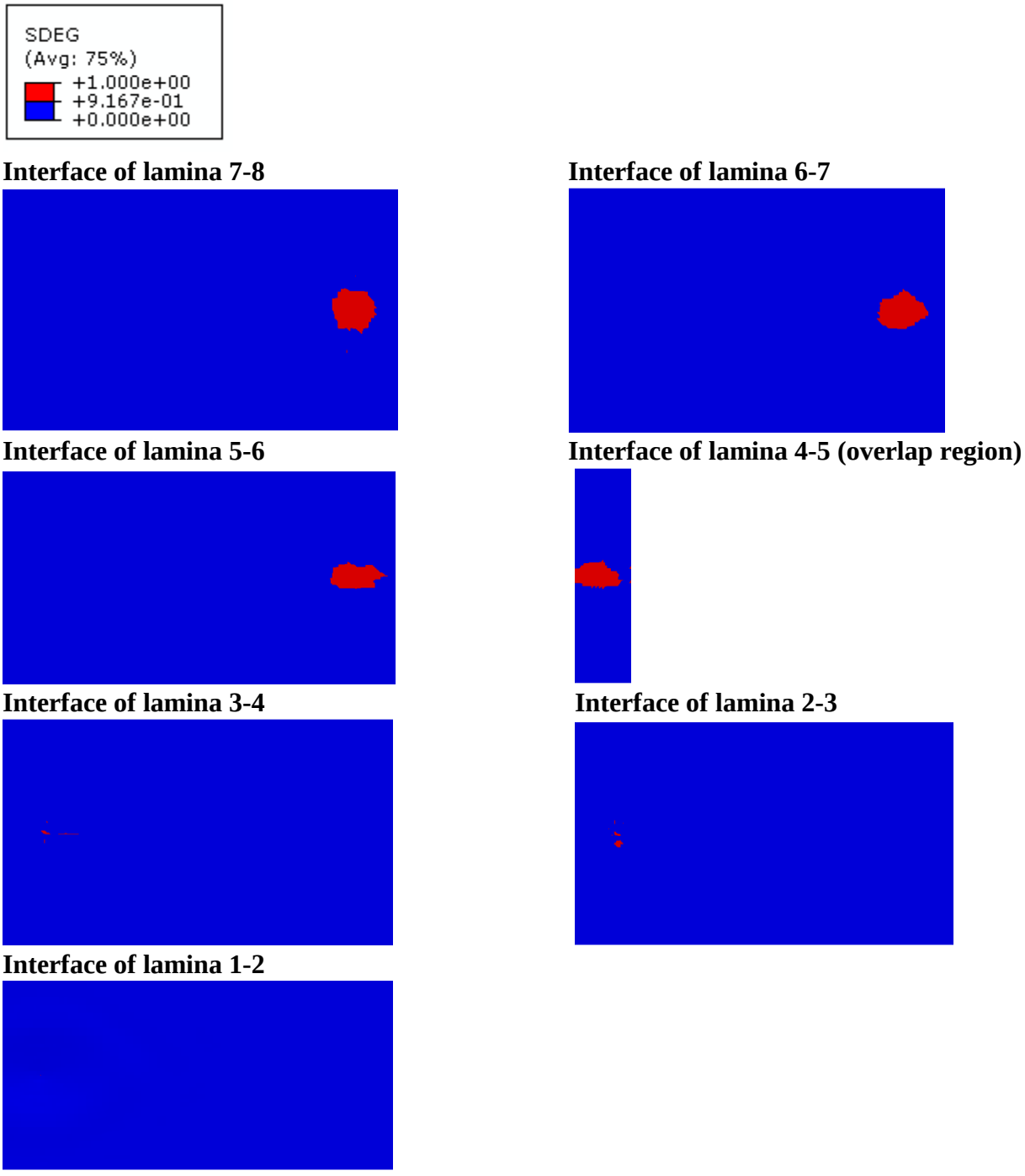

Fig 4. 9 FE based damage area plots for all interfaces of lap joints of 25 mm at 6.7 ms^{-1}

(iv) Impact Velocity 7.9 ms^{-1}

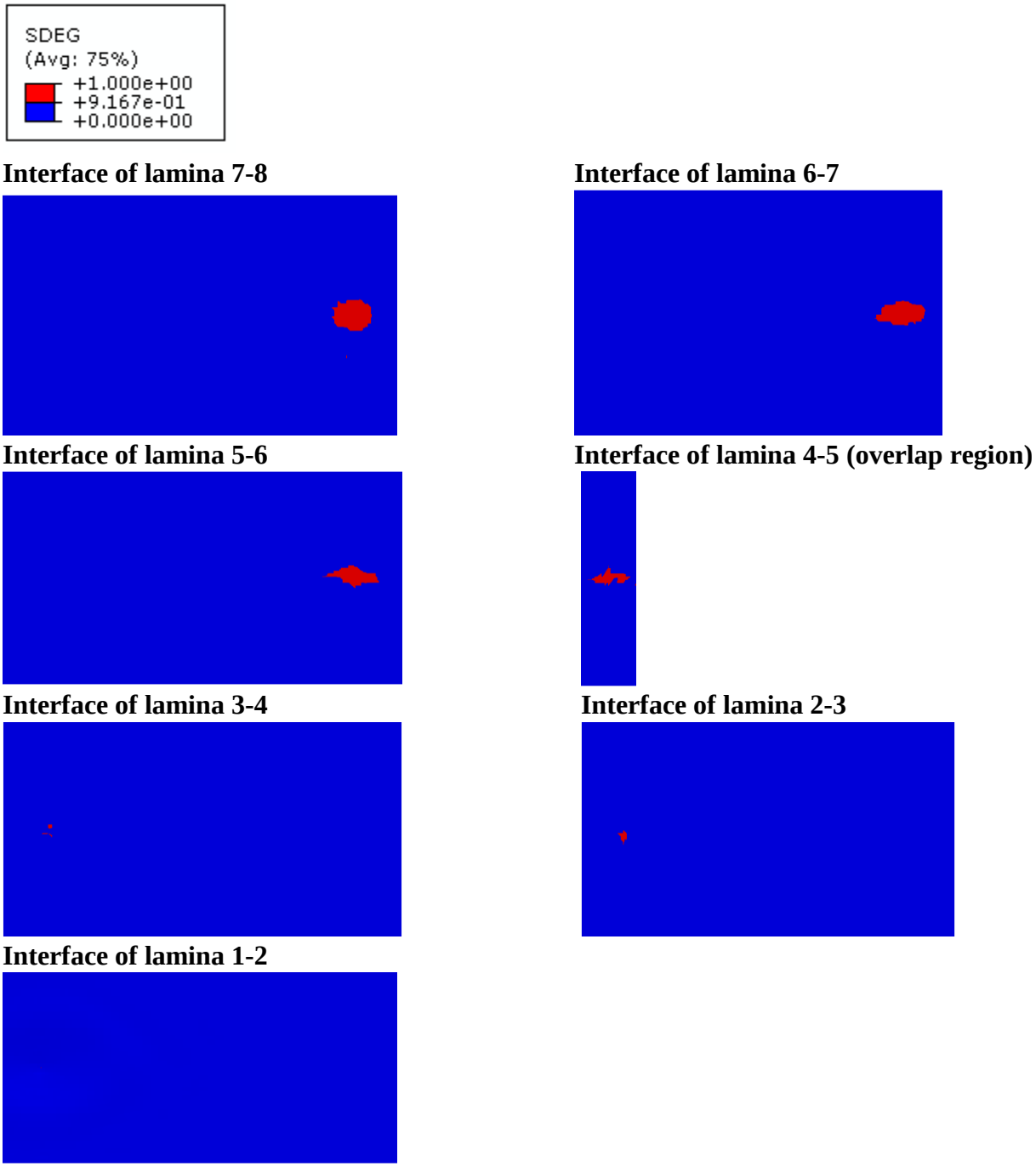

Fig 4. 10 FE based damage area plots for all interfaces of lap joints of 25 mm at 7.9 ms^{-1}

(v) Comparison of Case 2- 25 mm overlap joint results with respect to impact velocities

It has been observed that, the maximum delamination area arises at the interface of top two laminas at all impact velocities in 25 mm overlap joint. And the damage areas started to grow, as the impact velocities increases from 4 ms^{-1} to 7.9 ms^{-1}. The comparison of delamination areas expressed as percentage are of overlap is shown in Fig 4.11. These percentage delamination areas are calculated at the maximum delaminated interface. Fig 4.11 shows that, the percentage delamination area increases as impact velocities increases and the maximum percentage delaminated area is 6.73 % percent at 7.9 ms^{-1}.

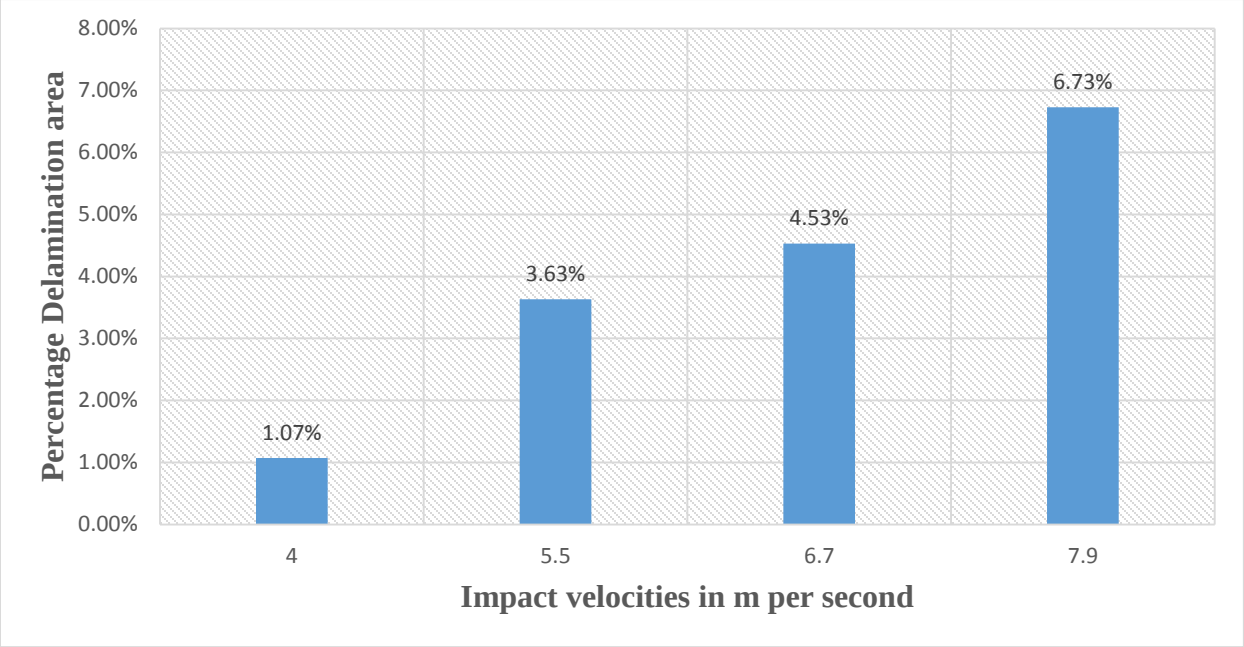

Fig 4. 11 Comparison of Percentage delamination area expressed as percentage of total area of overlap

4.2.3 Case Number 3- 36 mm overlap width

Damage area plots were calculated for each interface, which are shown below in Fig 4.12. The maximum damage was seen to be observed at first and second layer from the top as observed in last case for a 21 mm overlap width. Finite element based plots of all interfaces of 36 mm lap joint at 4ms^{-1} at1.81 ms after the first impact is shown in Fig 4.12.

(i) Impact Velocity 4.0 ms^{-1}

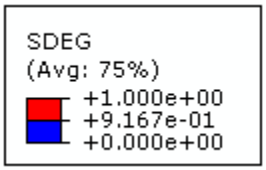

Interface of lamina 7-8

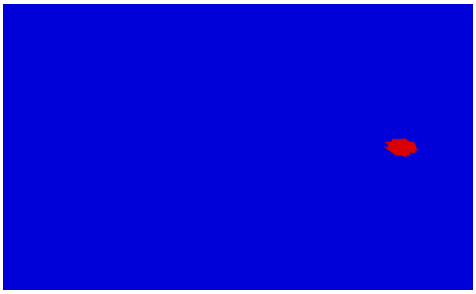

Interface of lamina 6-7

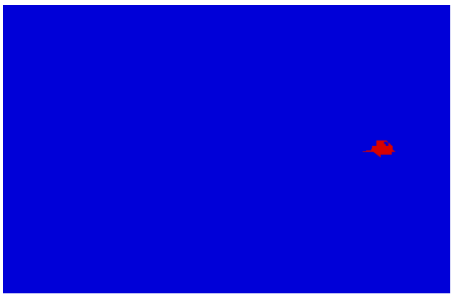

Interface of lamina 5-6

Interface of lamina 4-5 (overlap region)

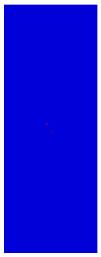

Interface of lamina 3-4

Interface of lamina 2-3

Interface of lamina 1-2

Fig 4. 12 FE based damage area plots for all interfaces of lap joints of 36 mm at 4.0 ms^{-1}

(ii) Impact Velocity 5.5 ms^{-1}

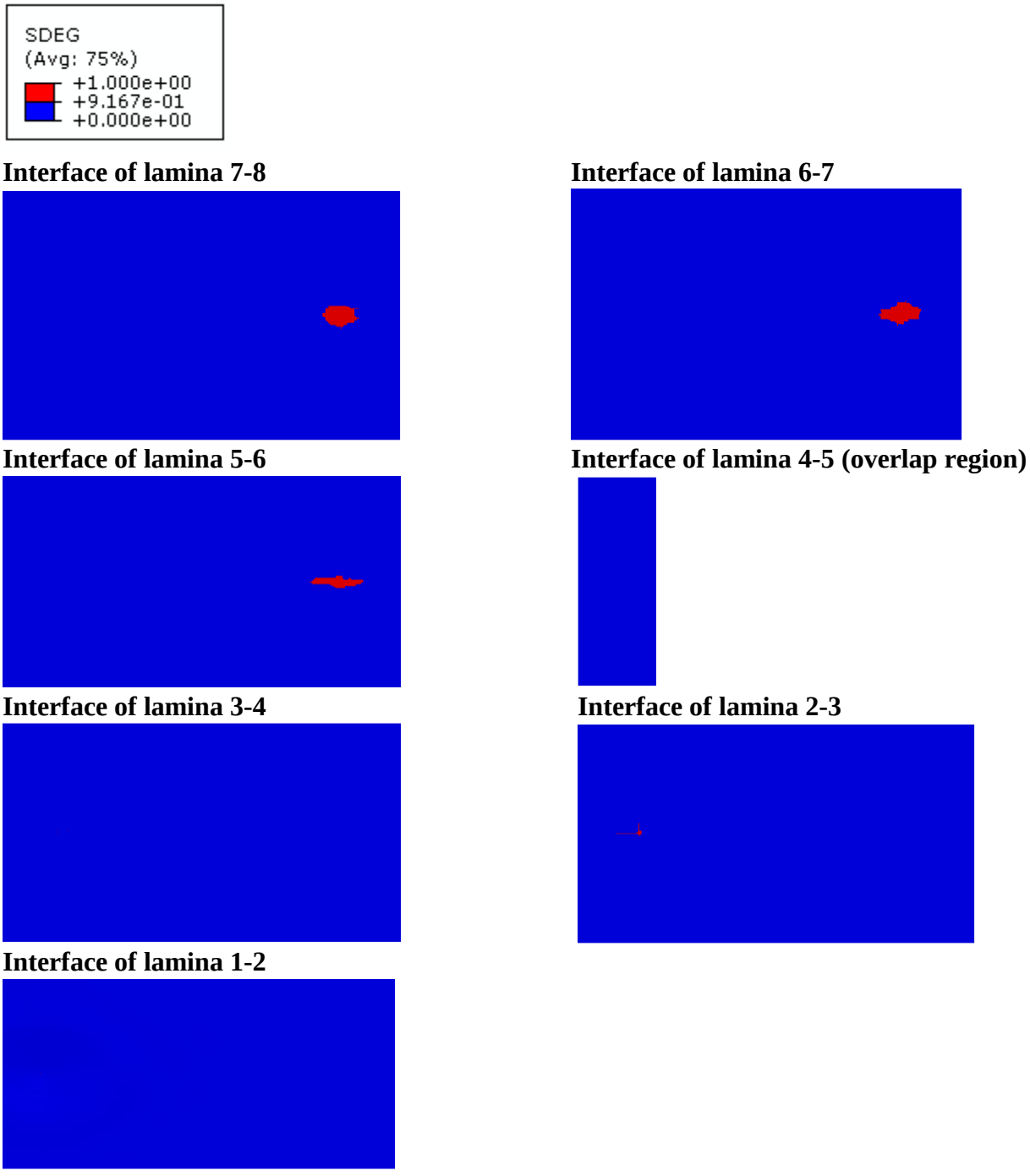

Fig 4. 13 FE based damage area plots for all interfaces of lap joints of 36 mm at 5.5 ms^{-1}

(iii) Impact Velocity 6.7 ms^{-1}

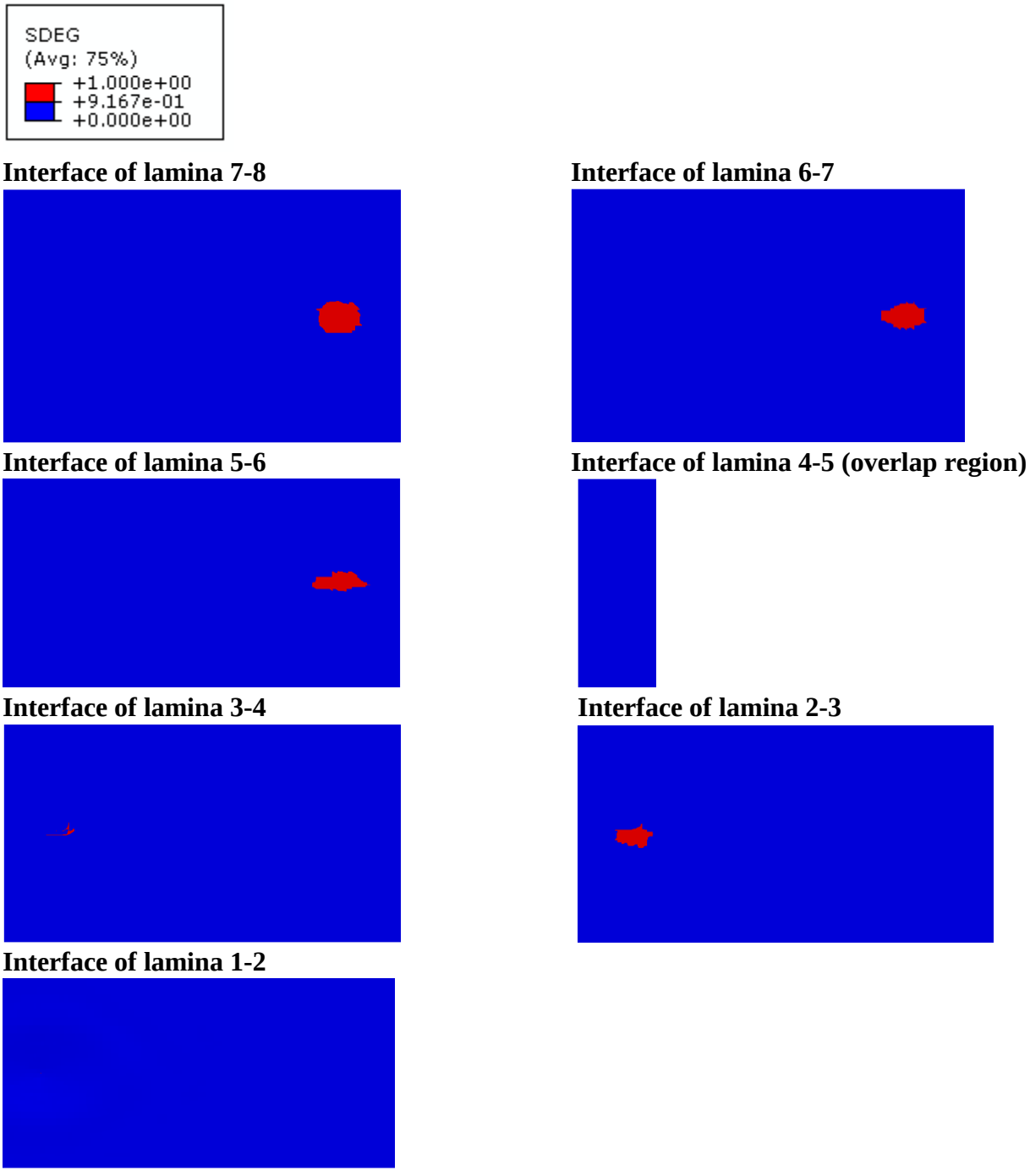

Fig 4. 14 FE based damage area plots for all interfaces of lap joints of 36 mm at 6.7 ms^{-1}

(iv) Impact Velocity 7.9 ms^{-1}

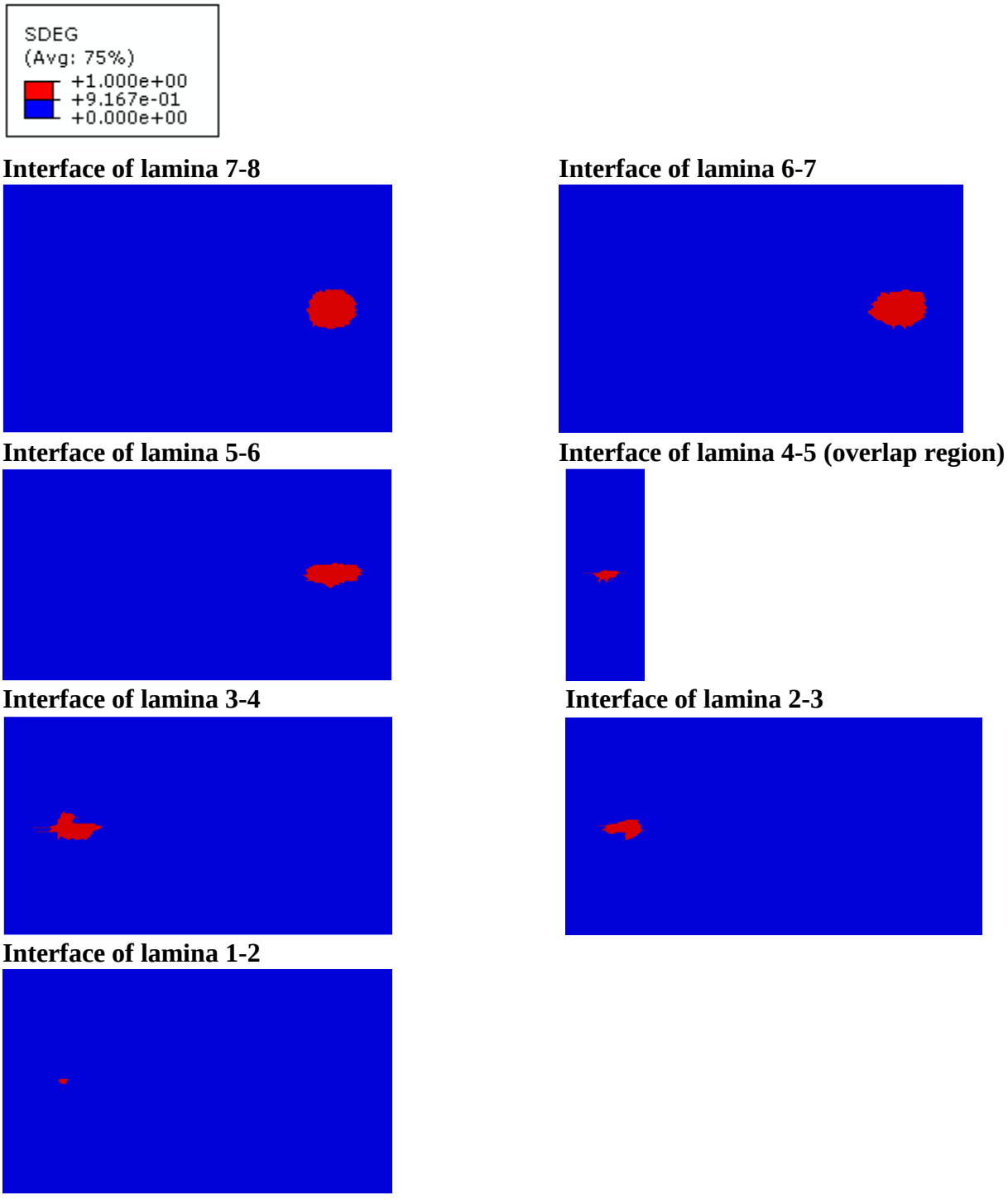

Fig 4. 15 FE based damage area plots for all interfaces of lap joints of 36 mm at 7.9 ms^{-1}

(v) Comparison of Case 3- 36 mm overlap joint results with respect to impact velocities

It has been observed that, the maximum delamination area arises at the interface of top two laminas at all impact velocities in 36 mm overlap joint. And the damage areas started to grow, as the impact velocities increases from 4 ms^{-1} to 7.9 ms^{-1}. The comparison of delamination areas expressed as percentage are of overlap is shown in Fig 4.16. These percentage delamination areas are calculated at the maximum delaminated interface. Fig 4.16 shows that, the percentage delamination area increases as impact velocities increases and the maximum percentage delaminated area is 5.53 % percent at 7.9 ms^{-1}.

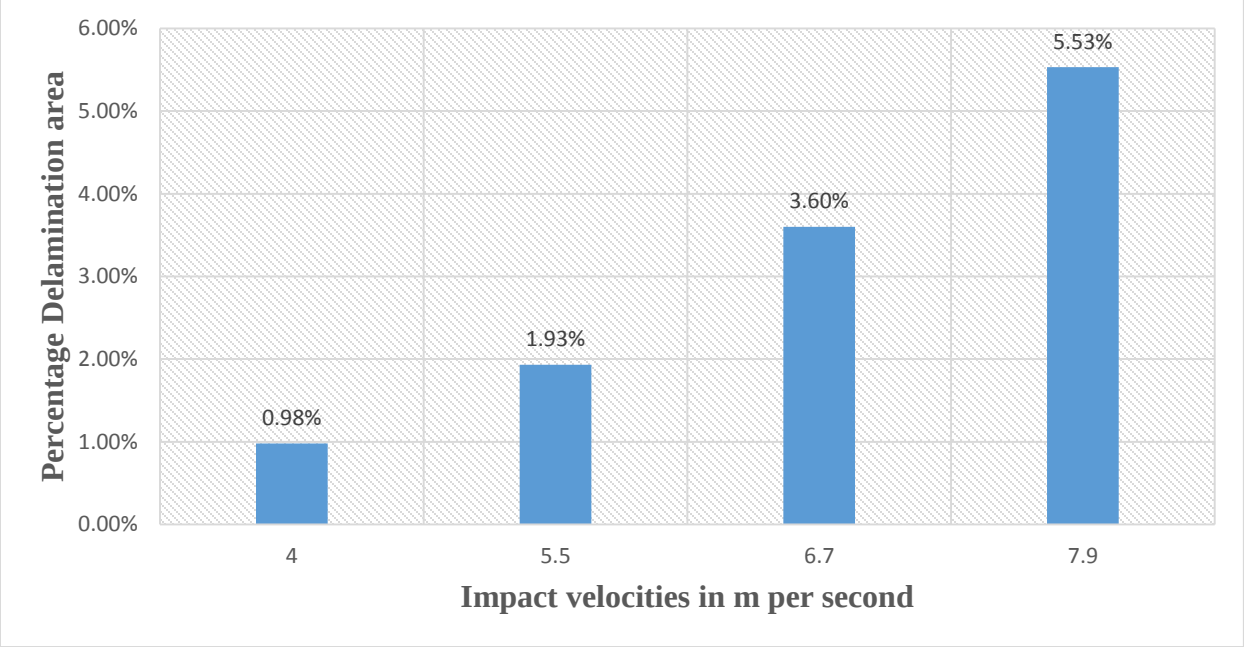

Fig 4. 16 Comparison of Percentage delamination area expressed as percentage of total area of overlap

4.2.4 Case Number 4- 46 mm overlap width

Damage area plots were calculated for each interface, which are shown below in Fig 4.17. The maximum damage was seen to be observed at first and second layer from the top as observed in last case for a 21 mm overlap width. Finite element based plots of all interfaces of 25mm lap joint at 4ms^{-1} at1.81 ms after the first impact is shown in Fig 4.17.

(i) Impact Velocity 4 ms^{-1}

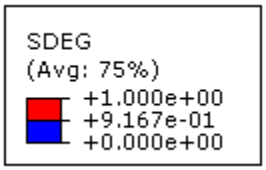

Interface of lamina 7-8

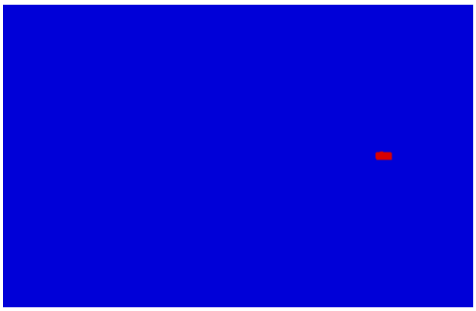

Interface of lamina 6-7

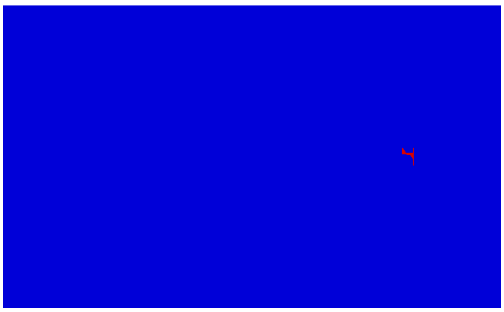

Interface of lamina 5-6

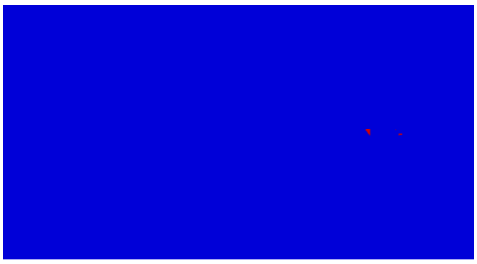

Interface of lamina 4-5 (overlap region)

Interface of lamina 3-4

Interface of lamina 2-3

Interface of lamina 1-2

Fig 4. 17 FE based damage area plots for all interfaces of lap joints of 46 mm at 4 ms^{-1}

(ii) Impact Velocity 5.5 ms^{-1}

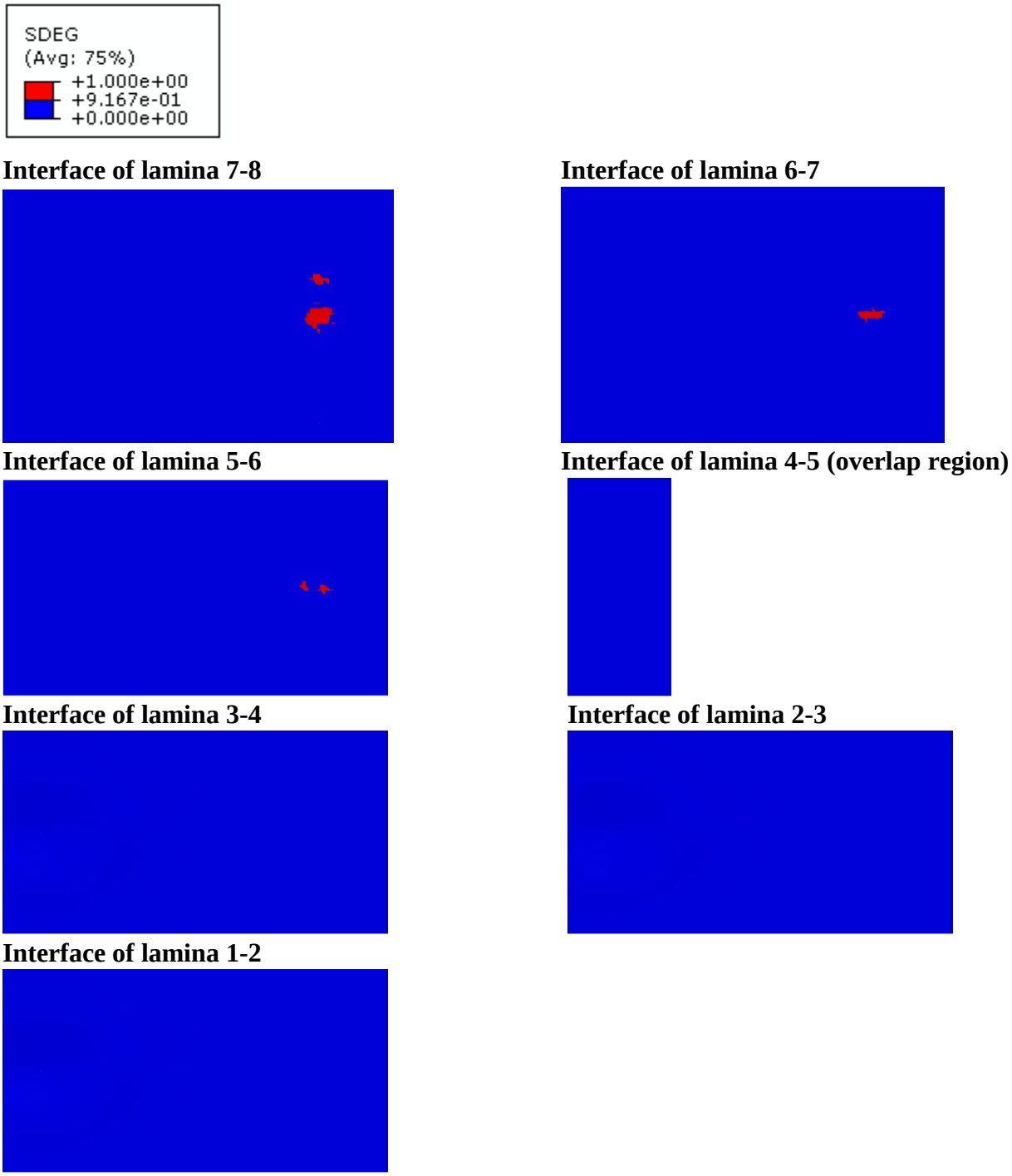

Fig 4. 18 FE based damage area plots for all interfaces of lap joints of 46 mm at 5.5 ms^{-1}

(iii) Impact Velocity 6.7 ms^{-1}

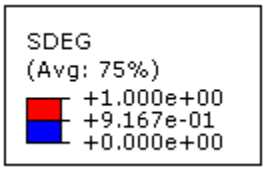

Interface of lamina 7-8

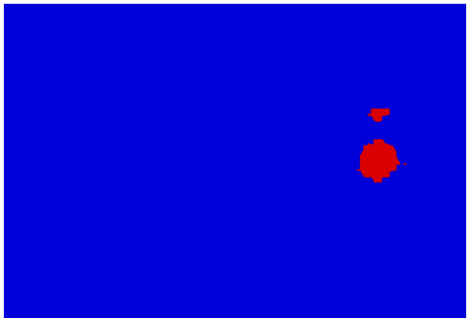

Interface of lamina 6-7

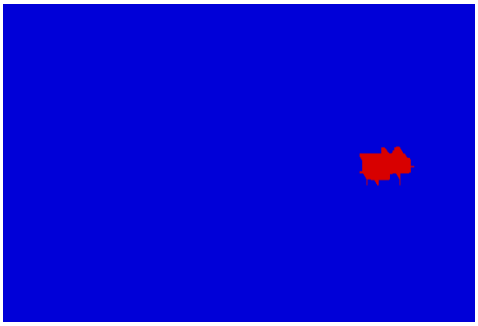

Interface of lamina 5-6

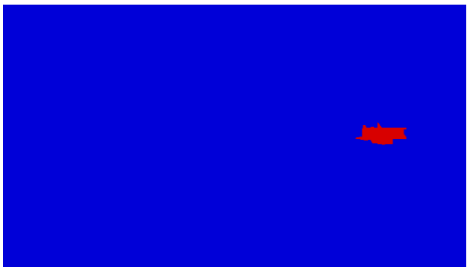

Interface of lamina 4-5 (overlap region)

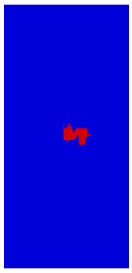

Interface of lamina 3-4

Interface of lamina 2-3

Interface of lamina 1-2

Fig 4. 19 FE based damage area plots for all interfaces of lap joints of 46 mm at 6.7 ms^{-1}

(iv) Impact Velocity 7.9 ms^{-1}

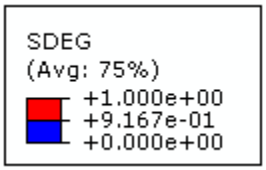

Interface of lamina 7-8

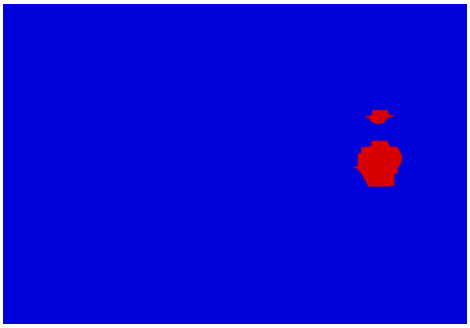

Interface of lamina 6-7

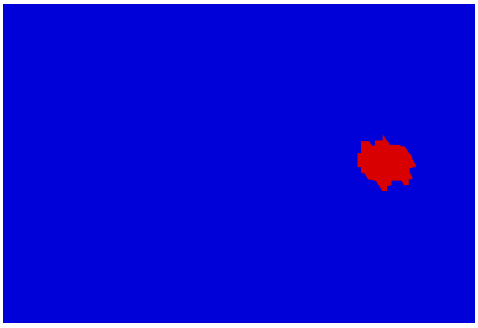

Interface of lamina 5-6

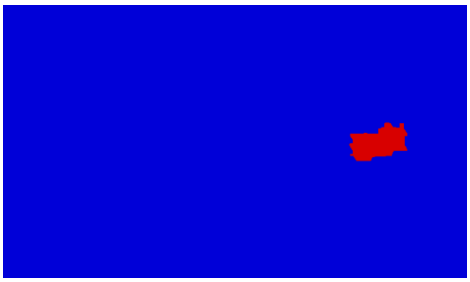

Interface of lamina 4-5 (overlap region)

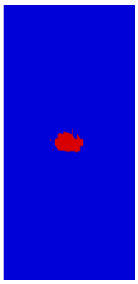

Interface of lamina 3-4

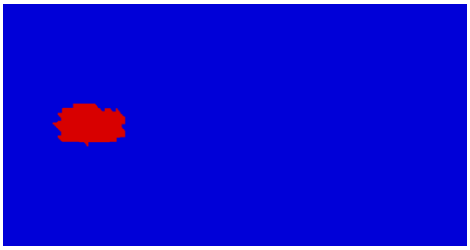

Interface of lamina 2-3

Interface of lamina 1-2

Fig 4. 20 FE based damage area plots for all interfaces of lap joints of 46 mm at 7.9 ms^{-1}

(v) Comparison of Case 4- 46 mm overlap joint results with respect to impact velocities

It has been observed that, the maximum delamination area arises at the top most interface at all impact velocities in 46 mm overlap joint. The comparison of delamination areas expressed as percentage are of overlap is shown in Fig 4.21. These percentage delamination areas are calculated at the maximum delaminated interface. Fig 4.21 shows that, the percentage delamination area increases as impact velocities increases and the maximum percentage delaminated area is 3.59 % percent at 6.7 ms^{-1}.

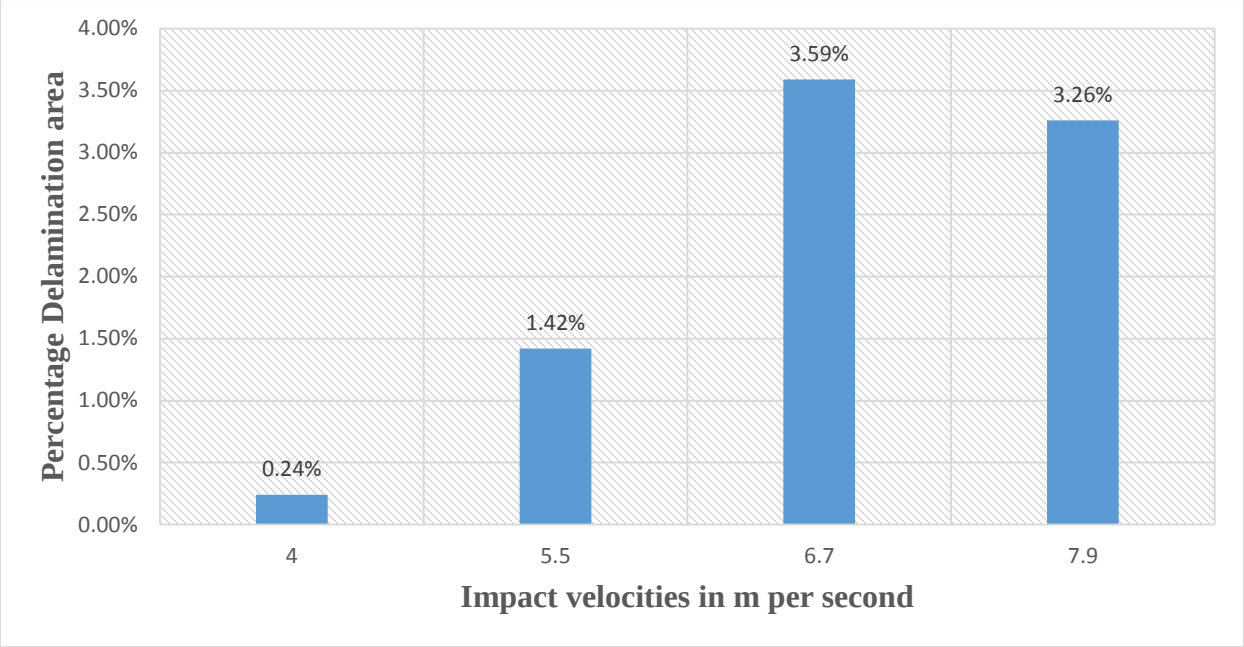

Fig 4. 21 Comparison of Percentage delamination area expressed as percentage of total area of overlap

4.2.5 Comparison of all 4 cases

Fig 4.22 is showing the overall delamination results of all overlap widths and all impact velocities. The trend remains the same in all cases that the maximum delaminated area is found to be observed at the top two interfaces. And the delaminated area increases as the velocity increases from 4 to 7.9 ms^{-1}. When we compare the results between overlap widths, an interesting phenomenon is perceived, as overlap width is increased the maximum delaminated area decreased as shown in Fig 4.22.

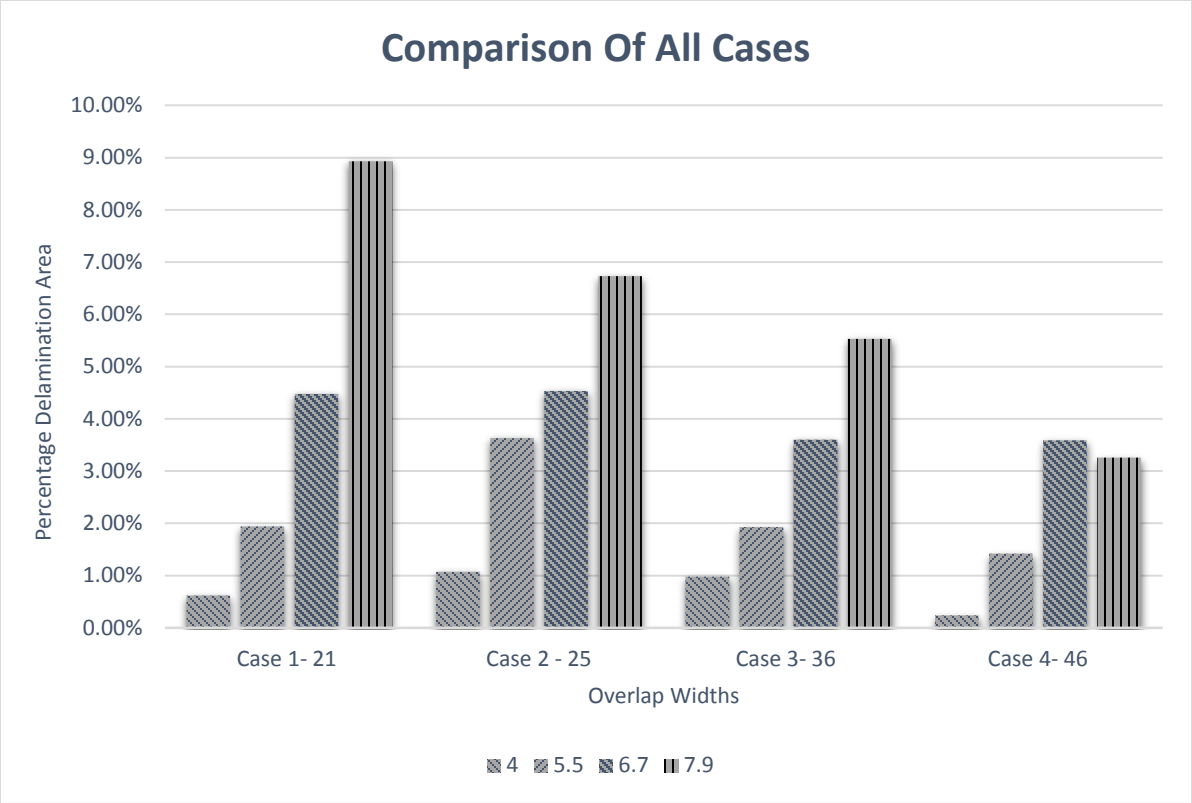

Fig 4. 22 Comparison of Percentage delamination area of all cases

4.2.6 Comparison of Delamination Results with the Experimental Results and the Previous FE simulations

It has been observed that for smaller velocities, this damage model gives much improved results as compared to previous damage model. For smaller characteristic overlap widths 21 and 25mm, and higher velocities (6.7 and 7.9) ms^{-1}, this damage model under predicted the percentage damage. For bigger overlap widths (36 and 46 mm), new damage model gives much improved results as compared to previous FE simulations. The percentage damage area results are improved up to 6 percent as compared to previous FE simulations in case of lower velocities and bigger overlap widths.

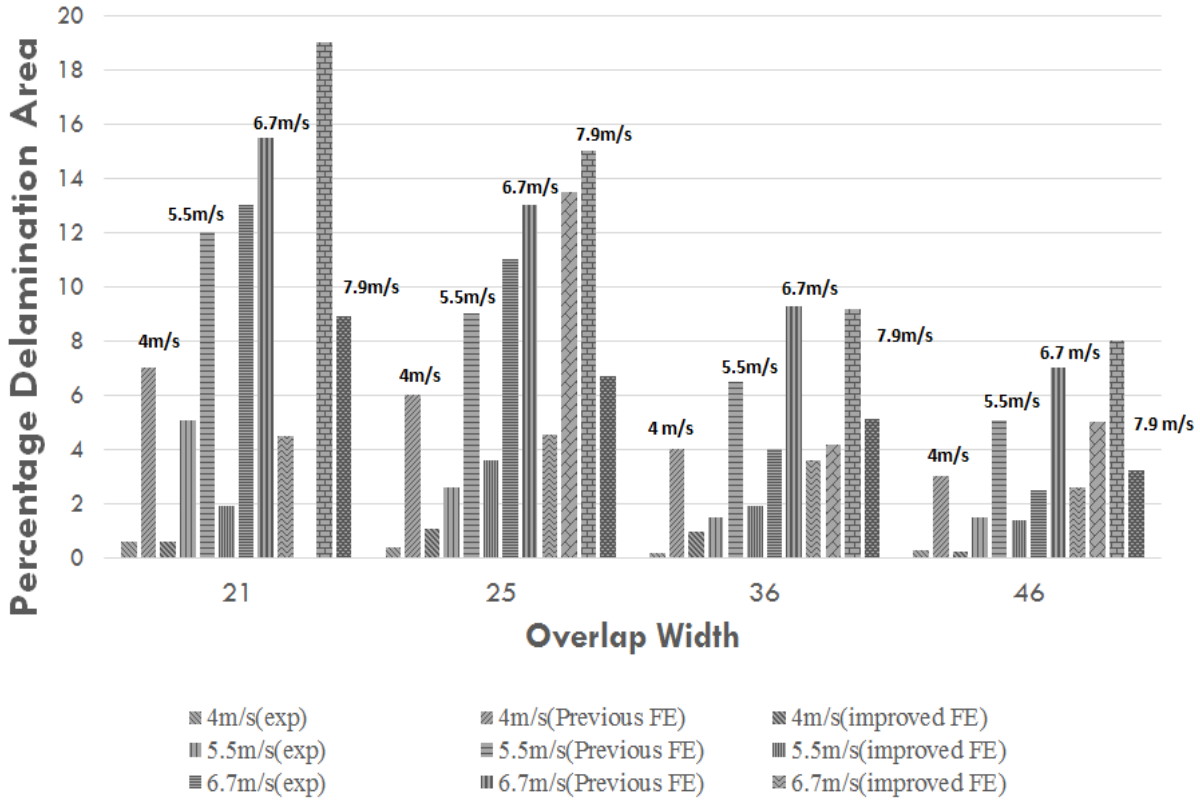

Fig 4. 23 Comparison of FE damage area prediction with the average experimental damage area values from C-Scan and previous FE simulations expressed as percentage of total area of overlap

4.3 Laminate Damage Results

Another important part of the study was to model inplane damage (laminate damage). Therefore, Hashin criteria was used for modeling laminate failure. There are four damage evolution variables (Damageft, Damagefc, Damagemt and Damagemc). Percentage areas for Damage evolution variables were calculated for modeling laminate failure. These damage areas were measured after 1.81ms of the first impact and the value of the scalar damage variable 'D' has been limited between 0.9 to 1 to focus only on the completely failed elements. The Ultrasonic C-Scan is a very popular and effective technique in the non-destructive analysis of metals, but in composites, it cannot be completely relied on due to the number of interfaces and irregular fibre patterns. These variables therefore make the scan less reliable and more complicated. C-Scan capture longitudinal fiber tension more accurately as compared to transverse (Matrix tension and Matrix compression). In order to compare our results with the experimental results, overall percentage damage area of lap

joint is computed in terms of longitudinal fiber tension. And the results were validated with the previous experimental results found in literature [8]. There will be four cases with respect to overlap regions (21, 25, 36 and 46) mm. In each case, percentage damage area of longitudinal fibre tension of all plies, with respect to four impact velocities will be shown and discussed.

4.3.1 Case-1 - 21 mm overlap joint

In this case, results of 4 impact velocities (4, 5.5, 6.7 and 7.9) ms^{-1} will be shown and discussed. Percentage damage areas were calculated, by plotting the damage variable (Damageft) for all laminas. These damage areas were measured after 1.81ms of the first impact.

(i) Impact Velocity 4 ms^{-1}

Damage area plots of longitudinal fiber tension (Damageft) were calculated for each lamina. The maximum damage was seen to be observed at top most ply (ply-8). As damage areas are calculated for lower plies, the damage areas decreases gradually. In this case with impact velocity $4ms^{-1}$, due to very low velocity, damage didn't reached to the bottom layers. As we will be moved towards the higher velocities, the damage started to grow, it will be discussed later on in next coming up cases. Finite element based plots of all plies of 21mm lap joint at $4ms^{-1}$ at 1.81 ms after the first impact is shown in Fig 4.24.

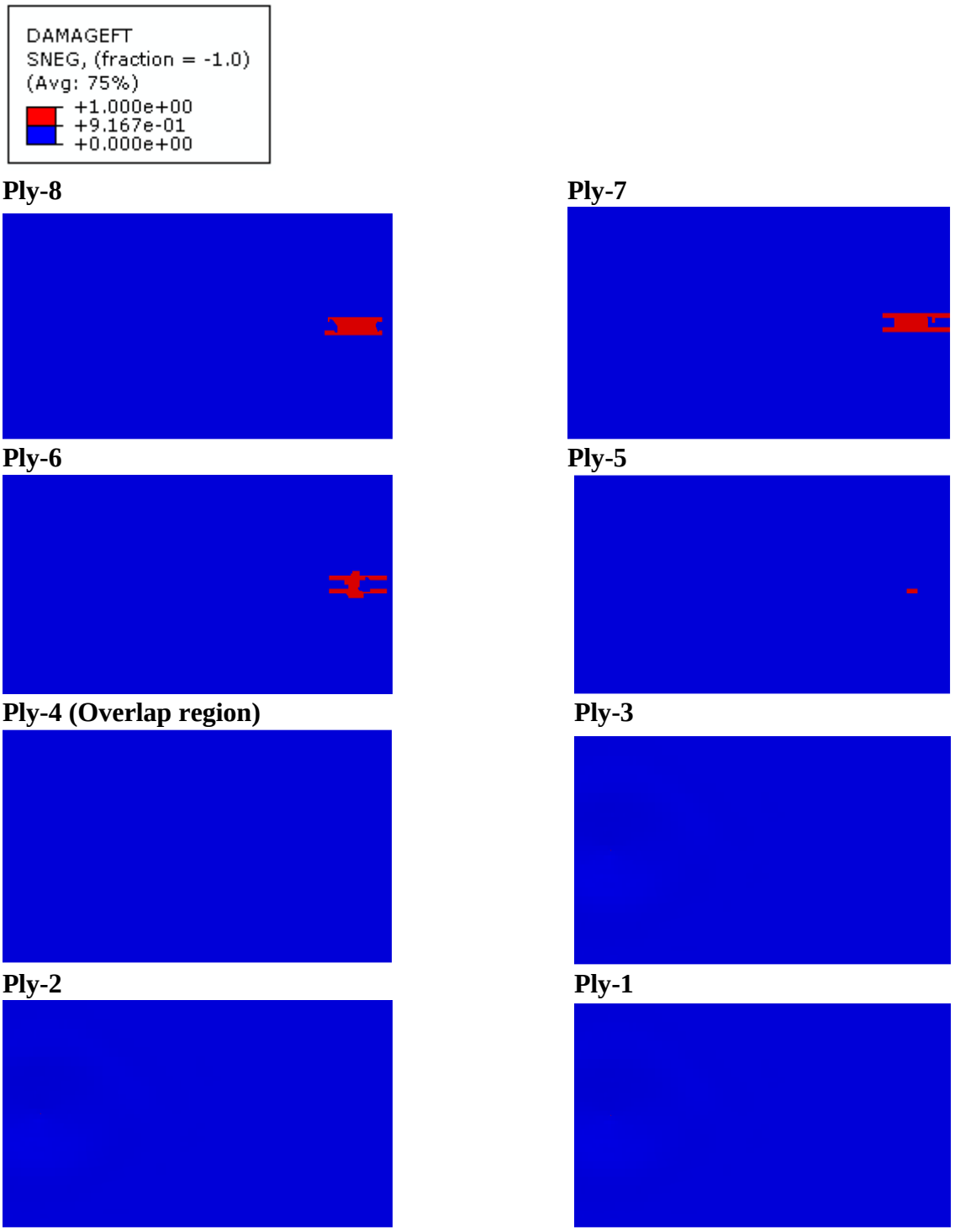

Fig 4. 24 FE based damage area plots for all Plies of lap joints of 21 mm at 4ms^{-1}

(ii) Impact Velocity 5.5 ms^{-1}

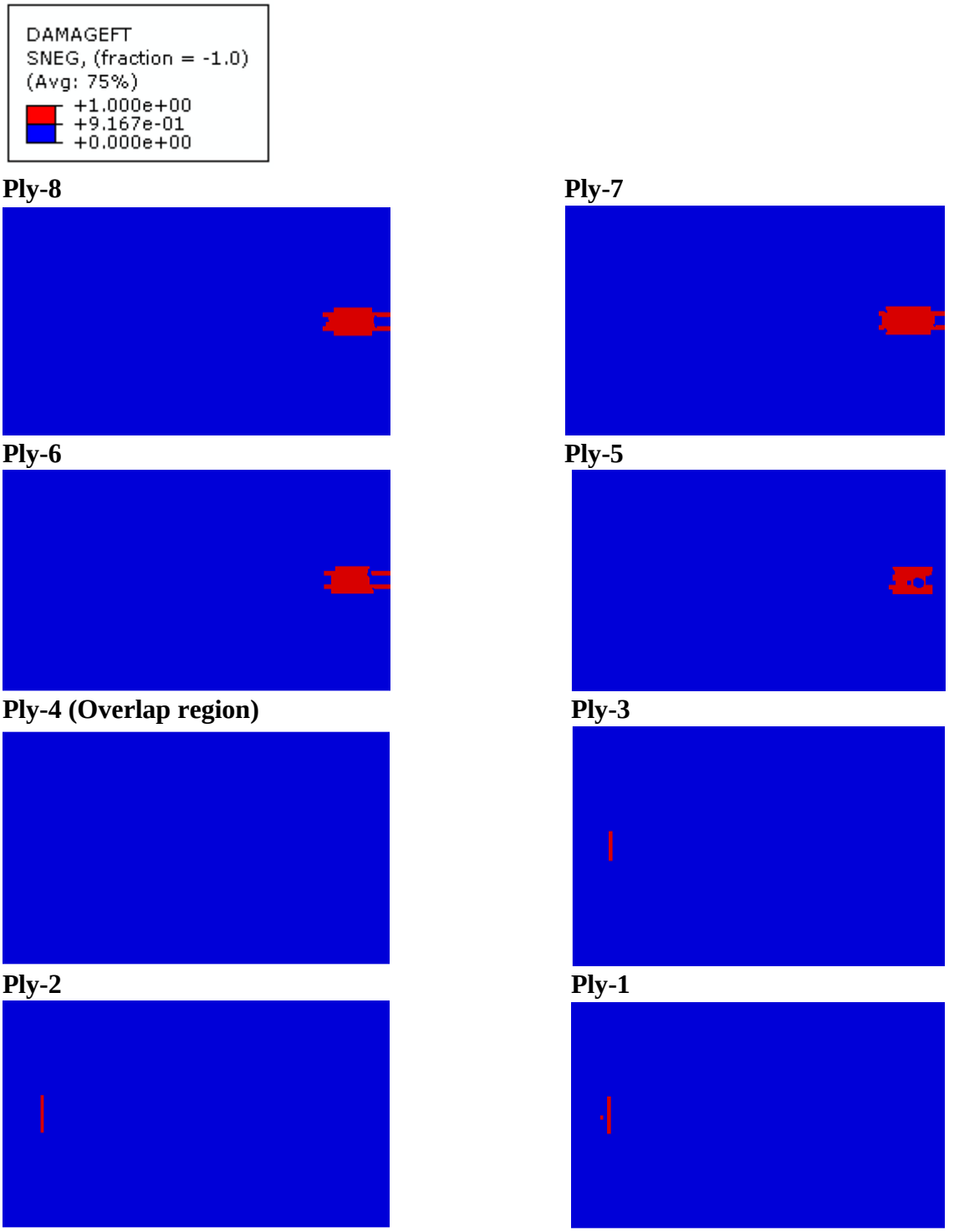

Fig 4. 25 FE based damage area plots for all Plies of lap joints of 21 mm at 5.5 ms^{-1}

(iii) Impact Velocity 6.7 ms^{-1}

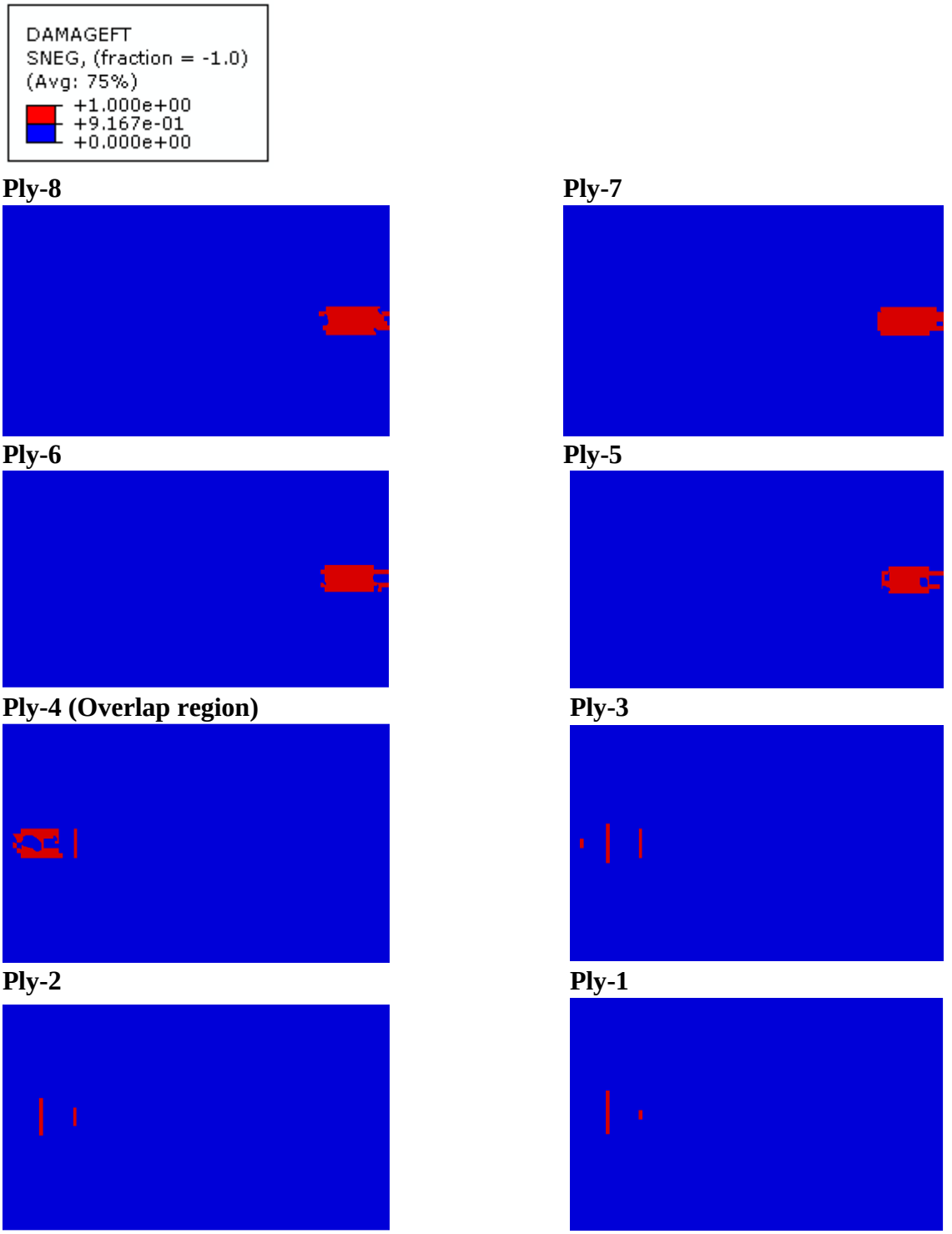

Fig 4. 26 FE based damage area plots for all Plies of lap joints of 21 mm at 6.7 ms^{-1}

(iv) Impact Velocity 7.9 ms^{-1}

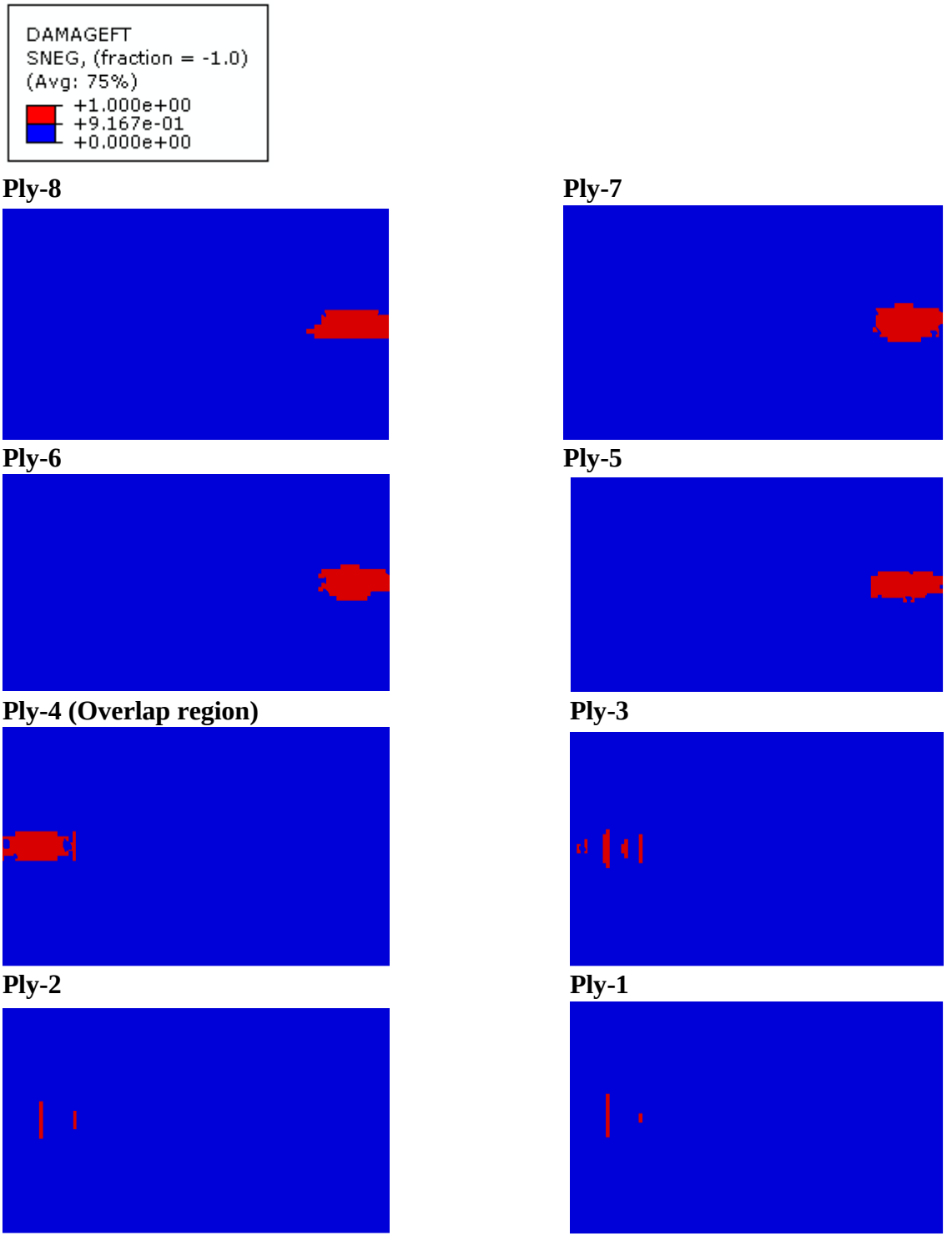

Fig 4. 27 FE based damage area plots for all Plies of lap joints of 21 mm at 7.9 ms^{-1}

(v) Comparison of Case 1- 21 mm overlap joint results with respect to impact velocities

It has been observed that, the maximum damage area arises at the top most ply-8 at all impact velocities in 21 mm overlap joint. And the damage areas started to grow, as the impact velocities increases from 4 ms^{-1} to 7.9 ms^{-1}. The comparison of damage areas expressed as percentage are of overlap is shown in Fig 4.28. These percentage damage areas are calculated at the maximum damaged ply, which in our case is top most ply. Fig 4.28 shows that, the percentage damage area increases as impact velocities increases and the maximum damage area is 11.42 % percent at 7.9 ms^{-1}.

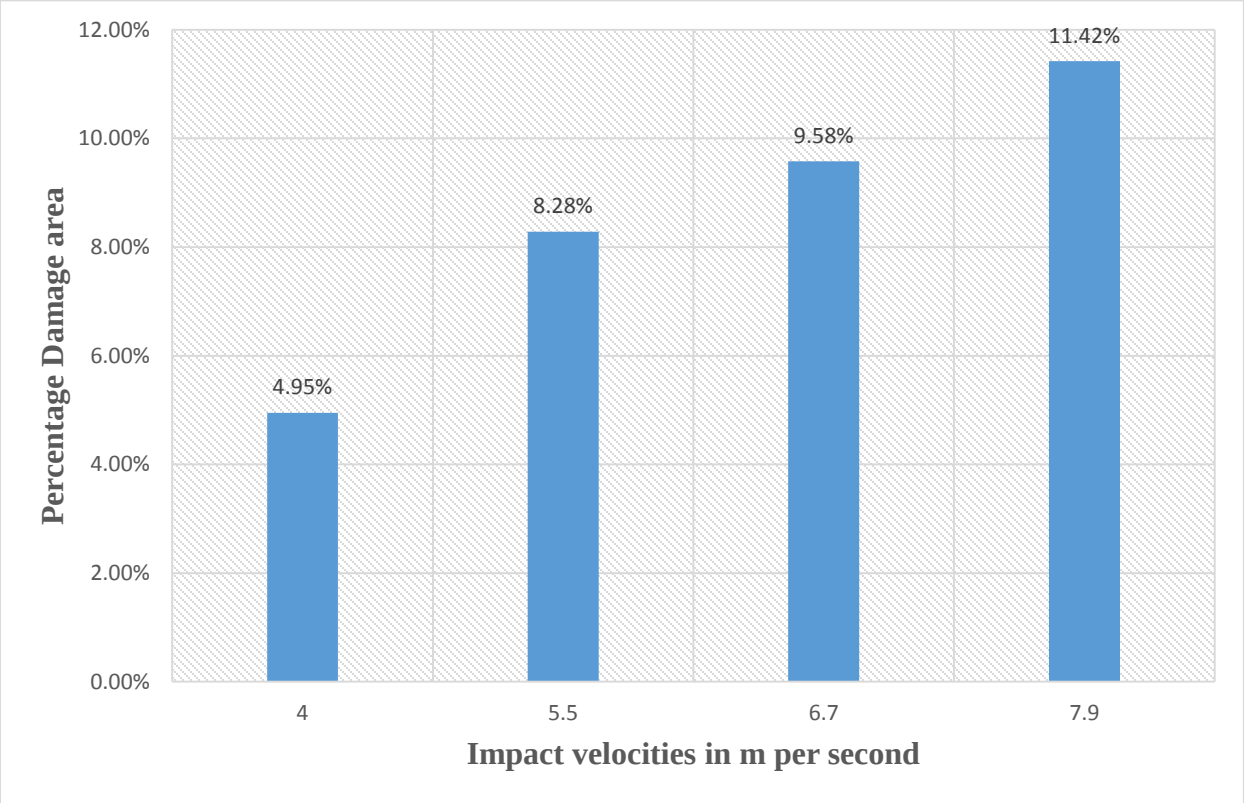

Fig 4. 28 Comparison of Percentage damage area expressed as percentage of total area of overlap

Similarly, damage area plots for longitudinal fiber tension are plotted for all laminas and the same trend is seen, as in first case-21 mm lap joint for all impact velocities.

4.3.2 Comparison of Case2- 25 mm overlap joint results with respect to impact velocities

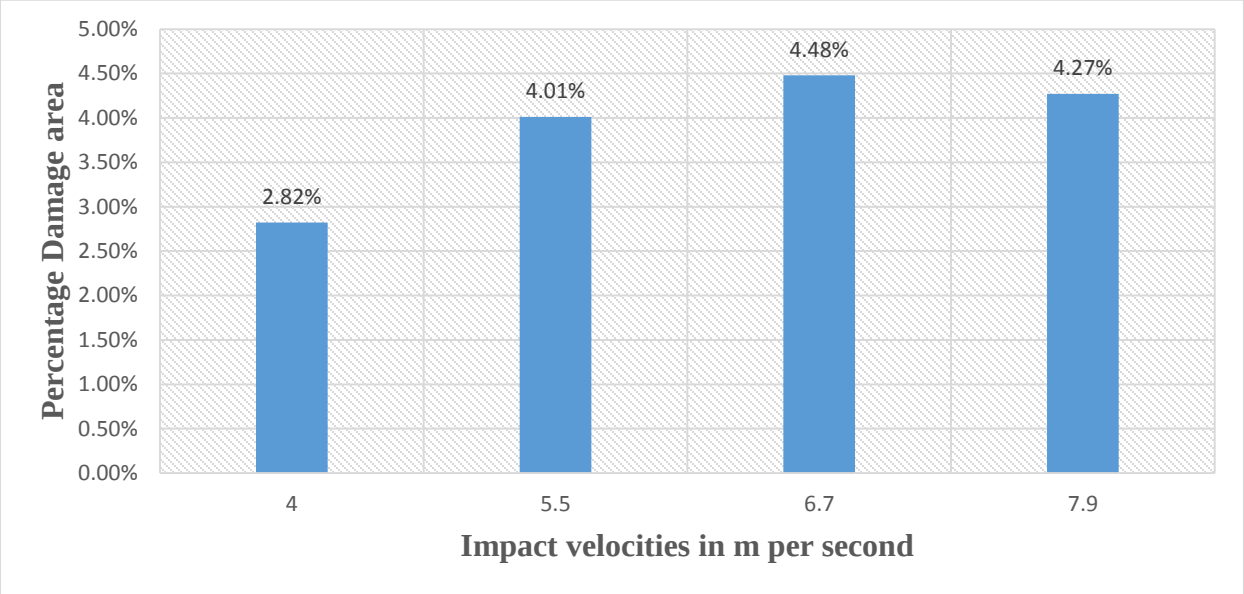

Fig 4. 29 Comparison of Percentage damage area expressed as percentage of total area of overlap

4.3.3 Comparison of Case3- 36 mm overlap joint results with respect to impact velocities

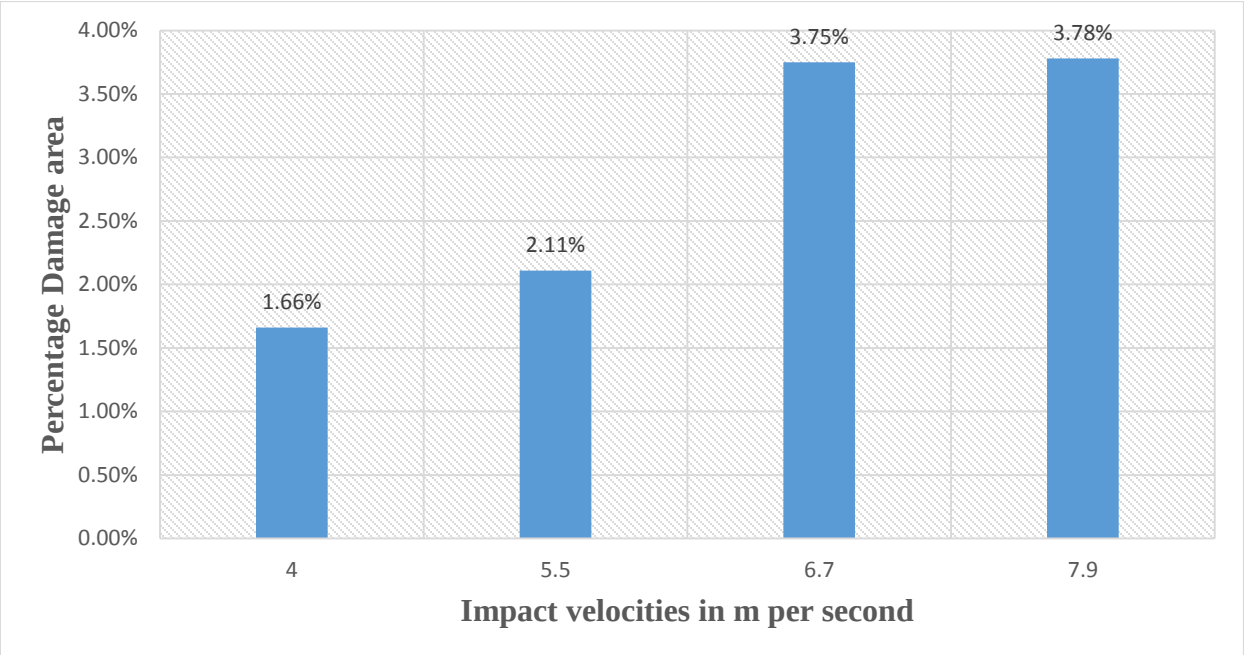

Fig 4. 30 Comparison of Percentage damage area expressed as percentage of total area of overlap

4.3.4 Comparison of Case4- 46 mm overlap joint results with respect to impact velocities

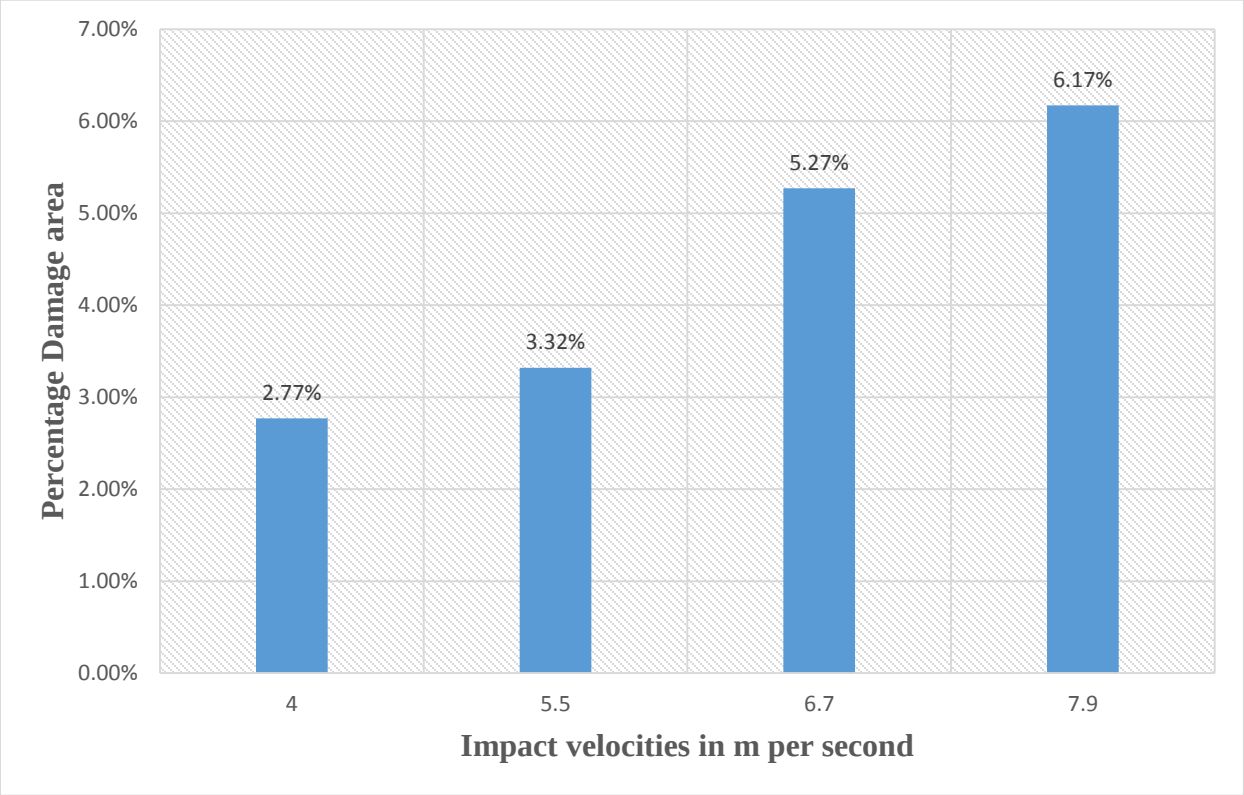

Fig 4. 31 Comparison of Percentage damage area expressed as percentage of total area of overlap

4.3.5 Comparison of all 4 cases

Fig 4.32 is showing the overall damage area results of all overlap widths and all impact velocities. The trend remains the same in all cases that the maximum damaged area is found to be observed at the top most ply. And the damaged area increases as the velocity increases from 4 to 7.9 ms^{-1}. When we compare the results between overlap widths, an interesting phenomenon is perceived, as overlap width is increased the damage areas calculated for longitudinal fiber tension decreased significantly as shown in Fig 4.32. This trend was also found in delamination case. Longitudinal fiber tensile mode is maximum for higher velocities and lower characteristic overlap widths. These results are deviating from the experimental results, as micro laminate failure was dominant for lower velocities (5.5 and 6.7) ms^{-1} in all overlap widths while in FE results shows the micro laminate failure dominated for higher velocity 7.9 ms^{-1}.

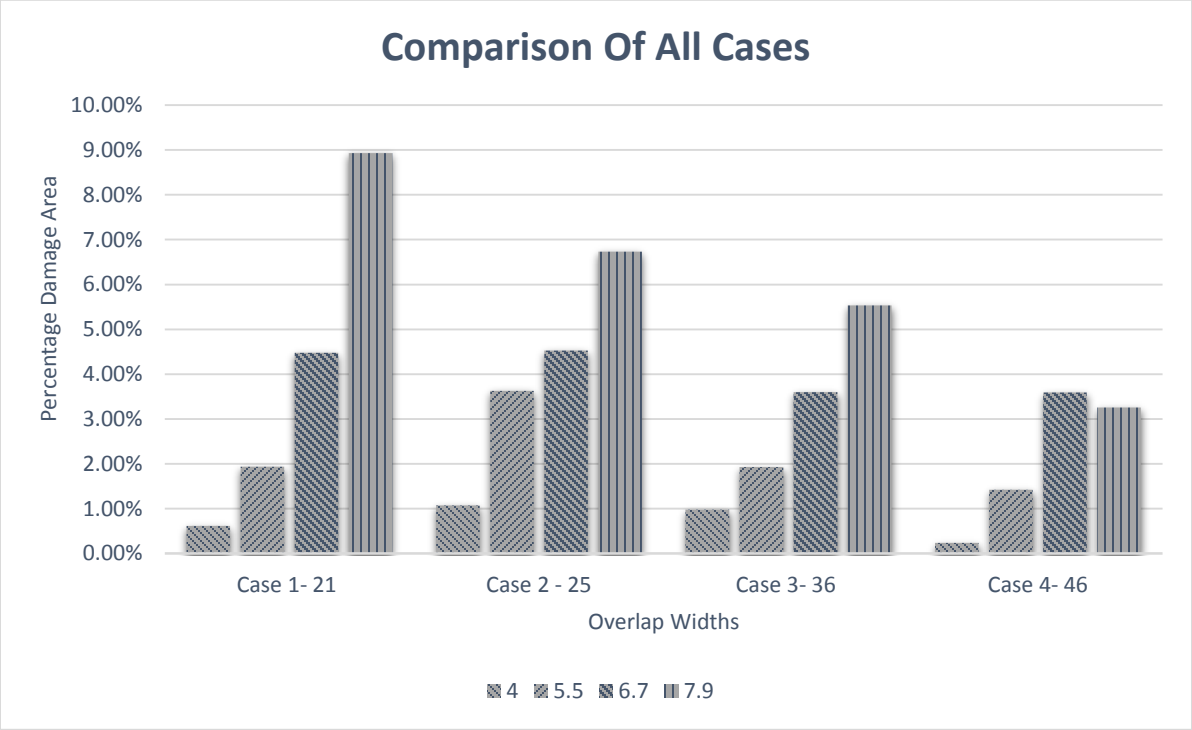

Fig 4. 32 Comparison of Percentage delamination area of all cases

Chapter 5
Conclusion

This is the closing chapter of this thesis. In this chapter, a conclusion of the study will be presented. There are some relevant streams which haven't been touched in this study. Based on that, a few future recommendations will also be made.

5.1 Conclusions

The basic objective of this study was to demonstrate the consistent set of methodology for measuring parameters for progressive damage model and for the validating this methodology by applying on single lap joint problem under transverse impact.

In particular, the study focused on improving the previous damage model [8] by including laminate damage in addition to delamination and bond failure with the ultimate aim to provide guidelines which will help a designer in deciding the extreme loading scenarios that must be considered to demonstrate that the design is safe.

This was achieved by proposing progressive damage model (Hashin) for modeling laminate failure by FE modeling of impact damage for four joints having different overlap widths (21, 25, 36 and 46 mm). The simulations were carried out at four different impact velocities – 4.0, 5.5, 6.7 and 7.9 ms^{-1} – all four of which fall under the low velocity regime.

In order to model delamination between the plies and disbond at the bond interface, cohesive zone approach based on the traction-separation law was used. The plies or adherends were modeled using 3D continuum shell elements. A total of 16 simulations were carried out to study the behavior of delamination and laminate damage as a function of overlap width and impact velocity.

ImageJ was used to process and analyze the simulation results and ascertain the percentage of delamination at interfaces and laminate damage. After detailed analysis of all the simulations, it has been observed that delamination and laminate are the function of overlap width. As the overlap width increases delamination and laminate damage decreases. Furthermore, it was observed that in both delamination and laminate damage the maximum damage occurs at the top most ply and interface.

The data taken from these simulations was compiled in the form of graphs which allowed for a comprehensive comparison of delamination/disbond and inplane damage on the basis of overlap width and impact velocity. In case of delamination damage, this model is safe to use for bigger overlap widths (36 and 46) mm. For smaller overlap regions, it is safe for lower velocities (4 and 5.5) ms^{-1}. For higher velocities, this damage model under predicts. The previous damage model was safer to use for higher velocities for lower characteristic overlap widths.

Through the parametric analysis of the data formulated by these simulations, it was concluded that if a designer wants to design a single lap joint of glass reinforced woven fiber polymeric composite subjected to transverse loading by considering the extreme loading scenarios, laminate failure should also be modeled in addition to delamination modeling for better results.

5.2 Future Recommendations

In this study, laminate failure is modelled by using mode longitudinal fiber tensile mode. If other modes of fracture toughnesses can be calculated in future studies, this will further improve the results and existing damage model.

There are few other parameters like material model, thickness of the lap joint and the boundary conditions, which can be varied, and their effects on the delamination, inplane damage and other modes of damage observed. Work could be done to develop an analytical formulation which would help us to define velocity ranges rather than working with discrete velocities and overlap widths.

References

[1] SergeAbrate, "Modeling of impacts on composite structures," *Composite Structures 51 (2001) 129-138*, 2001.

[2] P. M. Umar Farooq, "Finite element simulation of damage and failure predictions of relatively thick carbon fibre-reinforced laminated composite panels," *Thin-Walled Structures 104 :82–105,* 2016.

[3] M. ,. S. ,. H. M. E. Ali Kursun, "Experimental and numerical analysis of low velocity impact on a preloaded composite plate," *Advances in Engineering Software 90: 41–52.* 2015

[4] F. A. D. Feng, "Finite element modelling of damage induced by low-velocity impact on composite laminate," *Composite Structures 108: 161–171,* 2014.

[5] A. P. S.K. Parida, "Influence of curvature geometry of laminated FRP composite panels on delamination damage in adhesively bonded lap shear joints," *International Journal of Adhesion & Adhesives 54 : 57–66,* 2014.

[6] MeduriS.Naik, "Polymer matrix composites subjected to low velocity impact," *Compos Sci Technol, 2001*.

[7] D. K. B. A. Dutton S, "Composite materials for aircraft structures," *American Institute of Aeronautics and Astronautics,* 2006.

[8] S. F. H. ,. S. L. ,. R. D. R.S. Choudhry, "Damage in single lap joints of woven fabric reinforced polymeric composites subjected to transverse impact loading," *International Journal of Impact Engineering 80: 76-93,* 2015.

[9] F. C. R. R. T. W. E.J. Barbero, "Determination of material parameters for Abaqus progressive damage analysis of E-glass epoxy laminates," *Composites: Part B 46: 211–220,* 2013.

[10] R. Batra, "Damage and failure in low energy impact of fiber-reinforced polymeric composite laminates," *Composite Structures 94 :540–547,* 2012.

[11] M. H. P. D. U. K. V. Abhay R.S. Gautama, "Experimental- numerical studies of transverse impact response of adhesively bonded lap joints in composite structures," *International Journal of Adhesion & Adhesives 26: 184–198,2006*

[12] J. R. Reeder, "3d mixed mode delamination fracture criteria-an experimental prespective," *NASA Langley research center,M/S 188E.*

[13] Z.Hashin, "Failure criteria for unidirectional fiber composites".

[14] Donadon, "A progressive failure model for composite laminates subjected to low velocity impact damage," *Computers and Structures 86: 1232–1252,* 2008.

[15] P. Wang, "A novel predictive model for mechanical behavior of single-lap GFRP composite bolted joint under static and dynamic loading," *Composites Part B 79: 322-330,* 2015.

[16] U. S. G. Reyes, "Modeling and damage repair of woven thermoplastic composites subjected to low velocity impact," *Composite Structures, vol. vol.92, pp. 523-531, 2010.*

[17] D. L. C. Atasa, "Impact response of woven composites with small weaving angles," *International Journal of Impact Engineering, vol. 35 , no. 2, pp. 80-97, 2008.*

[18] T. B. B. P. Y. D. M. Keefeb, "Finite element modeling of transverse impact on a ballistic fabric," *International Journal of Mechanical Sciences, vol. 48, no. 1,pp. 33-43, January 2006.*

[19] S. P. ,. P. R. ,. A. M. M.J. Laffan, "Translaminar fracture toughness testing of composites: A review," *Polymer Testing 31 : 481–489,* 2012.

[20] ,. G. C. V. H. E. Martin, "Damage analysis of thin 3D-woven SiC/SiC composite under low velocity impact loading," *Composites Part A: Applied Science and Manufacturing, vol. 43, no. 2, pp. 247-253, February 2012.*

[21] J. Jerald N. Rajesh Mathivanan *, "Experimental investigation of low-velocity impact characteristics of woven glass fiber epoxy matrix composite laminates of EP3 grade," *Materials and Design,* vol. 31 , no. 9, pp. 4553–4560, October 2010.

[22] Y. A. D. M. Qin, "Analysis of single lap adhesive composite joints with," *Composites Part B: Engineering, vol. 32, no. 2, pp. 167–173,March 2003.*

[23] H. K. R. H. J. Neumayer, "An explicit cohesive element combining cohesive failure of the adhesive and delamination failure in composite bonded joints," *Composite Structures 146 :75–83,* 2016.

[24] D. W. R. D. S. B. H.-G. R. C. B. W. Wagnera, "Adhesive joints in composite laminates—A combined numerical/experimental estimate of critical energy release rates," *International Journal of Adhesion and Adhesives, vol. 32, pp.23-38, January,* 2012.

[25] X. Y. ,. X. Z. Shuchang Long, "Delamination prediction in composite laminates under low-velocity impact," *Composite Structures 132 ,Volume 132, Pages 290–298,2015*

[26] H. K. H. Parka, "Damage resistance of single lap adhesive composite joints by transverse ice impact," *International Journal of Impact Engineering, vol. 37, no. 2, pp.177-184, February 2010.*

[27] S. T. P. Soraia Pimenta n, "An analytical model for the translaminar fracture toughness of fibre composites with stochastic quasi-fractal fracture surfaces," *Journal of the Mechanics and Physics of Solids 66: 78–102,* 2014.

[28] R.S.Choudhry, "Characterisation and modelling of impact damage in bonded joints of woven fibre polymeric composites (PhD)Thesis," *The School of MACE. 2009, The University of Manchester, Manchester,* 2009.

[29] VUMAT - User Subroutine to define material behaviour Section 1.2.17, ABAQUS User Subroutines Reference Manual (v6.10-1), ABAQUS.Inc, 2010.

[30] Cohesive elements Section 29.5, ABAQUS Analysis User's Manual (v6.10.1), ABAQUS,Inc, 2010.

[31] Abaqus Section 21.3.2 -Damage initiation for fiber-reinforced composites, ABAQUS Theory Manual (v6.10.1), ABAQUS,Inc, 2010.

[32] Section 24.3.3 Evolution of damage variables for each mode ABAQUS Theory Manual (v6.12.1), ABAQUS Theory Manual (v6.12.1), Abaqus Inc,2012

[33] Figure 24.3.3-1 Equivalent stress versus Equivalent diplacement , ABAQUS Theory Manual (v6.12.1), Abaqus Inc., 2012.

[34] Hexcel 8552 IM7 Unidirectional prepreg 190 gsm & 35% RC Qualification Material Property Data Report FAA Special Project number.

[35] P. C. J. X. C. D. A. M. G. Catalanotti, "Measurement of resistance curves in the longitudinal failure of composites using digital image correlation,," *Composites Science and Technology 70: 1986–1993,* 2010.

[36] S. P. P. R. A. M. M.J. Laffan, " Translaminar fracture toughness: the critical notch tip radius of 0 degree plies in CFRP," *Composites Science and Technology 72: 97–102,* 2011.

[37] S. P. P. R. L. I. A. M. M.J. Laffan, "Measurement of the fracture toughness associated with mode I fibre compressive failure," *14th European Conference on Composite Materials, Budapest, Hungary, 2010.*

[38] R.S.Choudhry, "Micromechanical modeling of 8-harness satin weave glass fiber-reinforced composites," *Journal of Composite Materials 0(0) 1–16,* 2016.

[39] Image J [Image processing and analysis in Java]. [Online]., "http://jeb.biologists.org/content/210/13/2213/F3.expansion.html#," [Online].

[40] The Company of Biologists. (2007) The Journal of Experimental Biology. [Online]., "http://jeb.biologists.org/content/210/13/2213/F3.expansion.html#," [Online].

CERTIFICATE OF COMPLETENESS

It is hereby certified that the dissertation submitted by NS Salman Khalid, Reg No. NUST201362426MCEME35113F, Titled: *FE Modelling of interacting indentation, flexural and delamination damage in lap joints of composites* has been checked/reviewed and its contents are complete in all respects.

Supervisor's Name: Dr. Rizwan Saeed Choudhry Signature: _____

Date: _____